A MAIN SEQUENCE FOR QUASARS

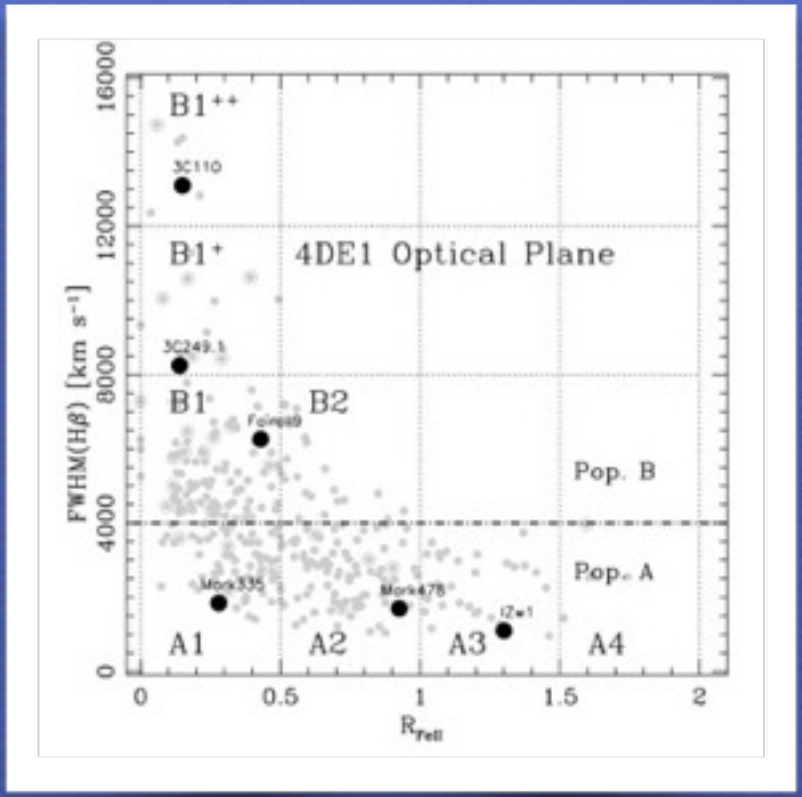

Paola Marziani

INAF, Osservatorio Astronomico di Padova, Italia

Deborah Dultzin (IA-UNAM, México), Jack W. Sulentic (IAA-CSIC, España), Alenka Negrete (IA-UNAM, México), Ascensión del Olmo, M. A. Martínez-Carballo (IAA-CSIC), España, Giovanna M. Stirpe, INAF, Osservatorio Astronomico di Bologna, Italia

Outline

Introduction: hints at quasar (type-1) spectral diversity at low z (<1)

The 4DE1 approach: observations and data analysis to provide a quantitative view of quasar properties

The "main sequence" of quasars organizes quasar diversity and allows to set observational constraints on dynamics and physical conditions within the broad line emitting region

Luminosity effects

Weak lined quasars: "solved" following the 4DE1 approach

 Quasar unification scheme(s)

Quasars lack stars' spherical symmetry.

Type 1 AGN are mainly unobscured accretors, probably seen at a viewing angle in between 0°/a few degrees and 45°-60° from the accretion disk axis.

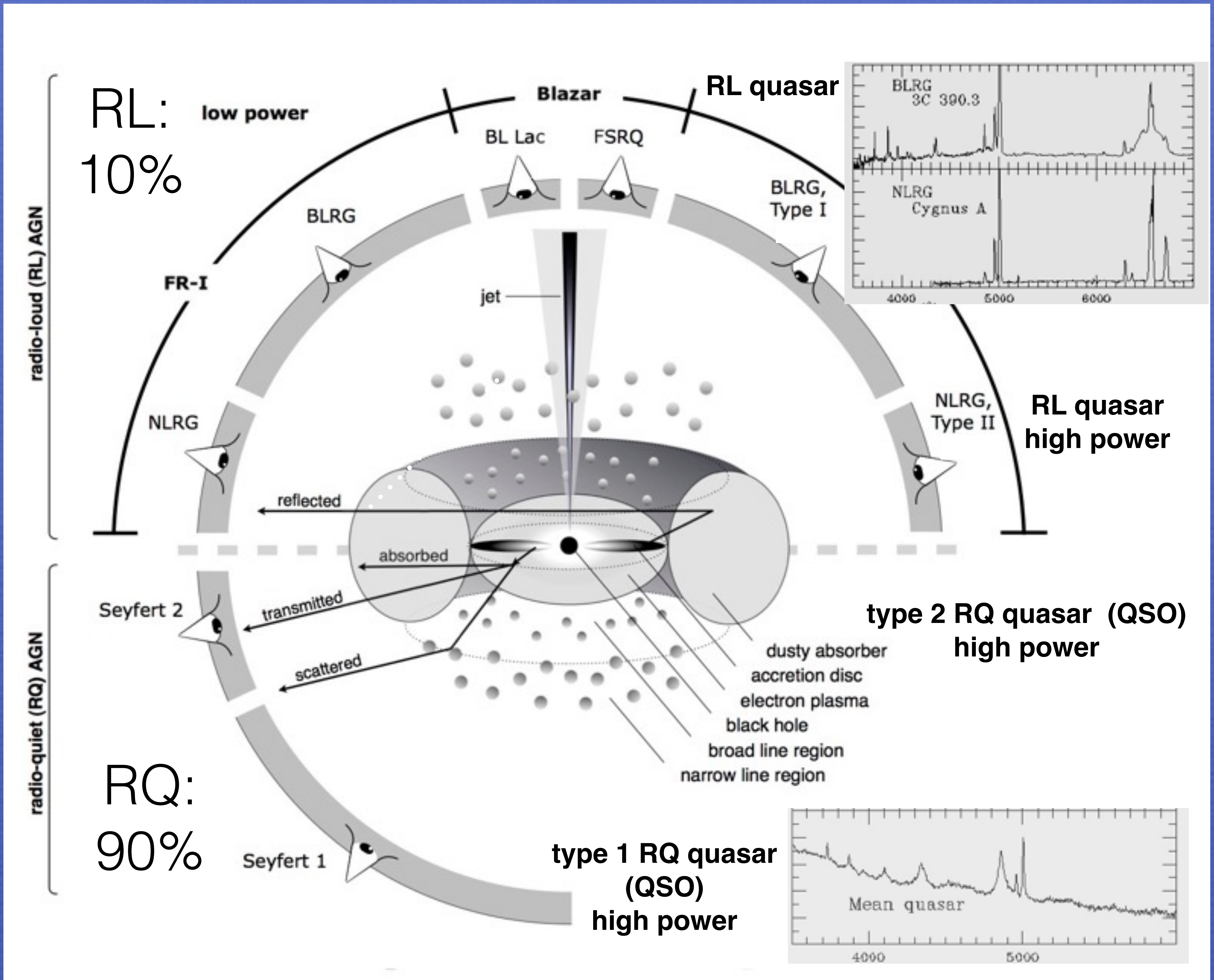

Adapted from Beckmann & Shrader 2013

Quasars' optical and UV spectrum

from the Sloan DSS: broad and narrow lines emitted by ionic species over a wide range of IPs

	Broad	Narrow
High Ionization	CIVλ1549, HeII	[OIII]λλ4959,5007, HeII,NeIII
Low Ionization	Balmer (Hβ), FeII, MgIIλ2800, CaII IR Triplet)	Balmer, [OI]λ6300,

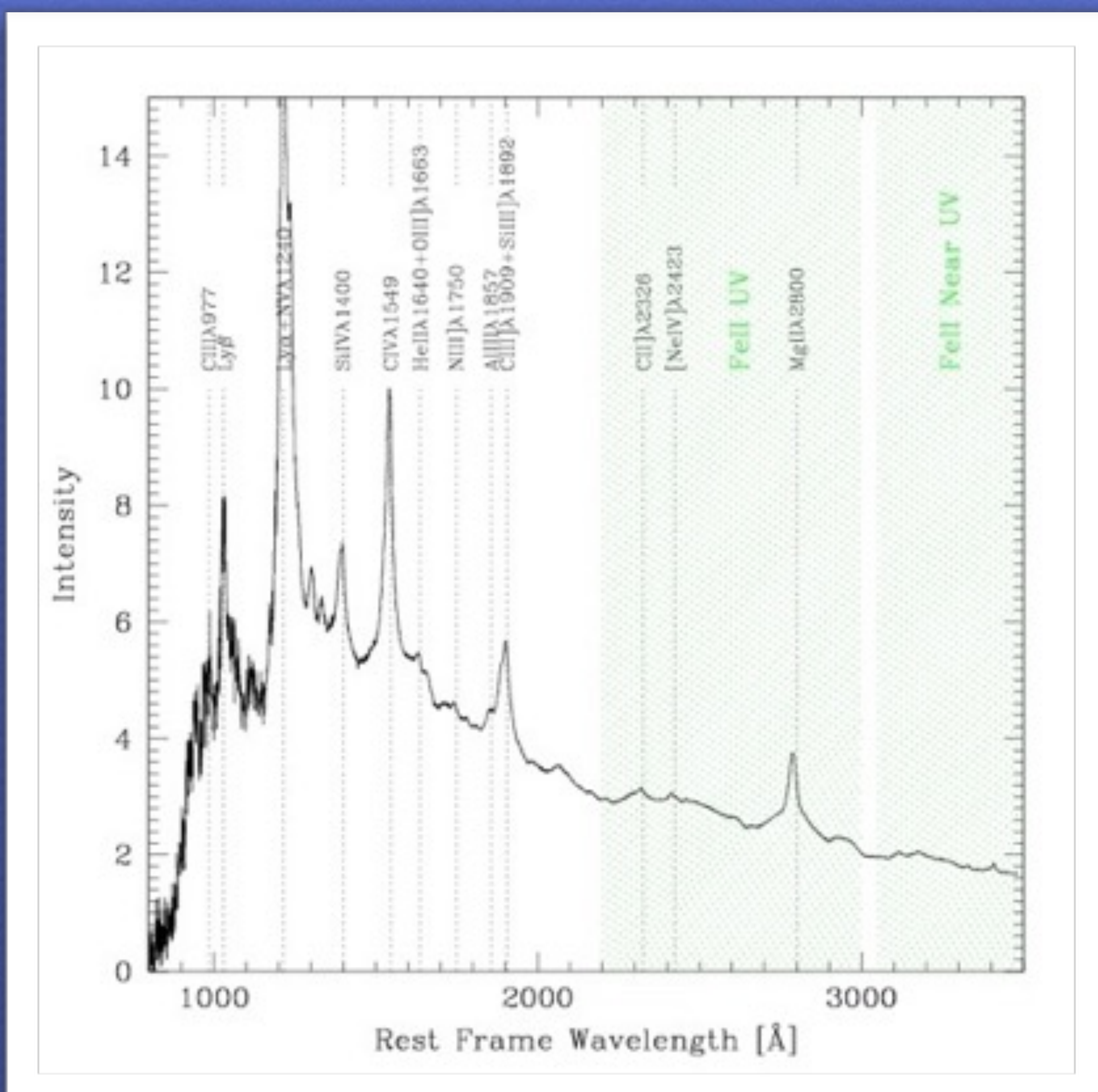

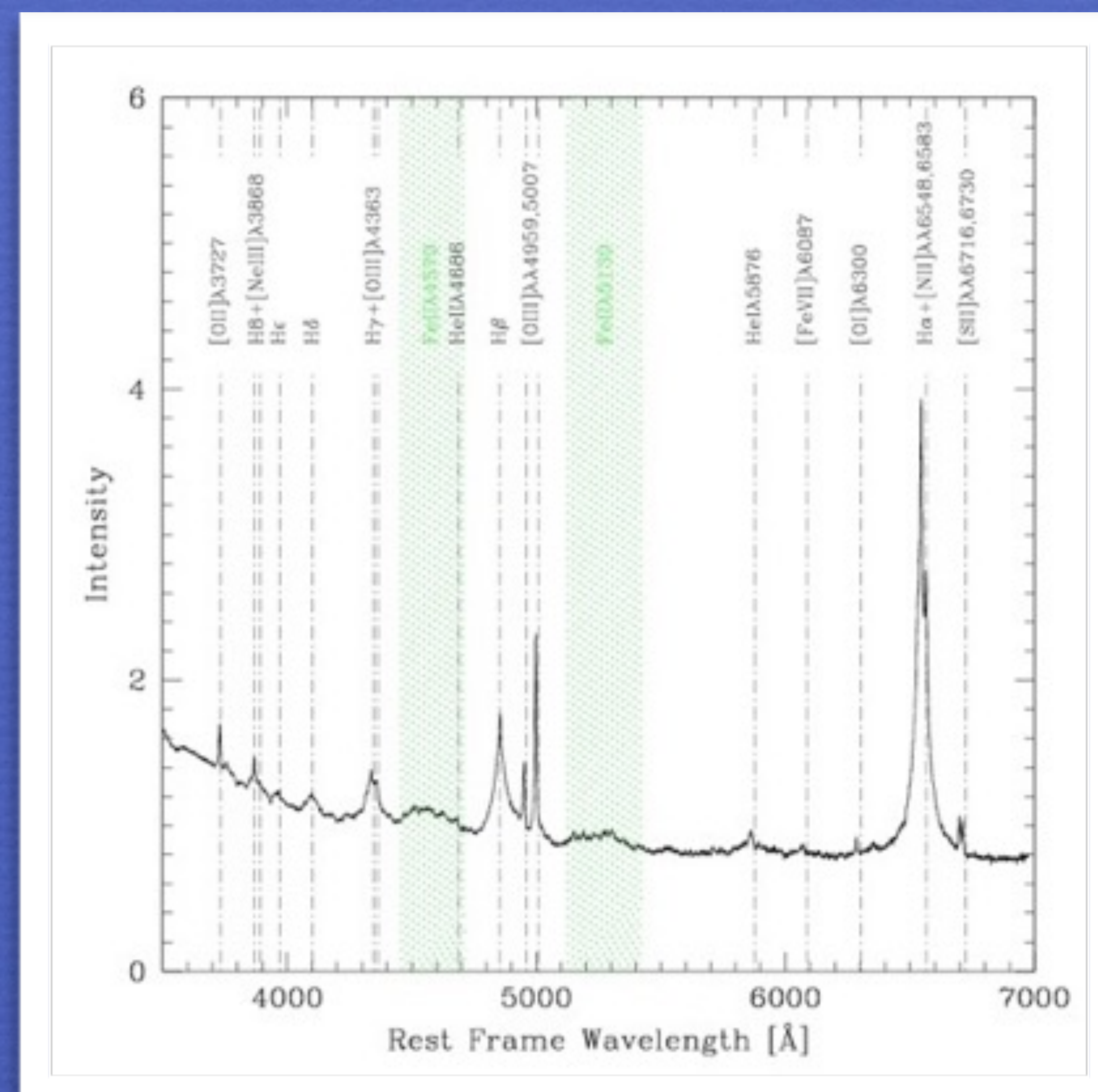

The composite quasar spectrum from the Sloan DSS (Van den Berk et al. 2001; Marziani et al. 2006)

Quasars do not all show the same spectrum!

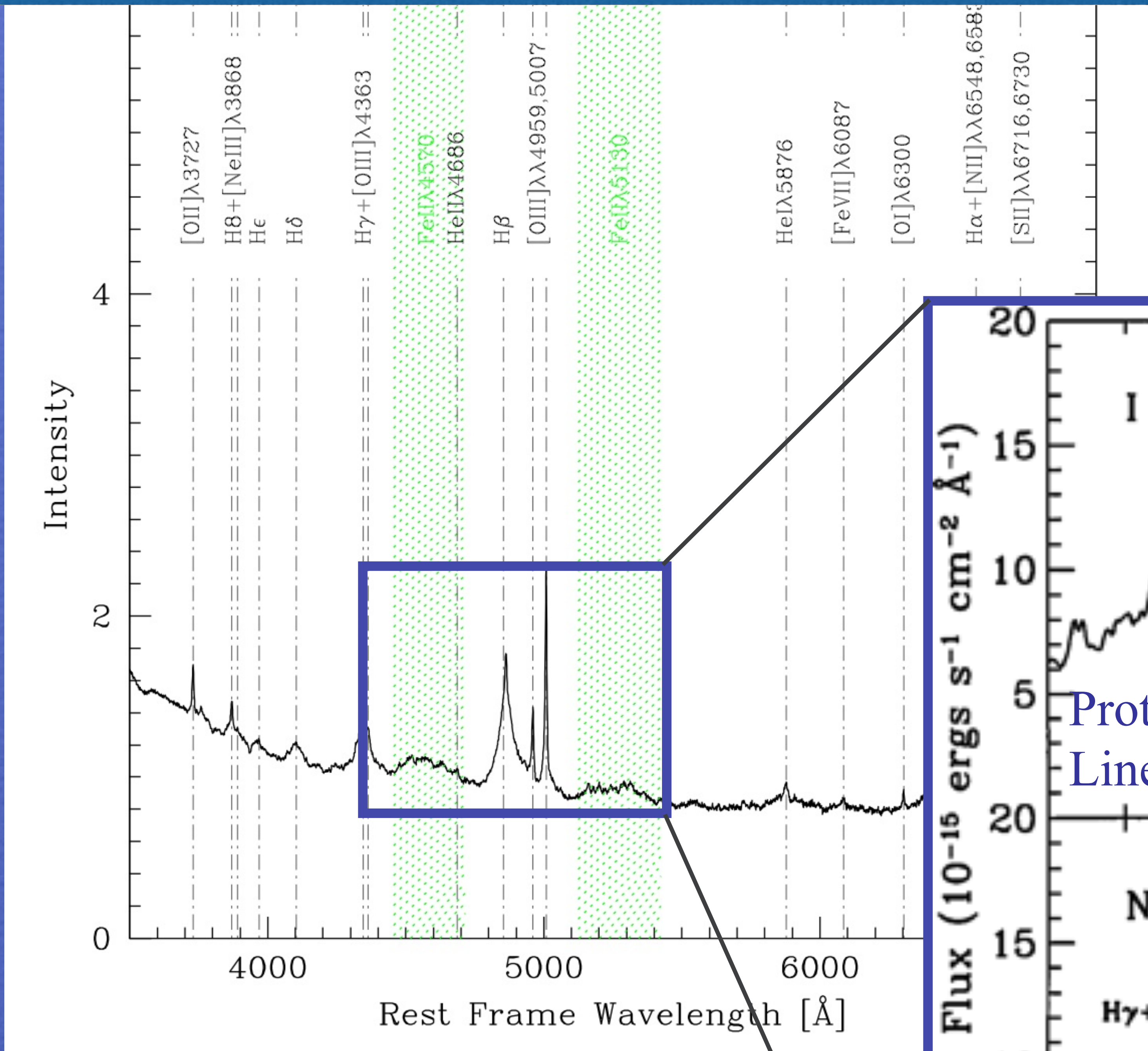

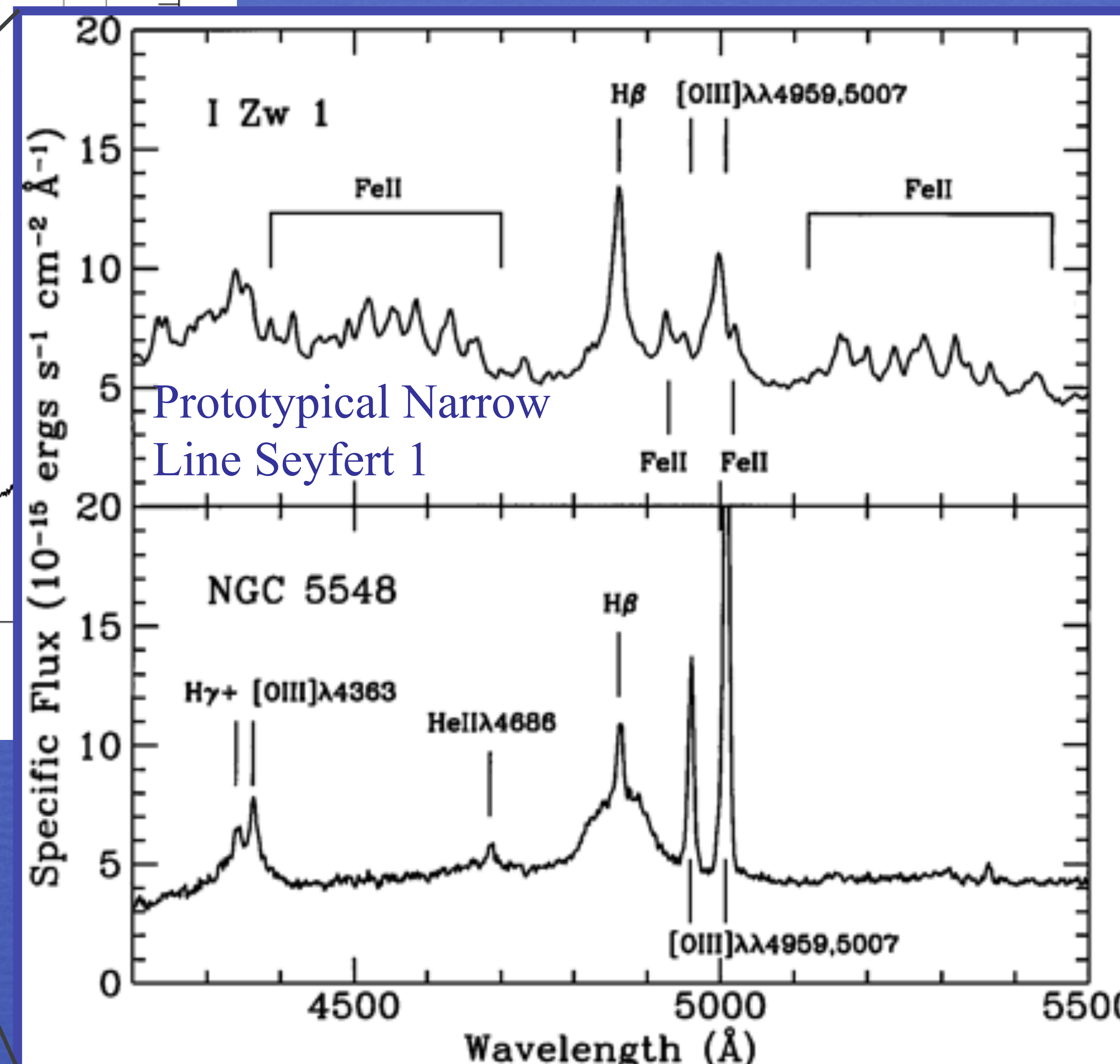

Widely different line profiles, intensity ratios, ionization level

Sulentic et al. 2000

Prediction of unification schemes on spectral properties of luminous Seyfert 1 and quasars (i.e., of type-1 AGN; log L>43):

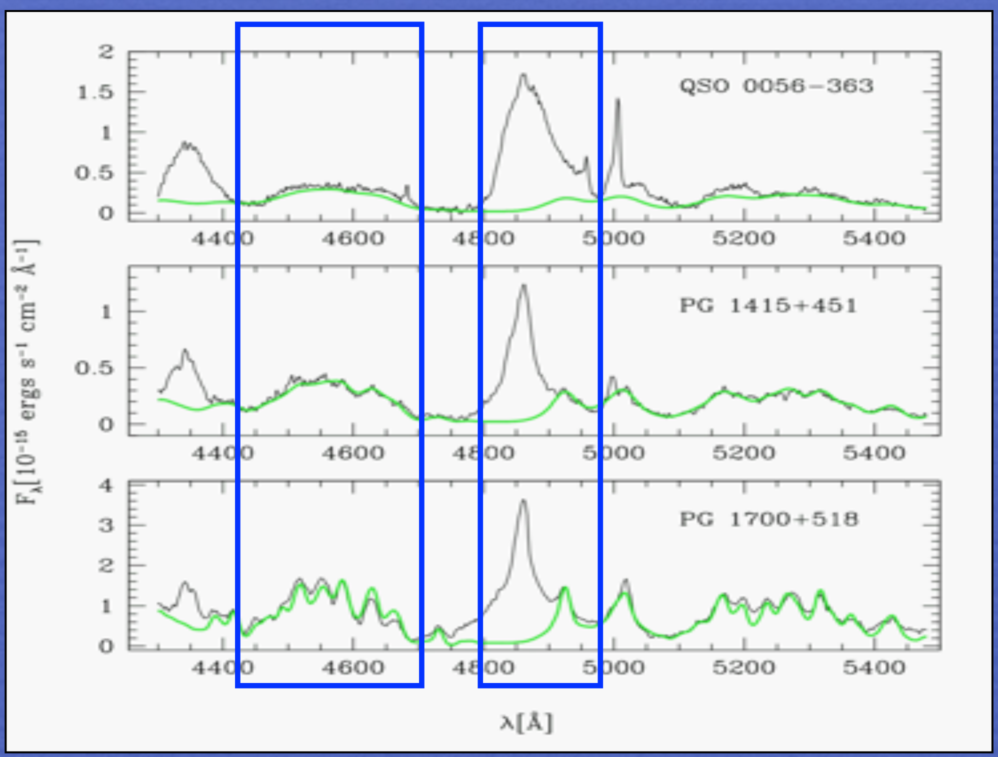

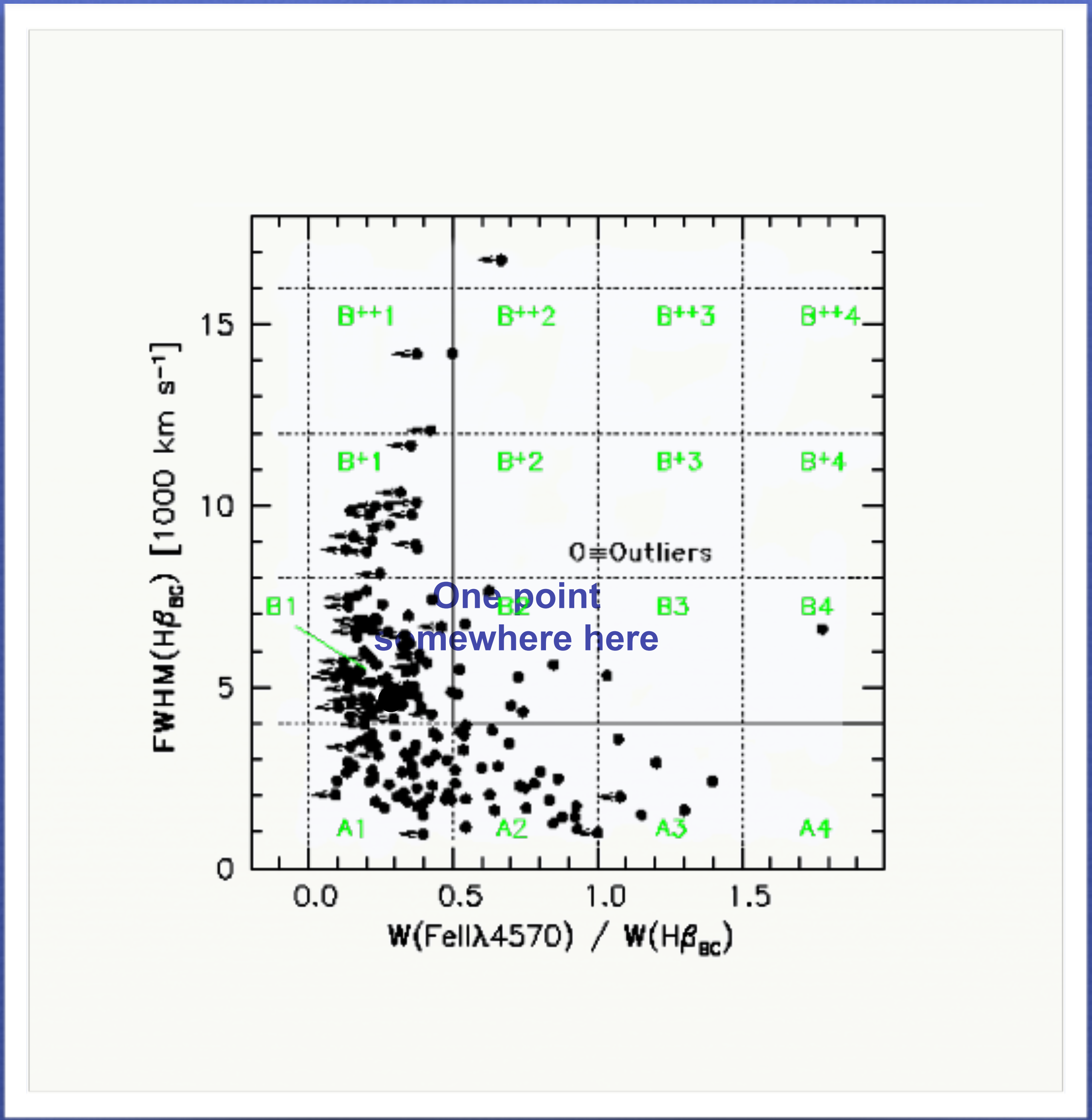

$$R_{\rm FeII} = \frac{I({\rm FeII}\lambda4570)}{I(H\beta)} \approx \frac{W({\rm FeII}\lambda4570)}{W(H\beta)}$$

Lines do not all show the same profiles!

Internal emission line shifts involve both broad and narrow lines.

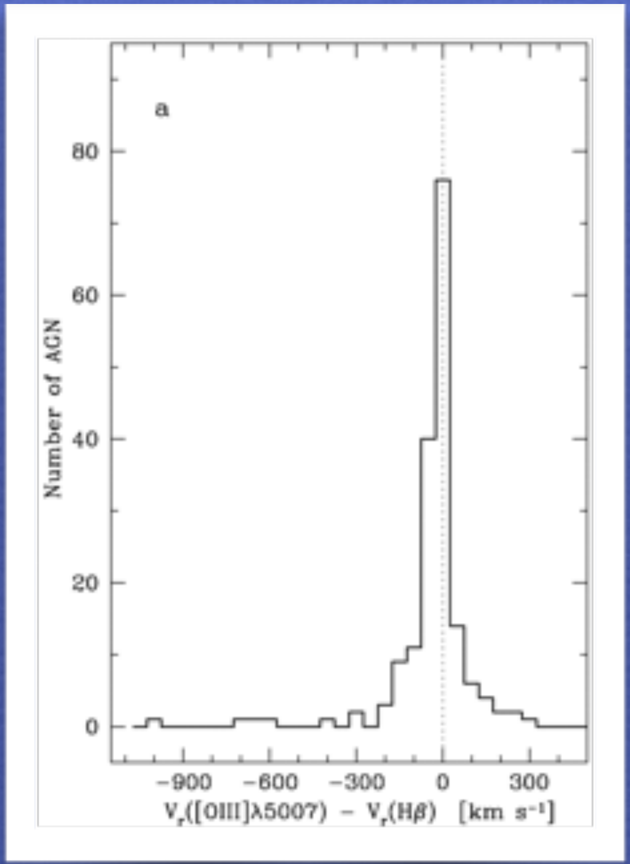

Zamanov et al. 2002

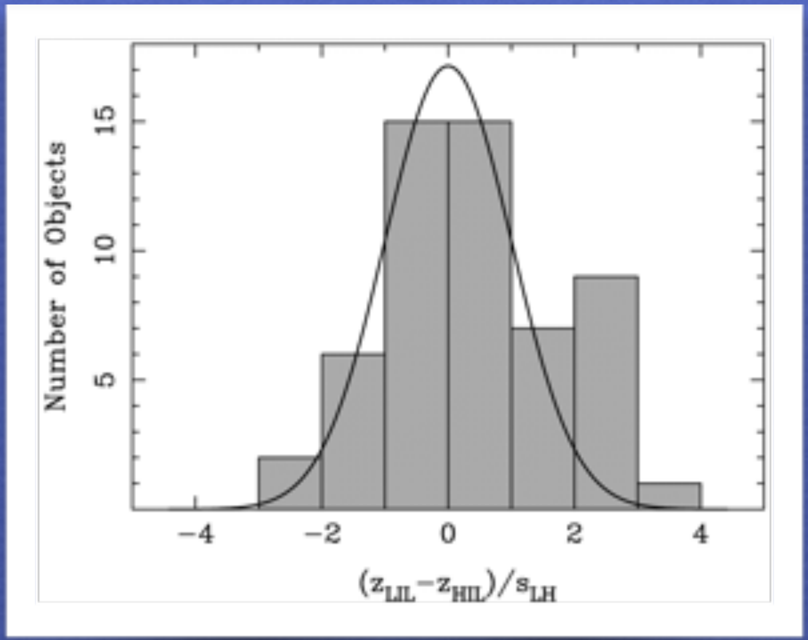

Eracleous & Halpern 2003
c.f. Hu et al. 2008

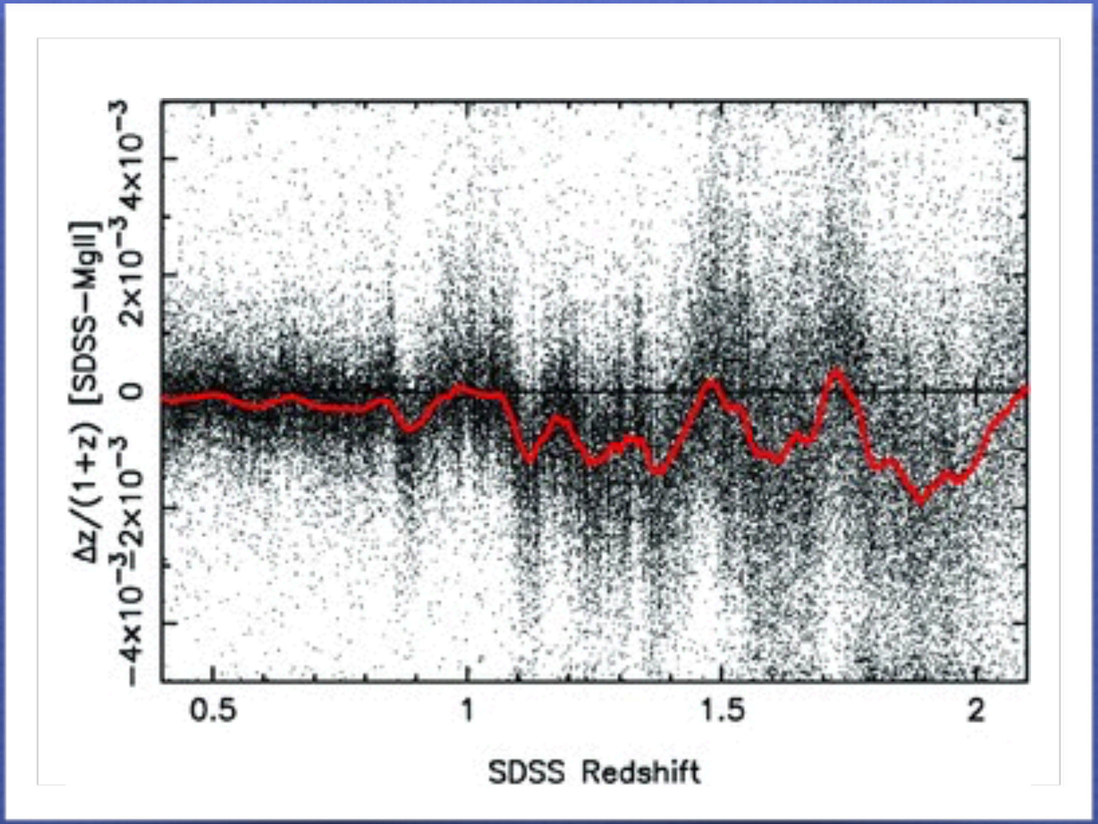

Hewett and Wild 2010

Narrow HILs such as [OIII]λ4959,5007 show blueshift

Narrow LILs such as narrow Hβ and [OII]λ3727
best for systemic redshift

Quasar systemic redshift more uncertain if z>1

Broad HIL blueshifts provide evidence of outflow require rest frame knowledge and proper contextualisation

Symmetric unshifted profiles are ascribed to virialized emitting regions

TABLE 1

PUBLISHED EMISSION-LINE VELOCITY SHIFTS

Line – Reference Line	Velocity[a] (km s^{-1})	N[b]	σ (km s^{-1})	Reference
High Ionization – Low Ionization				
C IV – [O II] λ3727	[illegible]	[illegible]	[illegible]	[illegible]
C IV – Hα	−1140 ± 290	17	1180	2
C IV – O I λ1304	−560 ± 120	23	...	3
C IV – O I λ1304	−1290 ± 180	19	800	4
C IV – C II λ1335	−1320 ± 400	7	1046	4
C IV – Mg II	−565 ± 100	17	...	3
C IV – Mg II	−460 ± 110	15	410	1
C IV – Mg II	[illegible]	[illegible]	[illegible]	[illegible]
C III] – Mg II	−600 ± 90	44	600	4
C III] – Hα	−880 ± 230	16	920	2
Lyα – Hα	−1770 ± 370[d]	11	1230	2
High Ionization – High Ionization				
C IV – C III]	120 ± 150	65	1200	4
C IV – C III]	−530 ± 110	25	570	5
C IV – Lyα	−400 ± 100	55	...	3
C IV – N V	−170 ± 100	26	...	3
Low Ionization – Low Ionization				
Mg II – [O II]	−200 ± 170	22	810	4
Mg II – [O II]	380 ± 80	12	270	1
Mg II – Hα	−140 ± 120	17	510	2
O I – Hα	−390 ± 470	4	930	2
[O III] – Hβ	−220 ± 150	23	730	4
[O II] – [O III]	100 ± 130	6	310	4

[a] Mean velocity of first ion in the reference frame of the z given by second ion, $\pm\sigma/\sqrt{N}$.
[b] Number of QSOs.
[c] Reduces to −780 when two QSOs with −4400 and −2500 are excluded.
[d] Reduces to −1420 when one outlier value of −5200 is excluded.
REFERENCES.—(1) Junkkarinen 1989; (2) Espey et al. 1989; (3) Gaskell 1982; (4) Wilkes 1986; (5) Corbin 1990—excluding BAL QSOs.

Tytler & Fan 1992; Gaskell 1982

A first contextualisation (radio quiet vs. radio loud) showed remarkable differences

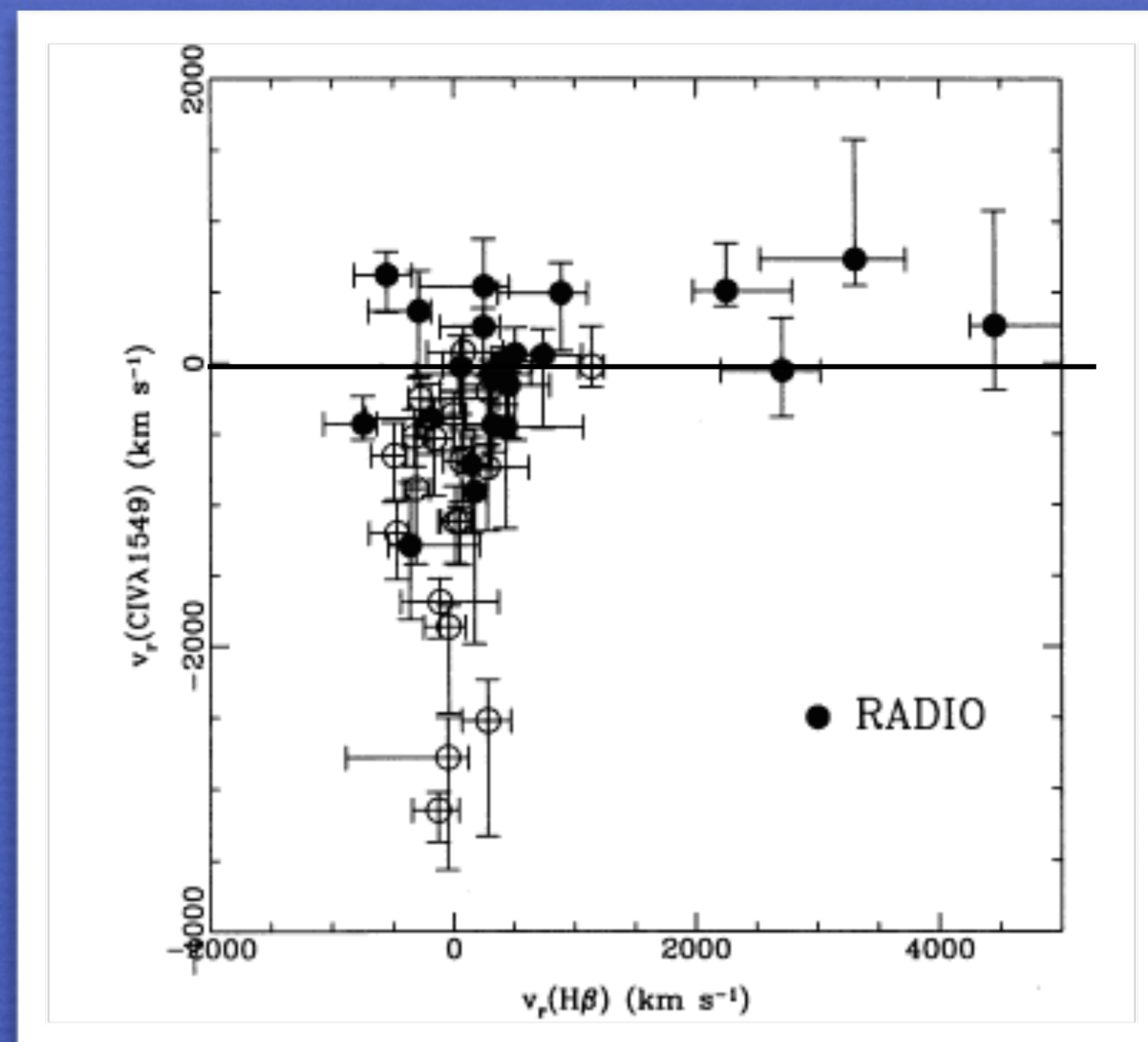

Sulentic et al. 1995

Unification schemes do not provide any clue for type-1 sources.

Huge quasar samples (~10^5 sources) are now available from major surveys completed and in progress (LBQS, SDSS, 2dF, BOSS).

Internal line shifts, profiles of spectral lines, as well as multifrequency spectrophotometric measures need proper contextualization.

Several present-day analyses are still affected by separation in classes that somewhat arbitrary (i.e., Narrow Line Seyfert 1 vs. broader type-1 quasars; radio loud / radio quiet), and by the assumption that type-1 quasar spectra are almost undistinguishable.

The 4DE1 approach

The 4DE1 approach Dedicated observations

HST (archive)

FOS

R = λ/δλ~1000

1000-3400

UV

CIV 1549

low *z*

ESO VLT

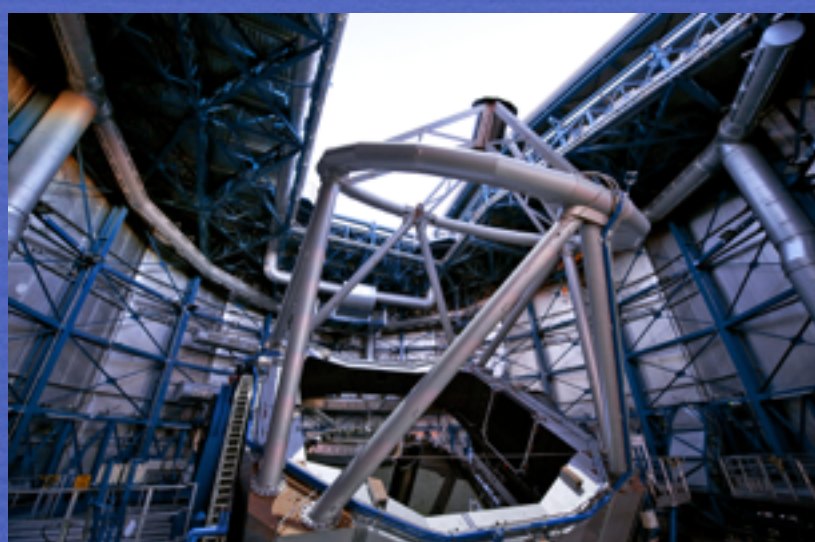

ISAAC

R = λ/

δλ~1000

sZ,J,H,K

Hβ high *z*(>1)

FORS

R = λ/δλ~

1000 - 1500

optical

UV high

z(>1.4)

SPM (OAN) Galileo TNG

Dolores, B&C

R = λ/

δλ~500-1000

optical

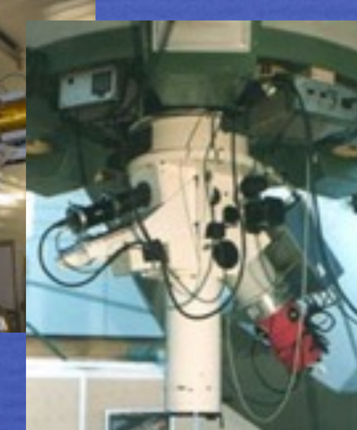

UV high

z(>1.4)

Hβ low *z*

Data samples: defined by limits in multiplexing

- ~ 300 mainly low-z (<1) quasars observed at San Pedro Martir, ESO, KPNO, Asiago, Calar Alto, in the last 20 years: flux limited at $m_B = 16.5$; (Hβ). Dedicated observations of ~100 fainter sources from GranTeCan, ESO/VLT, Galileo TNG Marziani et al. 2003a,b; Sulentic et al. 2004

- ~50 ESO-Hamburg quasars with VLT/ISAAC spectra with $0.9 < z < 3$ (Hβ), most with matching VLT/FORS optical data (CIV and UV lines) Sulentic et al. 2004, 2006; Marziani et al. 2009

- SDSS sample of 450 sources of r<17.5 and z< 0.7 (Hβ); SDSS sample with r<18.5 and z< 0.7 (Hβ and MgII λ2800; 680 quasars) Zamfir et al. 2008, 2010; Marziani et al. 2013

- ~700 HST archived FOS/STIS spectra of 140 low-z AGNs (CIVλ1549 + UV em. Lines), most with matching Hβ coverage Bachev et al. 2004, Sulentic et al. 2007

Data with spectral resolution $R = \lambda/\delta\lambda \sim 1000$ and S/N>20

The 4DE1 approach The limits of single epoch spectroscopy

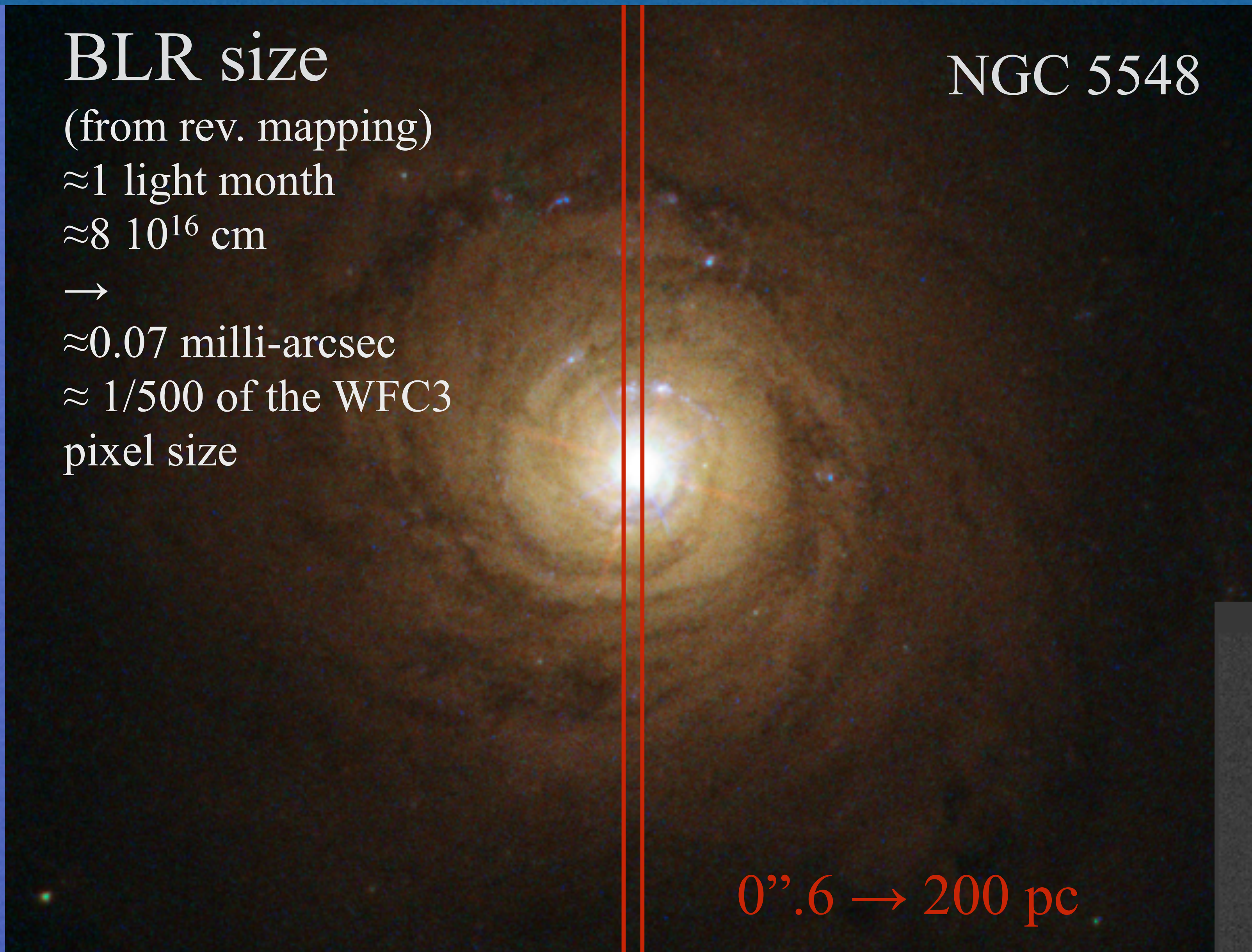

Single epoch, long-slit spectroscopy

Until recently, limited spectral coverage, lack of synoptical view

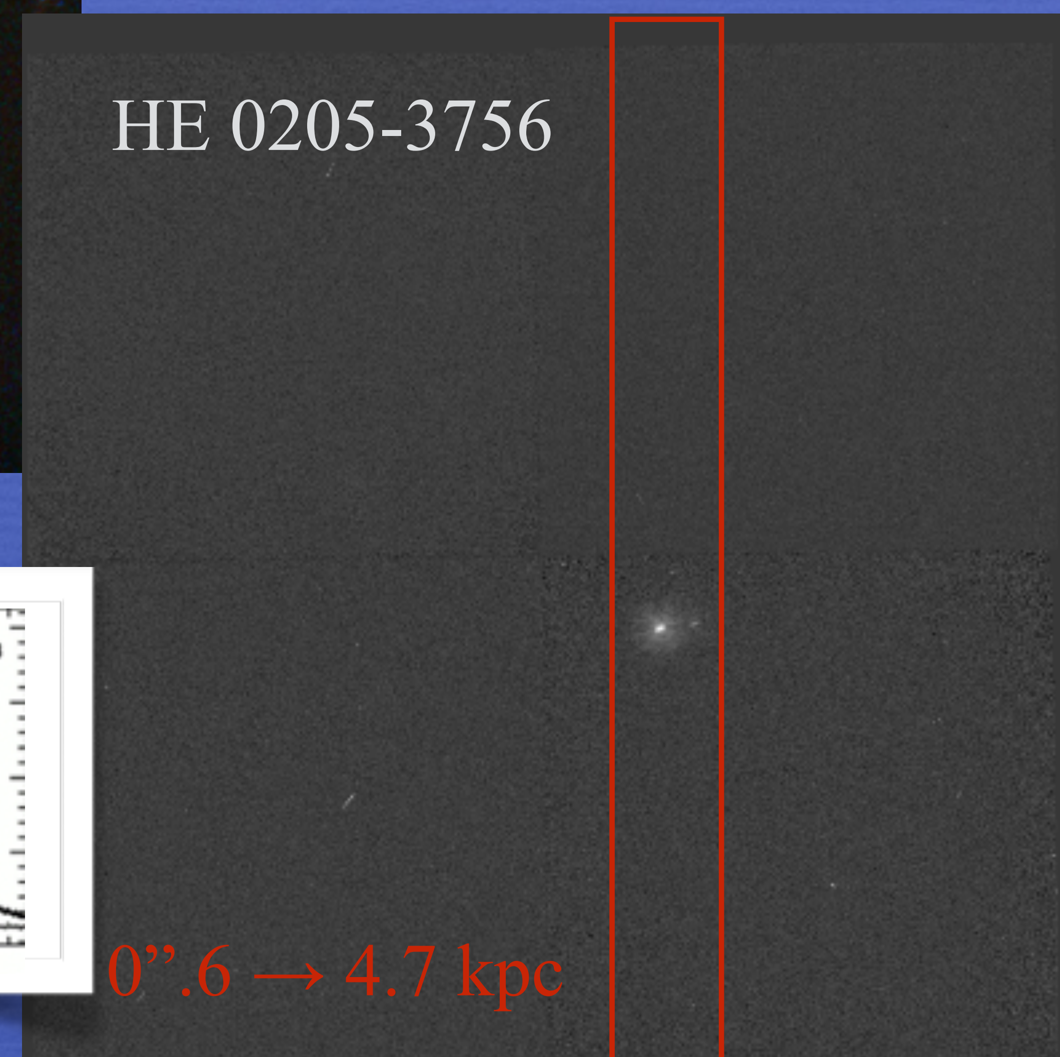

Composite emission line profile resulting from the unresolved, integrated contribution of emission over a wide range of spatial scales

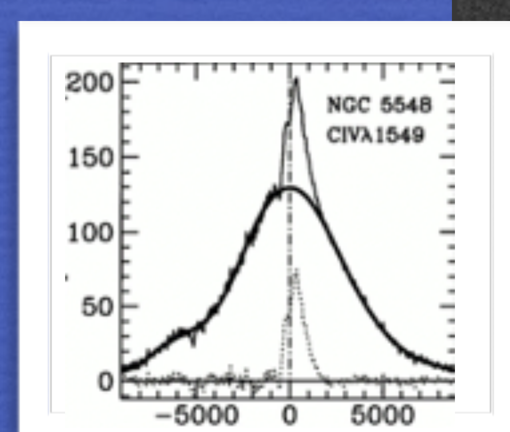

Uniform reduction and analysis applied to composite and individual spectra alike

1) Quasar rest frame determination

2) Host galaxy subtraction (if needed)

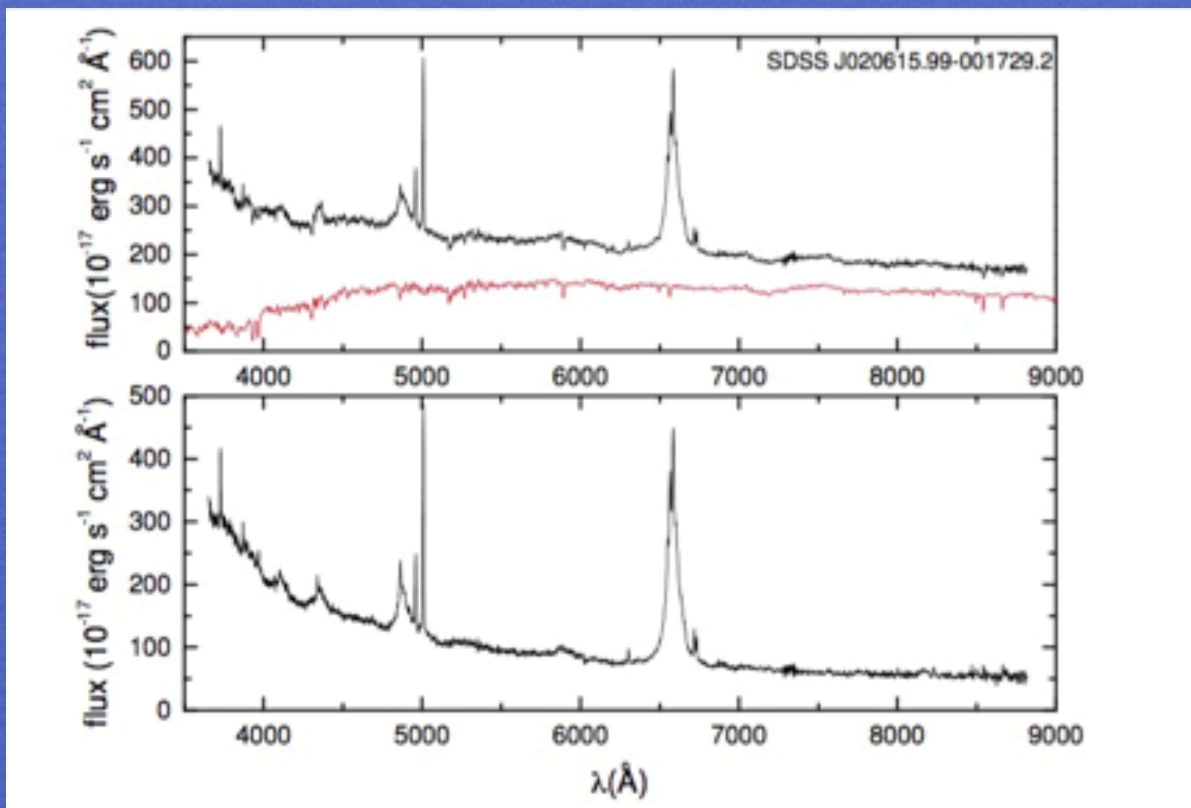

3) Quasar continuum subtraction

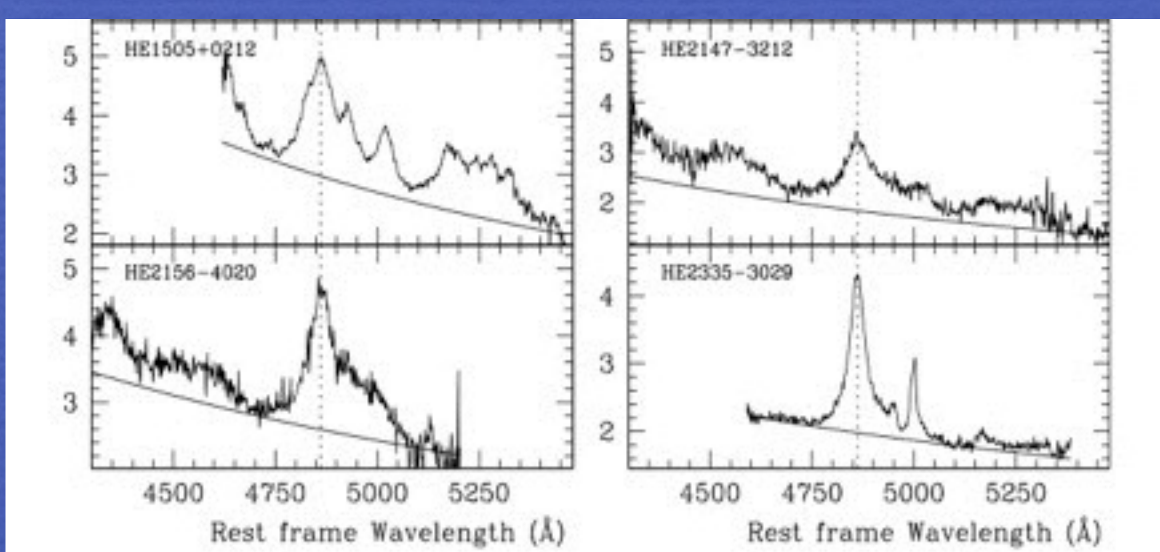

4) Analysis of emission lines + FeII blends

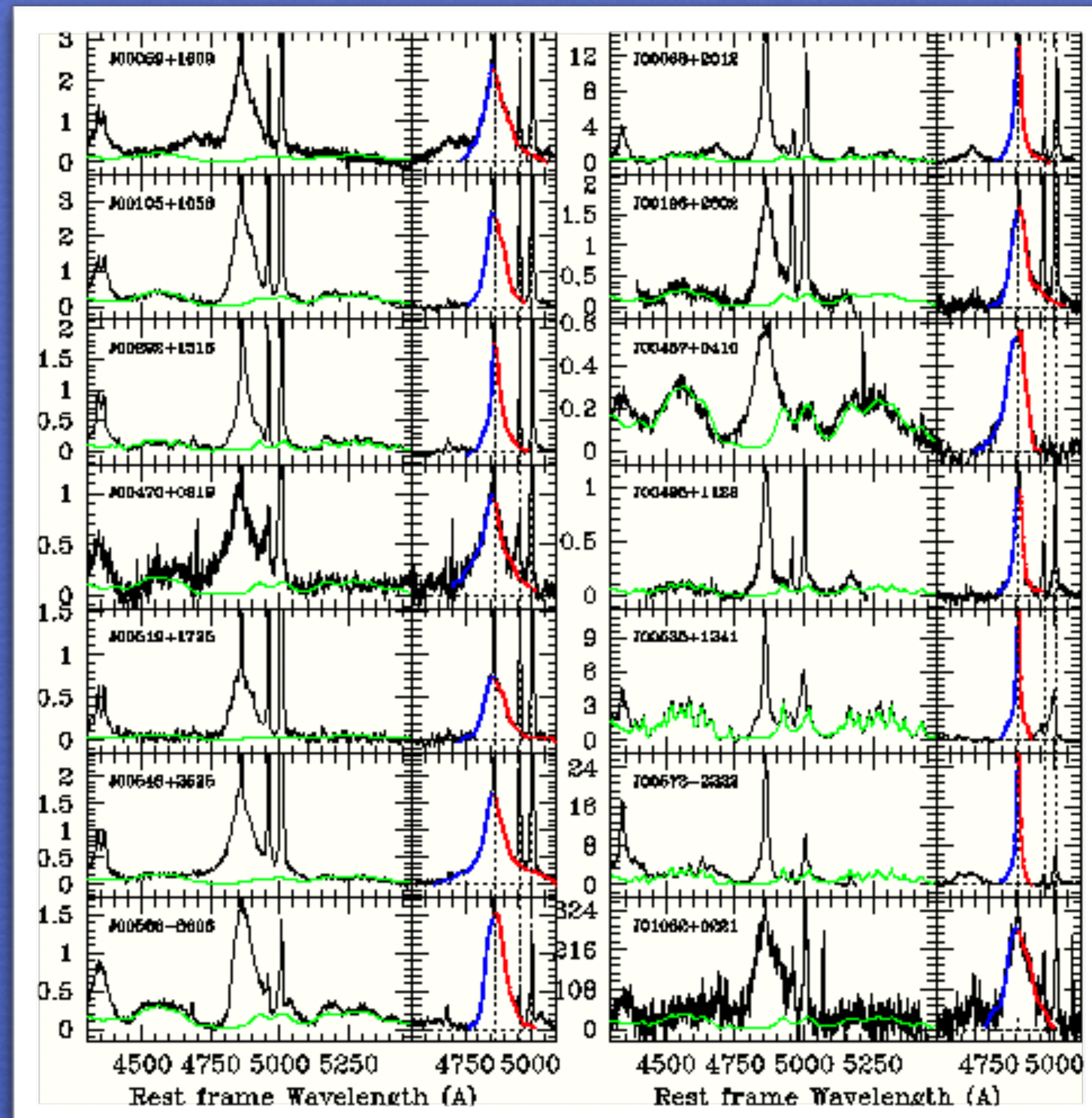

Continuum-subtracted spectra in the Hβ range
from Marziani et al. 2003a, A Spectral atlas of 215 low-z AGNs

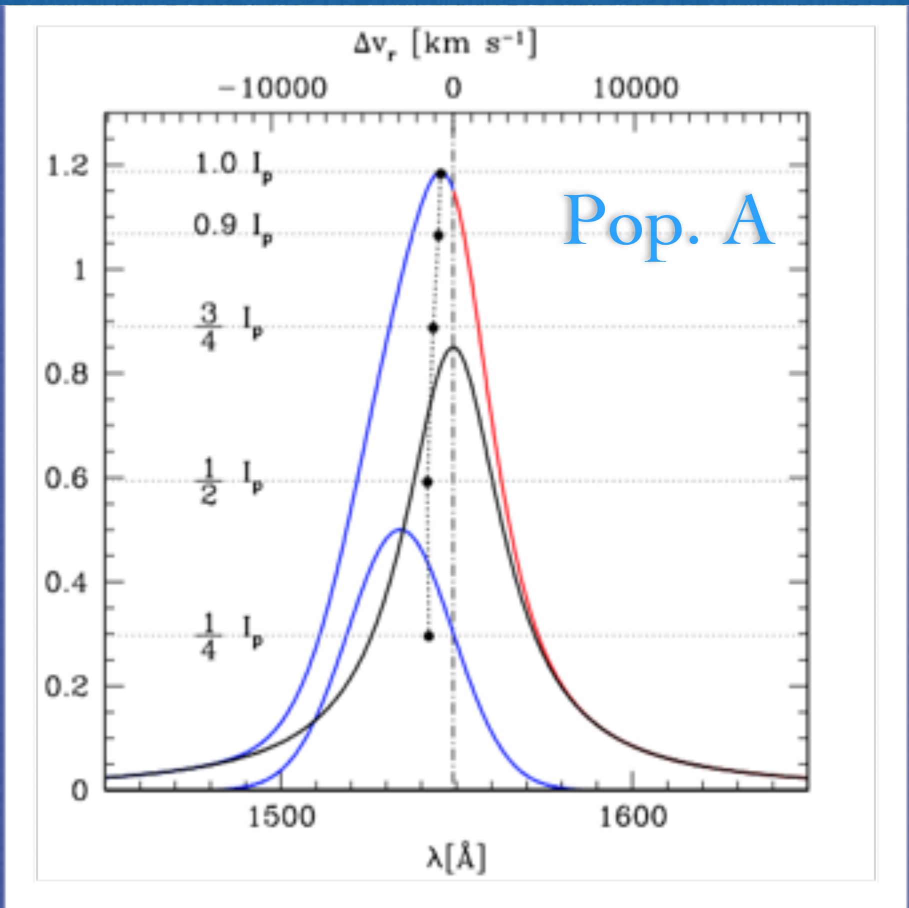

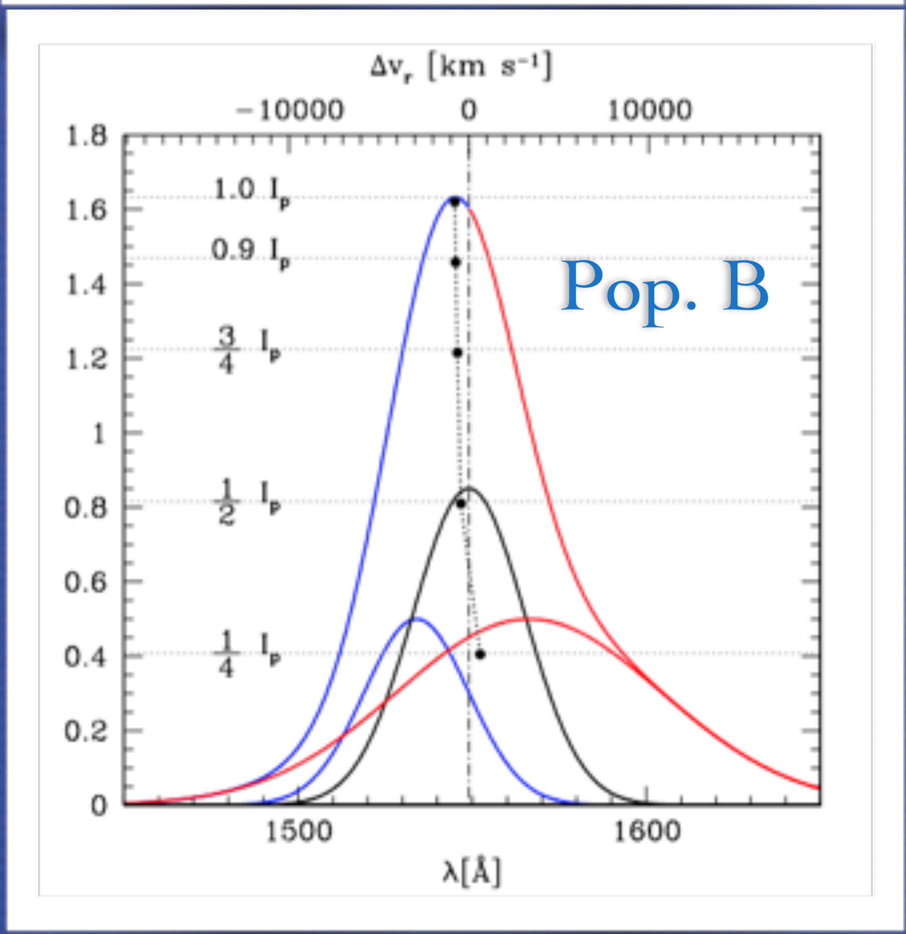

Broad emission line profile parameterization

Referred to line peak λ_P

$$c\left(\frac{i}{4}\right) = \frac{\lambda_B(i/4) + \lambda_R(i/4)}{2} - \lambda_0 \; \forall i = 0, \ldots 4$$

$$AI\left(\frac{i}{4}\right) = \frac{\lambda_B(i/4) + \lambda_R(i/4) - 2 \cdot \lambda_P}{\lambda_R(i/4) - \lambda_B(i/4)} \; \forall i = 0, \ldots 4$$

Referred to rest frame

line centroids at fractional intensity independent from(any) multi-component decomposition

S/N> 20 and resolution $\lambda/\delta\lambda$ ~ 1000 enough to:

measure profile parameters and fluxes of relevant lines (e.g., HβBC, LIL, & CIVλ1549BC, HIL);

Deconvolve broad and narrow components of blended linesusing minimum χ2 techniques.

Quasars' Eigenvector 1

Boroson & Green 1992; see also Gaskell et al. 1999

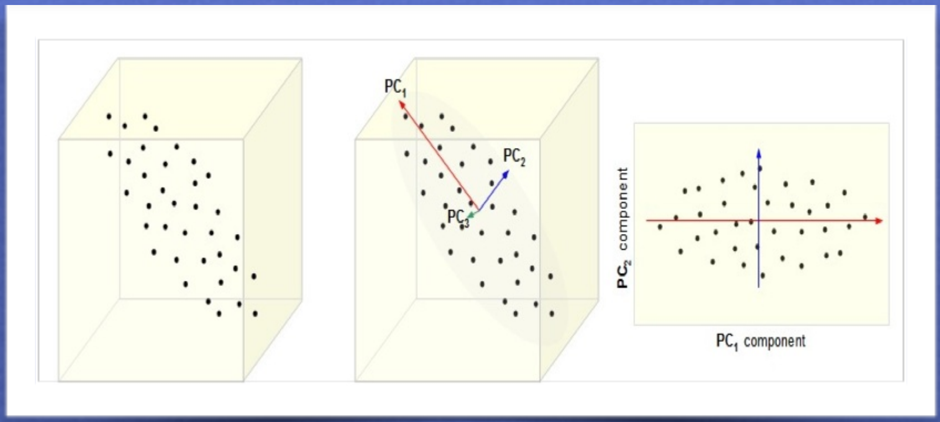

Principal Component Analysis (PCA): n×m matrix with m parameters for n objects find axes in m-dimensional space that maximize projection onto versors.

Eigenvector 1: Originally defined by a PCA of 82 PG quasars, and associated with an anticorrelation between strength of FeIIλ4570 (or [OIII] 5007 peak intensity) and width of Hβ.

Since 1992, has been found in several independent and increasingly large samples.

(Dultzin-Hacyan et al. 1997; Shang et al. 2003, Yip et al.2004, Sulentic et al. 2000, 2007; Kruzcek et al 2011; Tang et al. 2012; Kuraszkiewicz et al. 2008; Mao et al. 2009; Grupe 2004, Wang et al. 2006; Bachev et al. 2004; SDSS data : Shen & Ho 2014, Sun & Ho 2015.

The 4DE1 space of Sulentic et al.

width of Hβ

strength of FeIIλ4570
emitting gas

$$R_{\mathrm{FeII}} = \frac{I(\mathrm{FeII}\lambda4570)}{I(H\beta)} \approx \frac{W(\mathrm{FeII}\lambda4570)}{W(H\beta)}$$

CIVλ1549 line shift
emitting region

soft-X ray photon index

Separation of Population A (FWHM Hβ<4000 km/s) and Population B(roader) sources.

The 4DE1 approach: Defining the main sequence

Optical plane of 4DEigenvector 1: Spectral types in bins to account for quasars' diverse properties

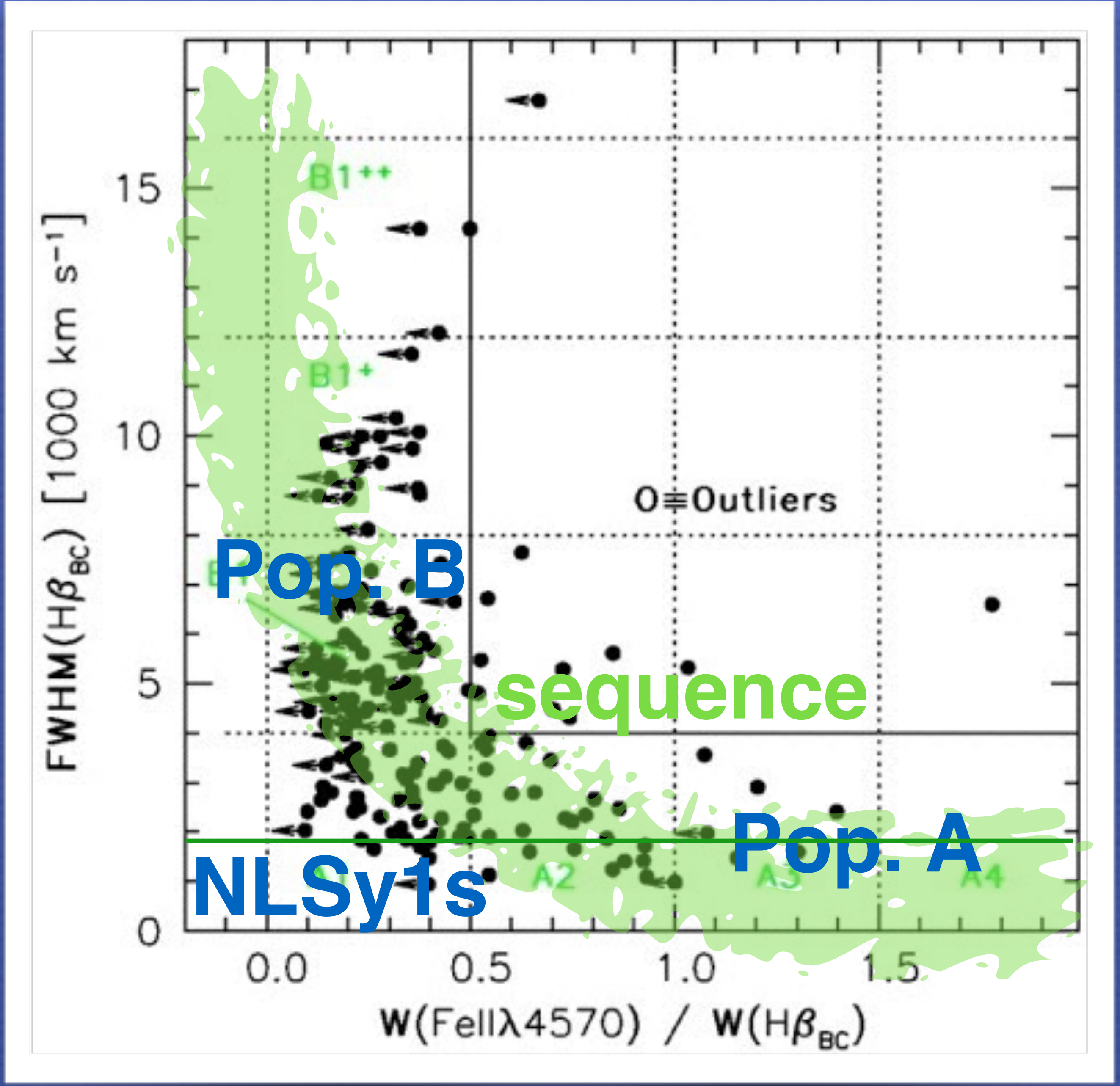

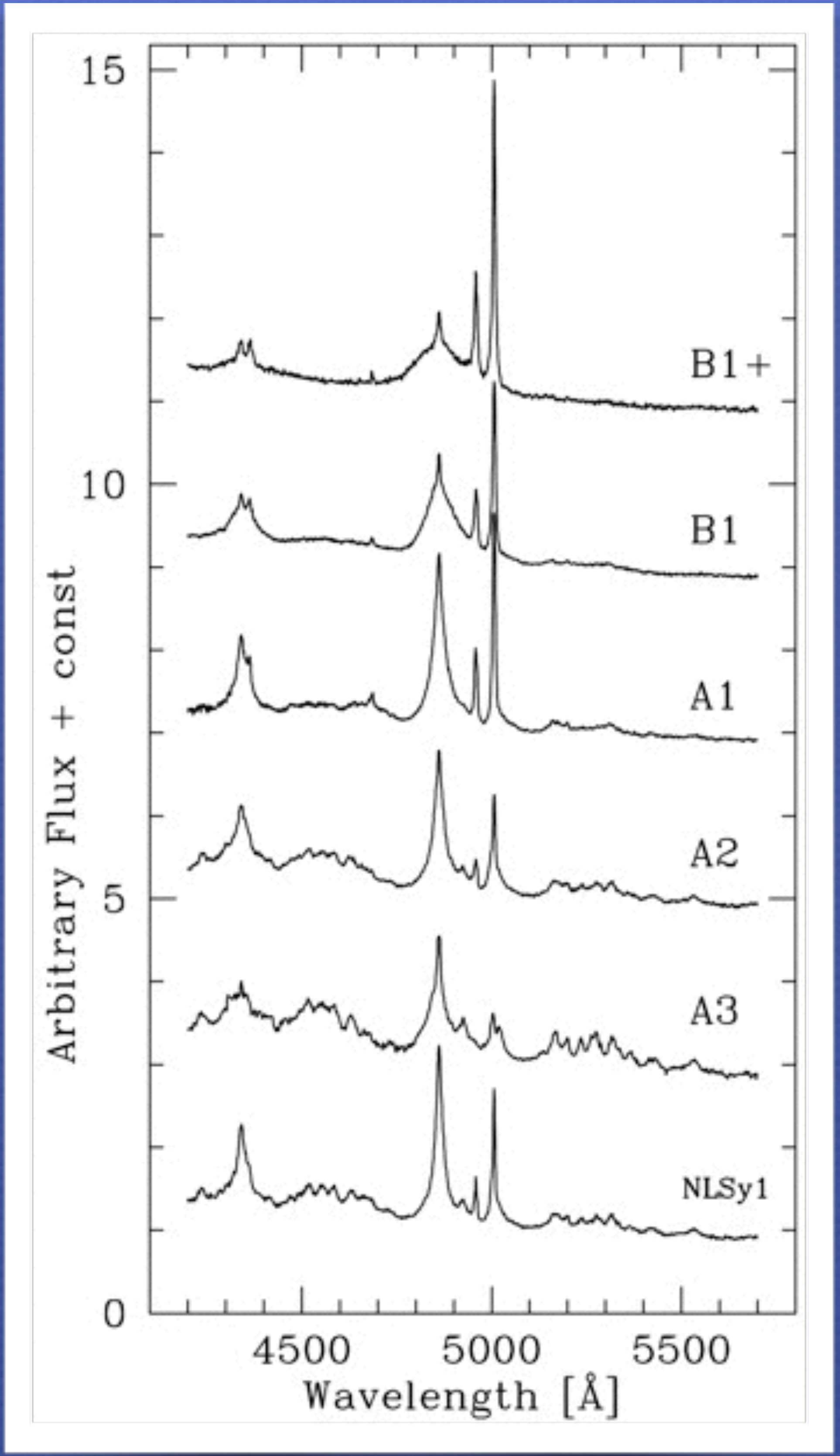

The Hβ profile

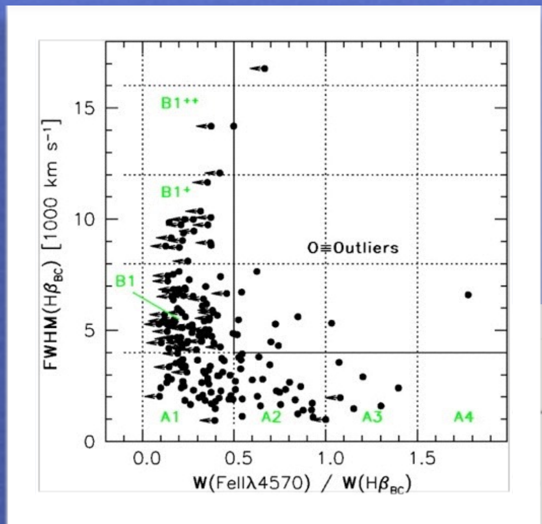

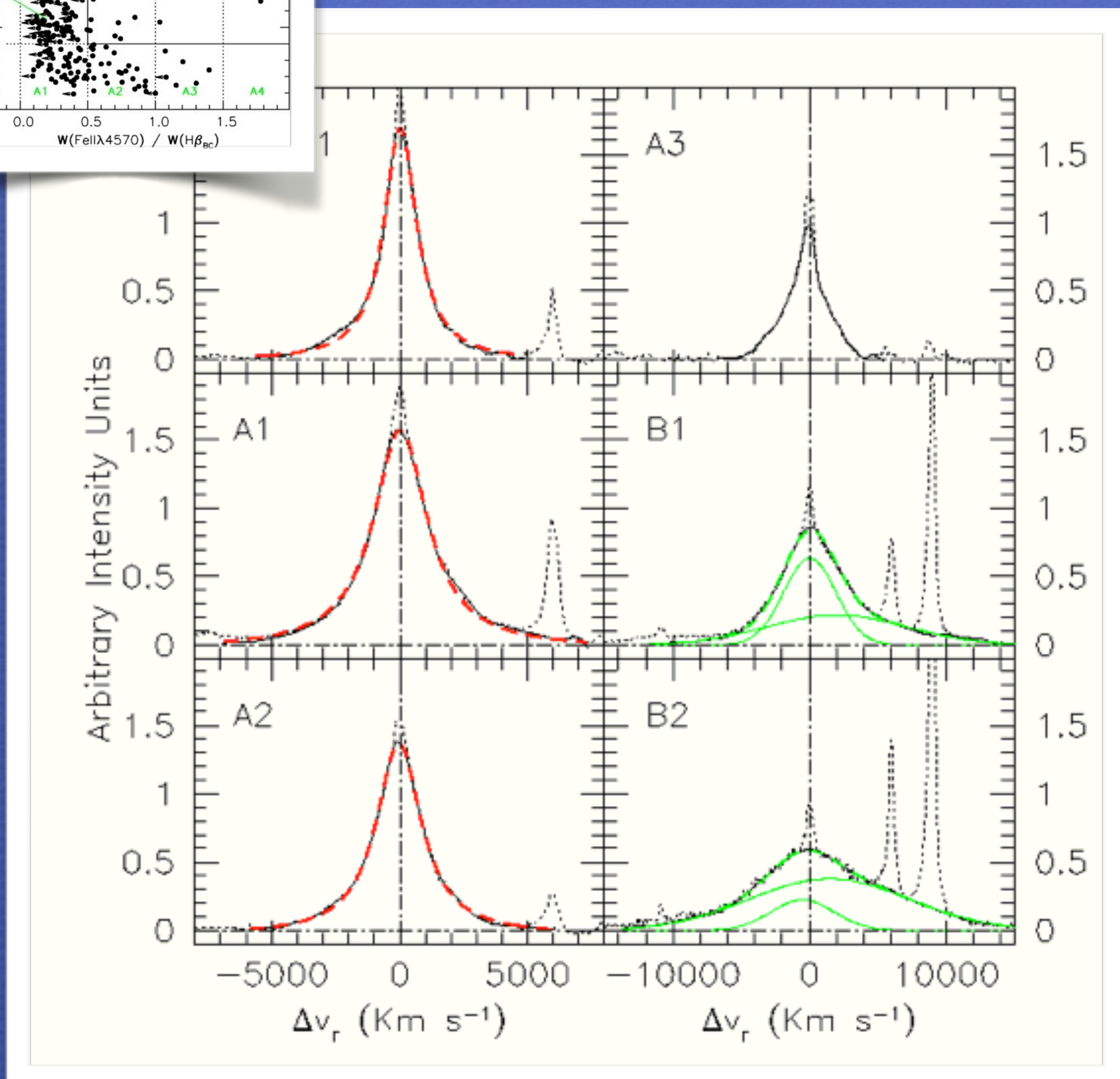

Pop. A.: Lorentzian $H\beta_{BC}$, symmetric unshifted (most often),

Pop. B.: Double Gaussian, most often redward asymmetric

A very broad component

$H\beta_{BC}$+$H\beta_{VBC}$

Sulentic et al. 2002 (z < 1, log L < 47 [erg/s]

Hβ profiles at one extreme of the sequence

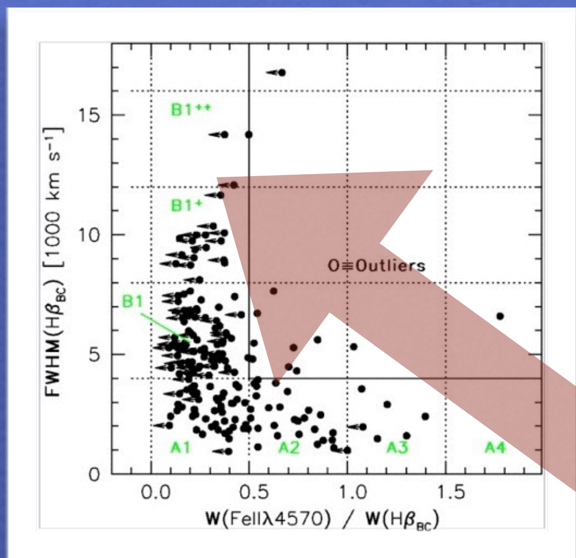

Accretion disk line emission:
likely in some of the broadest objects
but difficult to assess in general
lowest $L_{\mathrm{bol}}/L_{\mathrm{Edd}}$

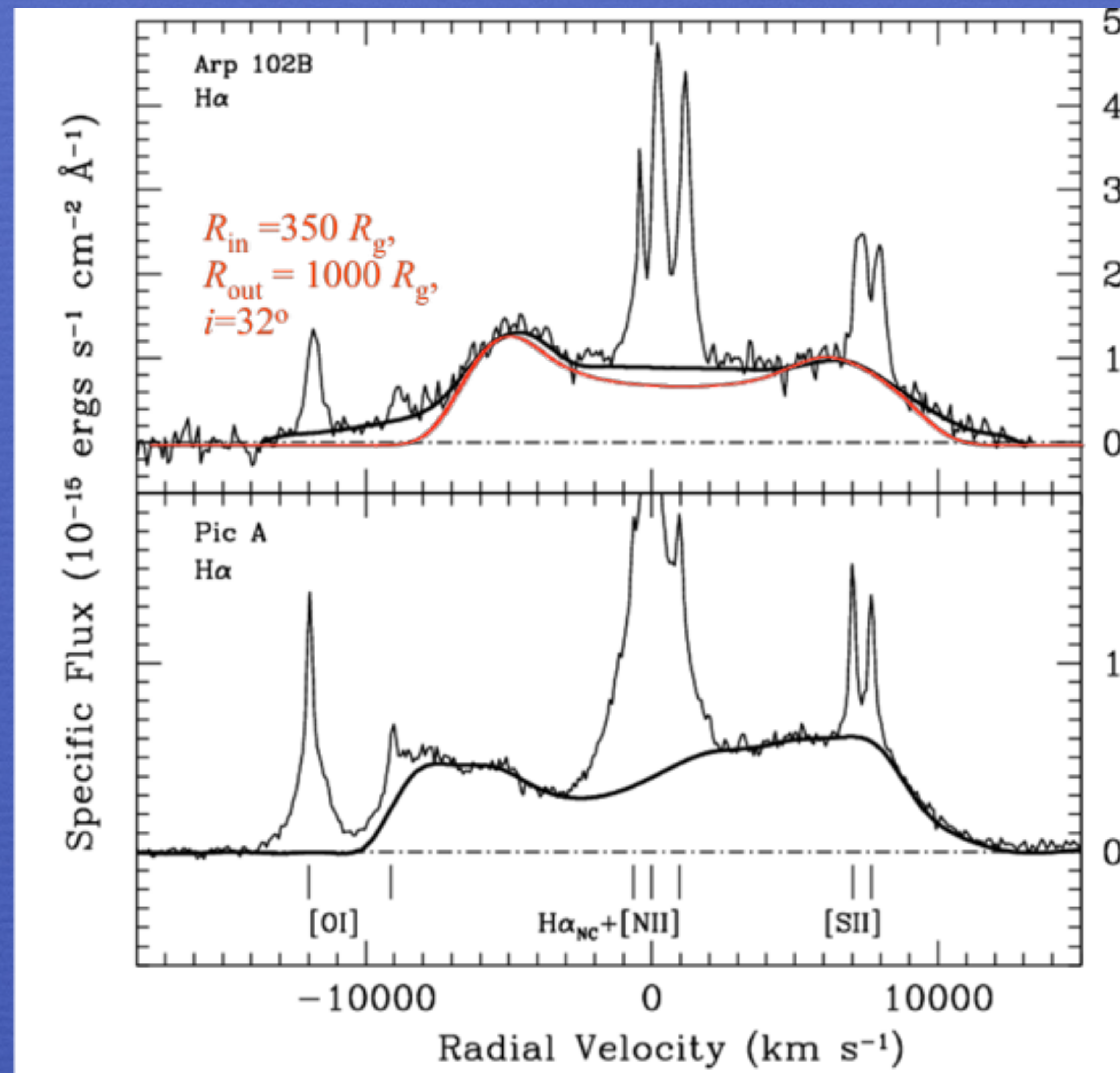

Chen & Halpern 1989;
Popovič et al. 2004; Bon et al. 2009;
Strateva et al. 2003, 2007

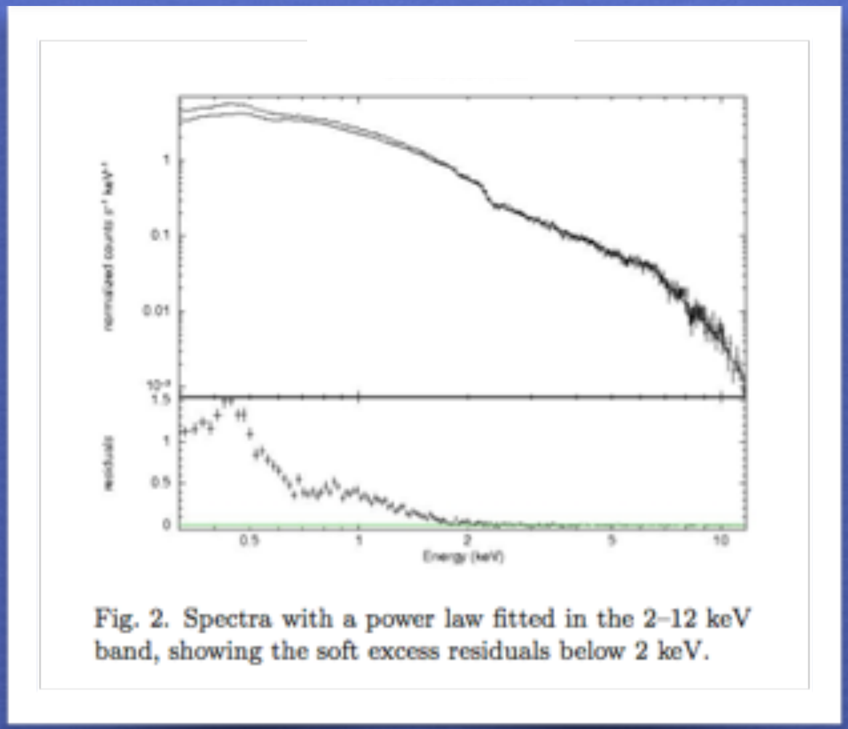

Γ_{soft} : measure of the soft-X excess (0.2 - 2 KeV)

$\Gamma_{soft} > 2$ mainly for FWHM(Hβ) < 4000 km/s (Pop.A)

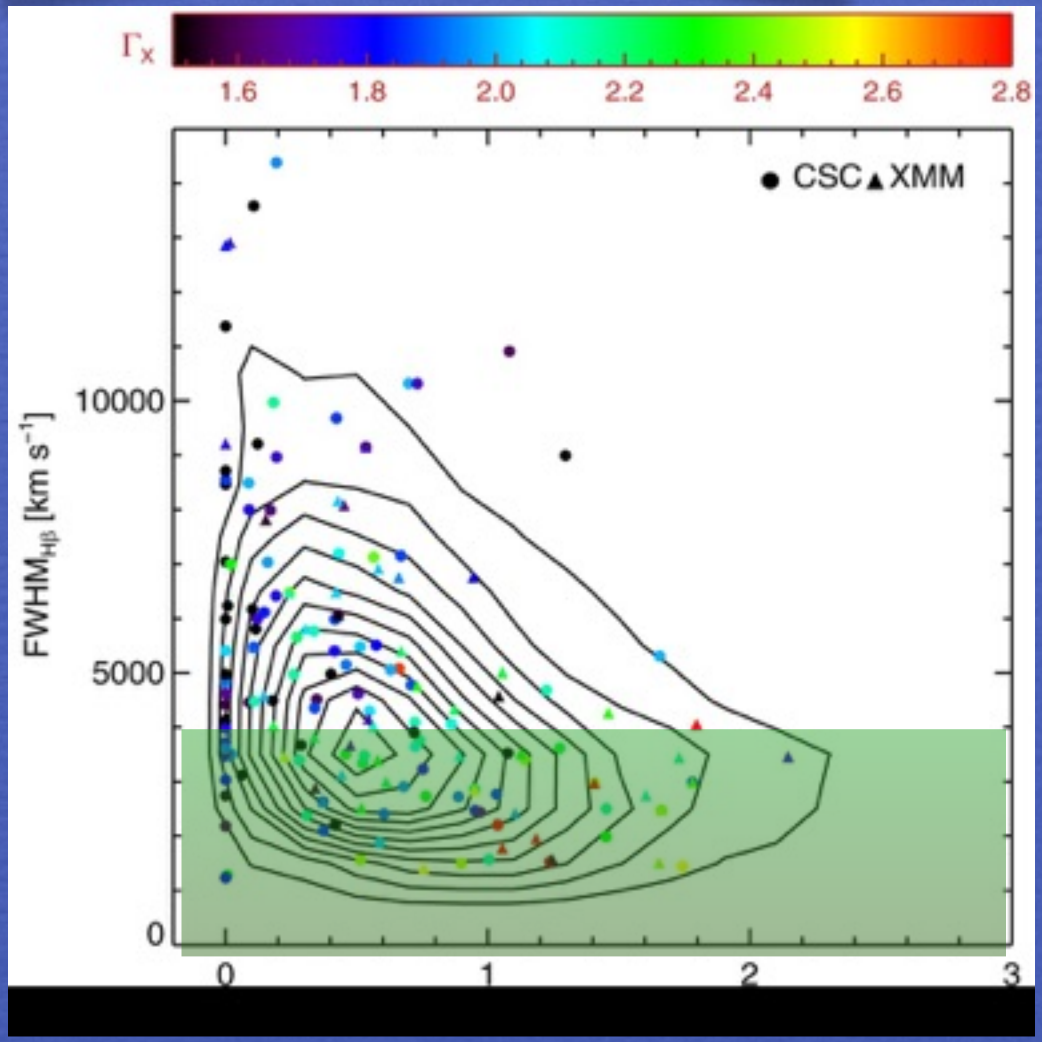

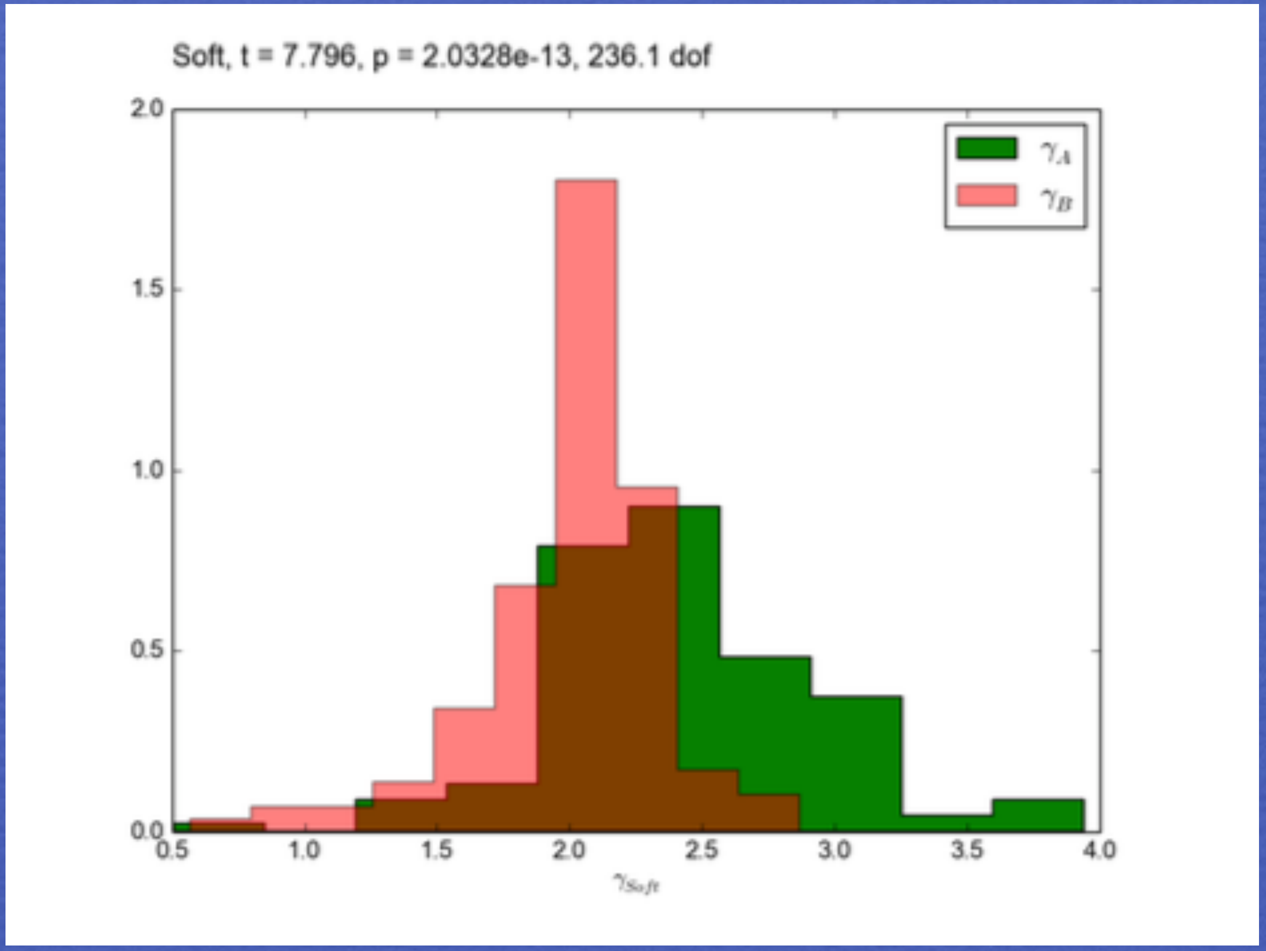

Shen & Ho 2014: Bensch et al. 2015

Correlations between 4DE1 parameters FWHM(Hβ), $R_{\rm FeII}$=F(FeIIλ4570)/F(Hβ), $\Gamma_{\rm soft}$ and CIV shift

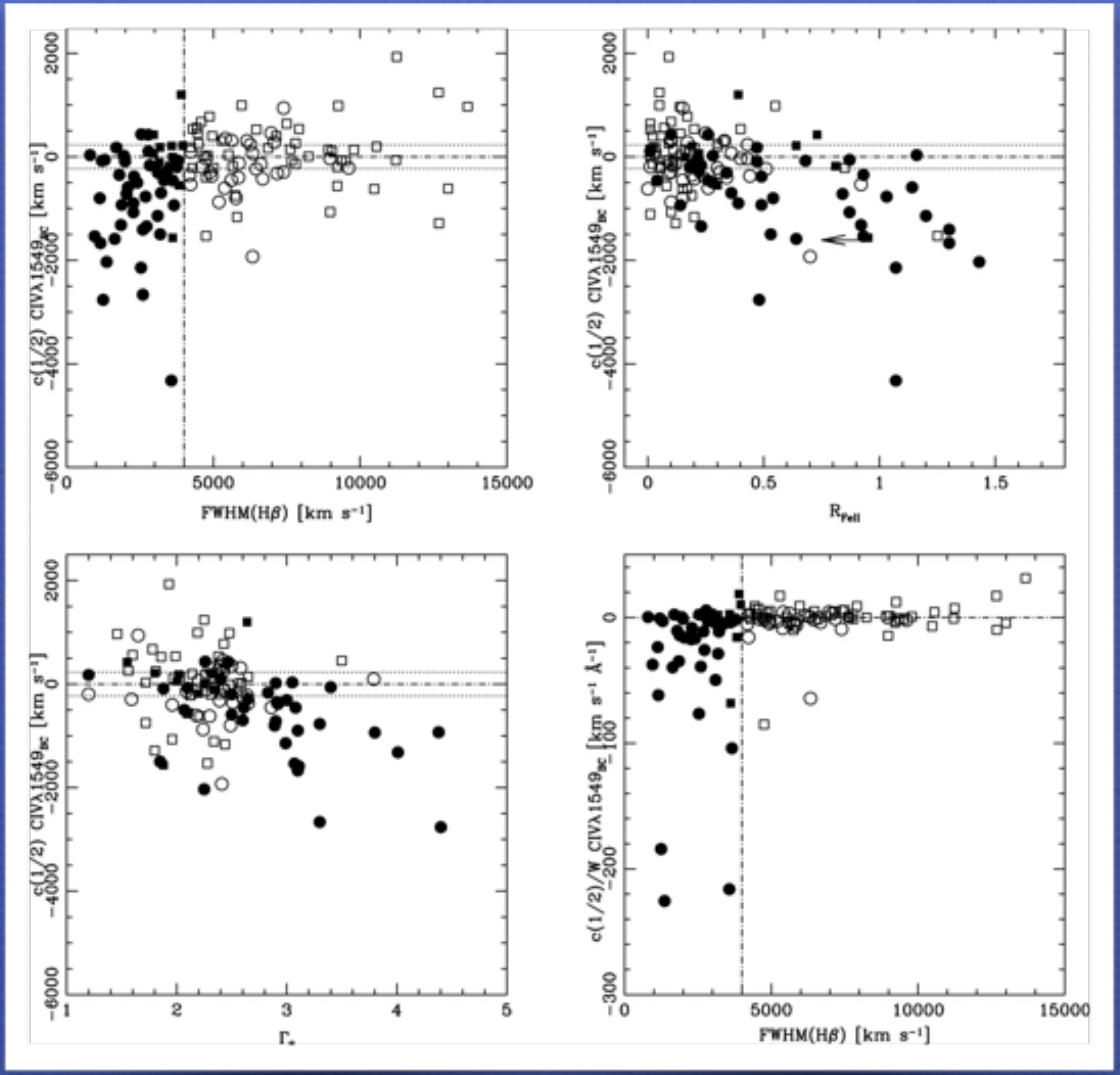

Filled: Pop. A
Open: Pop. B
Circles: RQ
Squares: RL

Sulentic et al. 2007

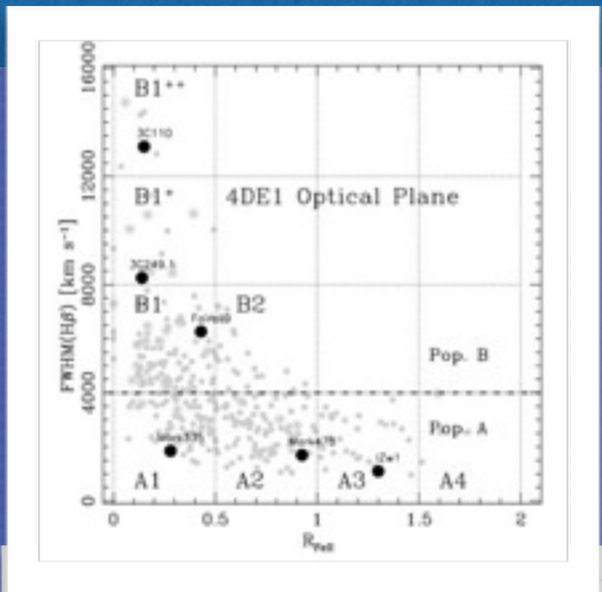

The CIVλ1549 line profile
scaled Hβ + blueshifted emission

Leighly 2000, Bachev et al. 2004, Marziani et al. 2010

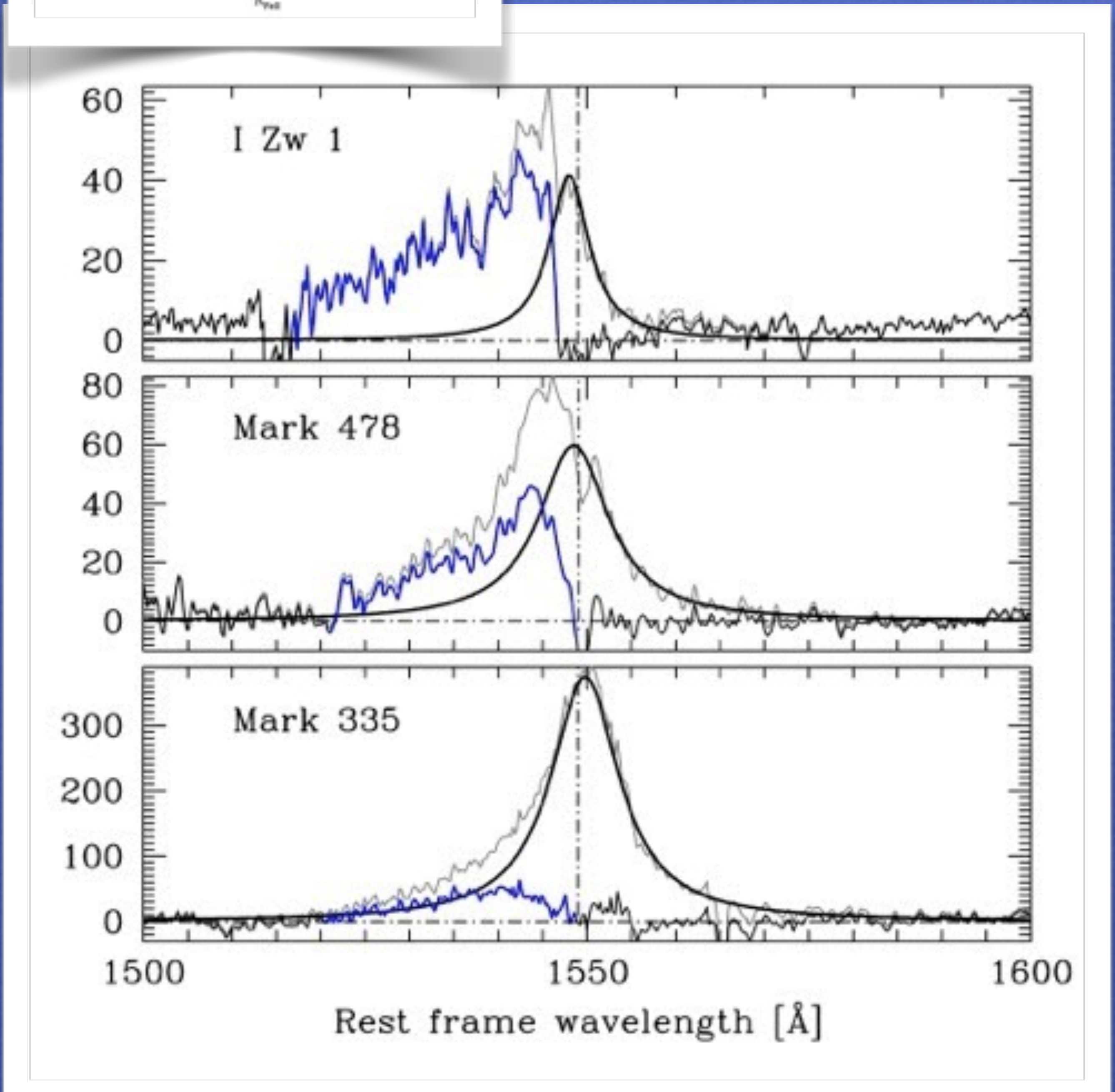

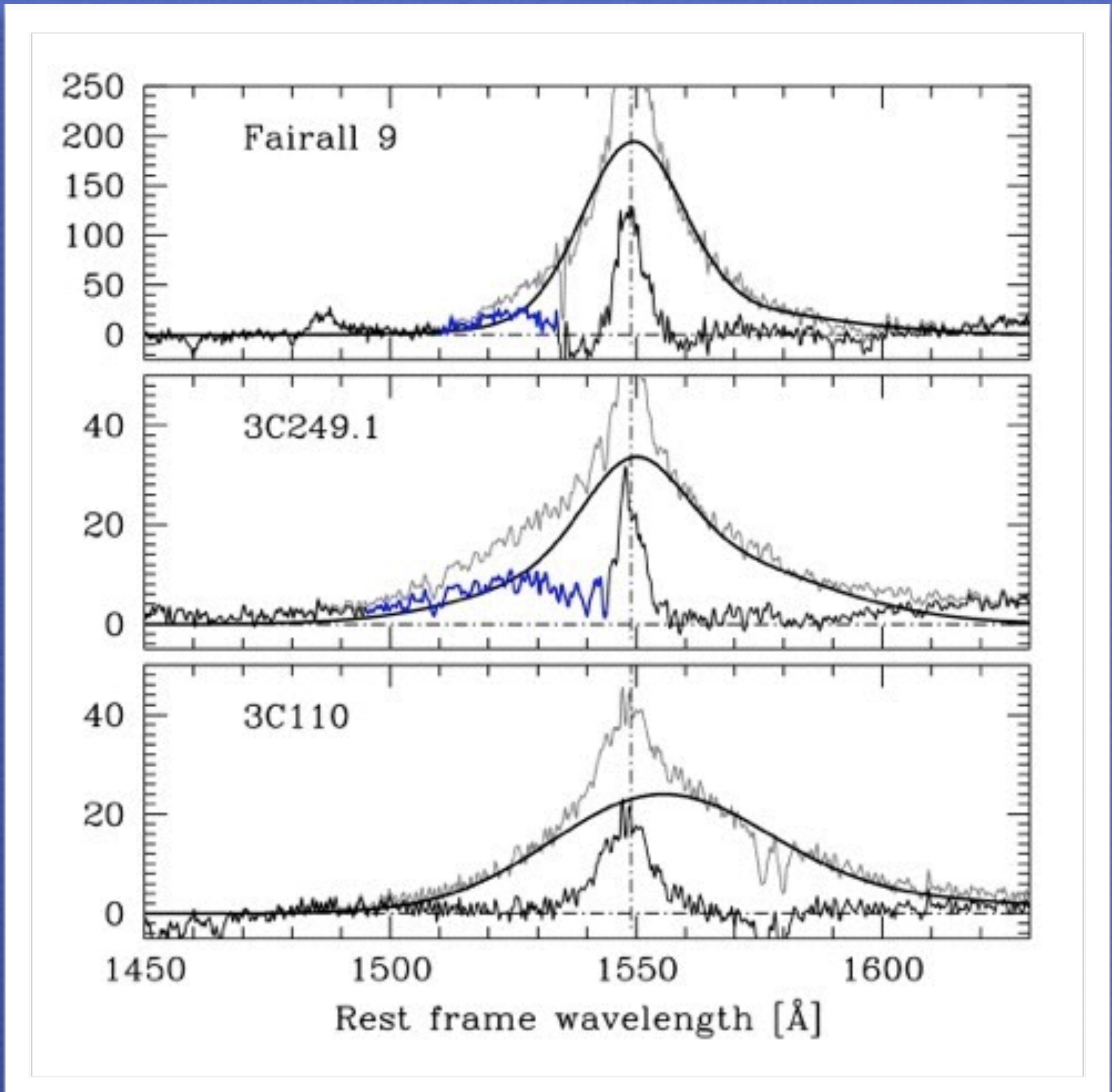

Correlations FWHM(CIVλ1549) vs. c(1/2) CIVλ1549

Increase in FWHM(CIVλ1549) associated with blueshifted excess

Filled: Pop. A
Open: Pop. B
Circles: RQ
Squares: RL

low *z* sample UV FOS data
+HE high L sample (red)

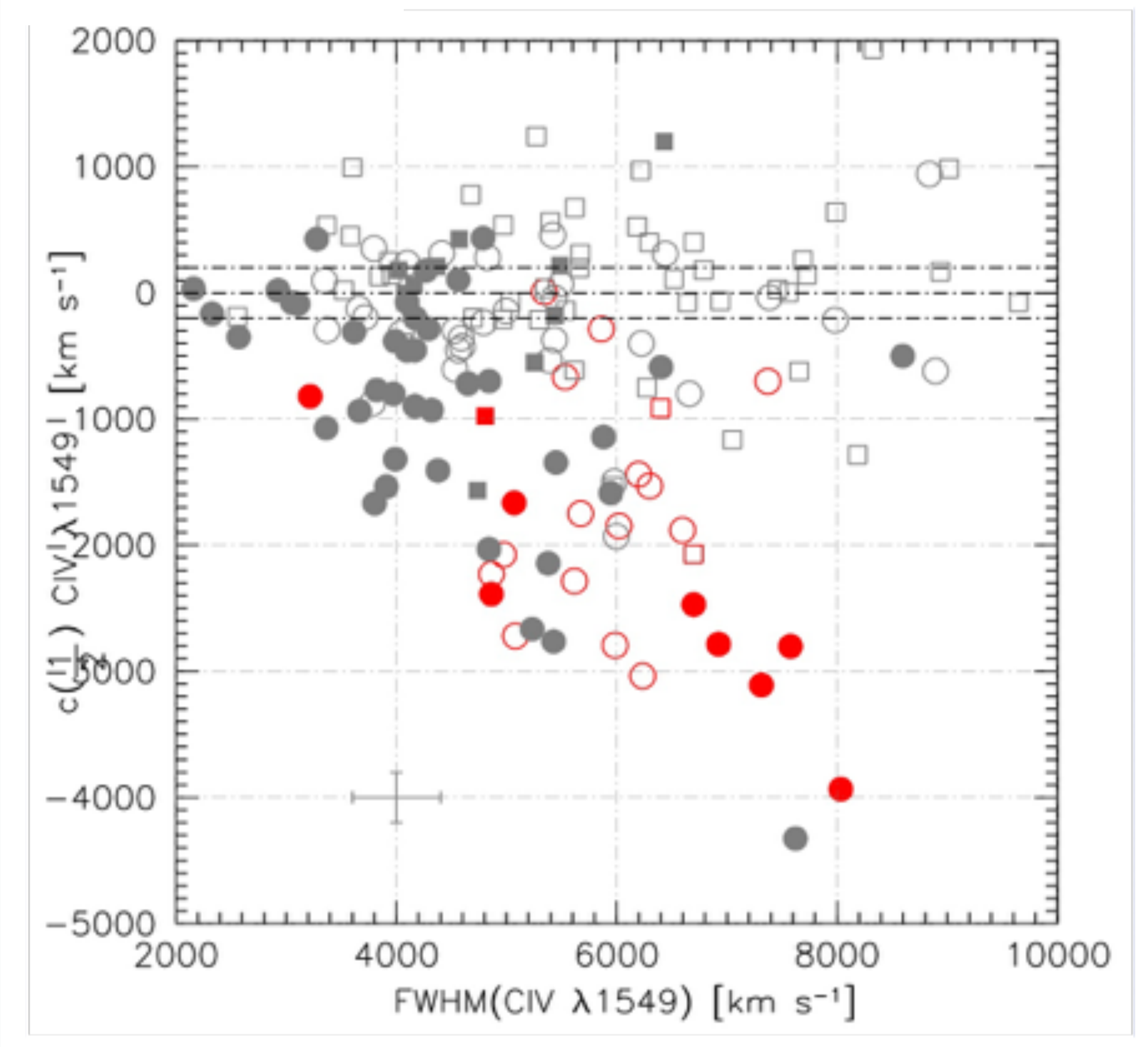

Pop. A RQ only

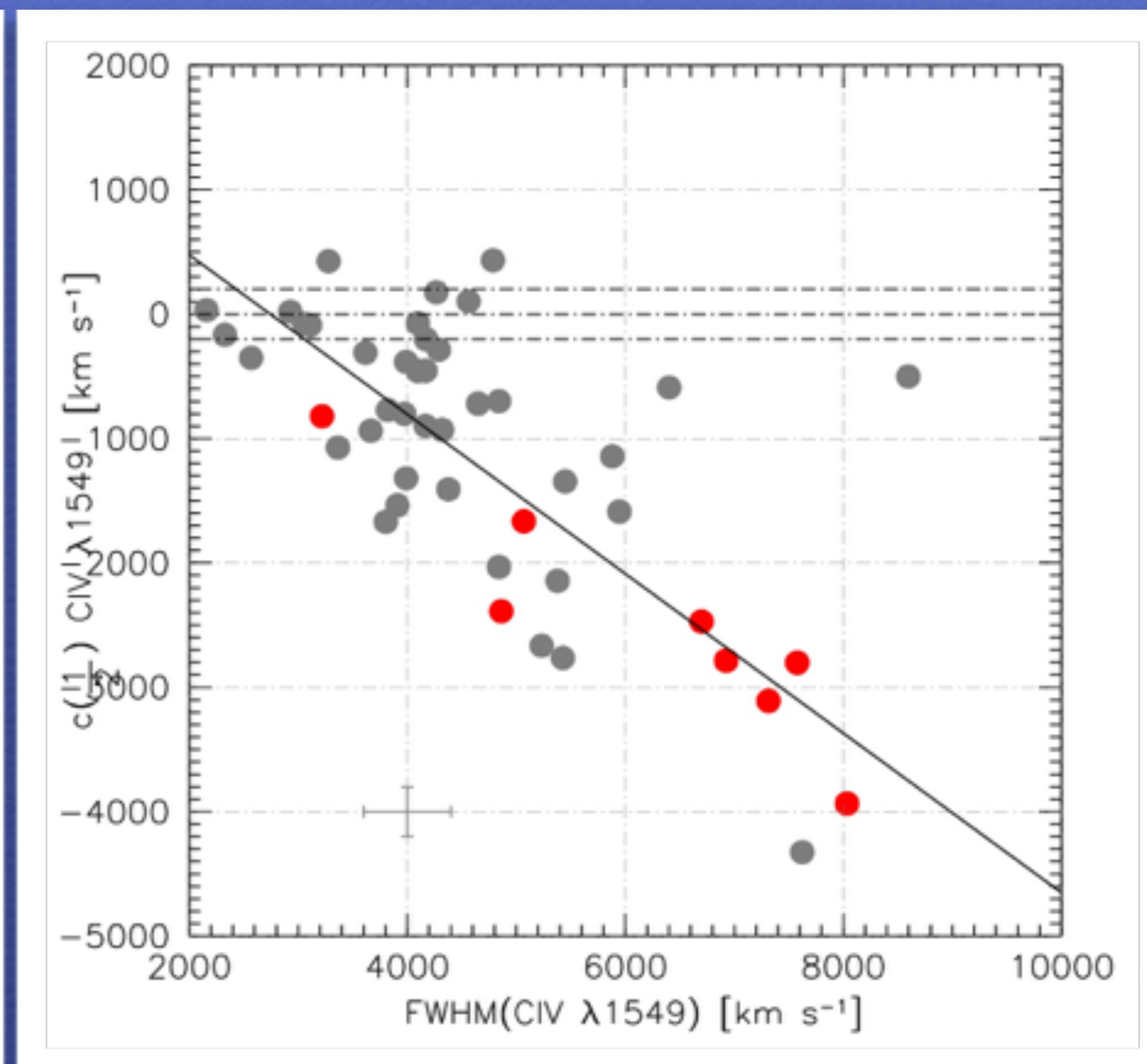

CIV shifts

Marziani & Sulentic 2012; Sulentic et al. 2007

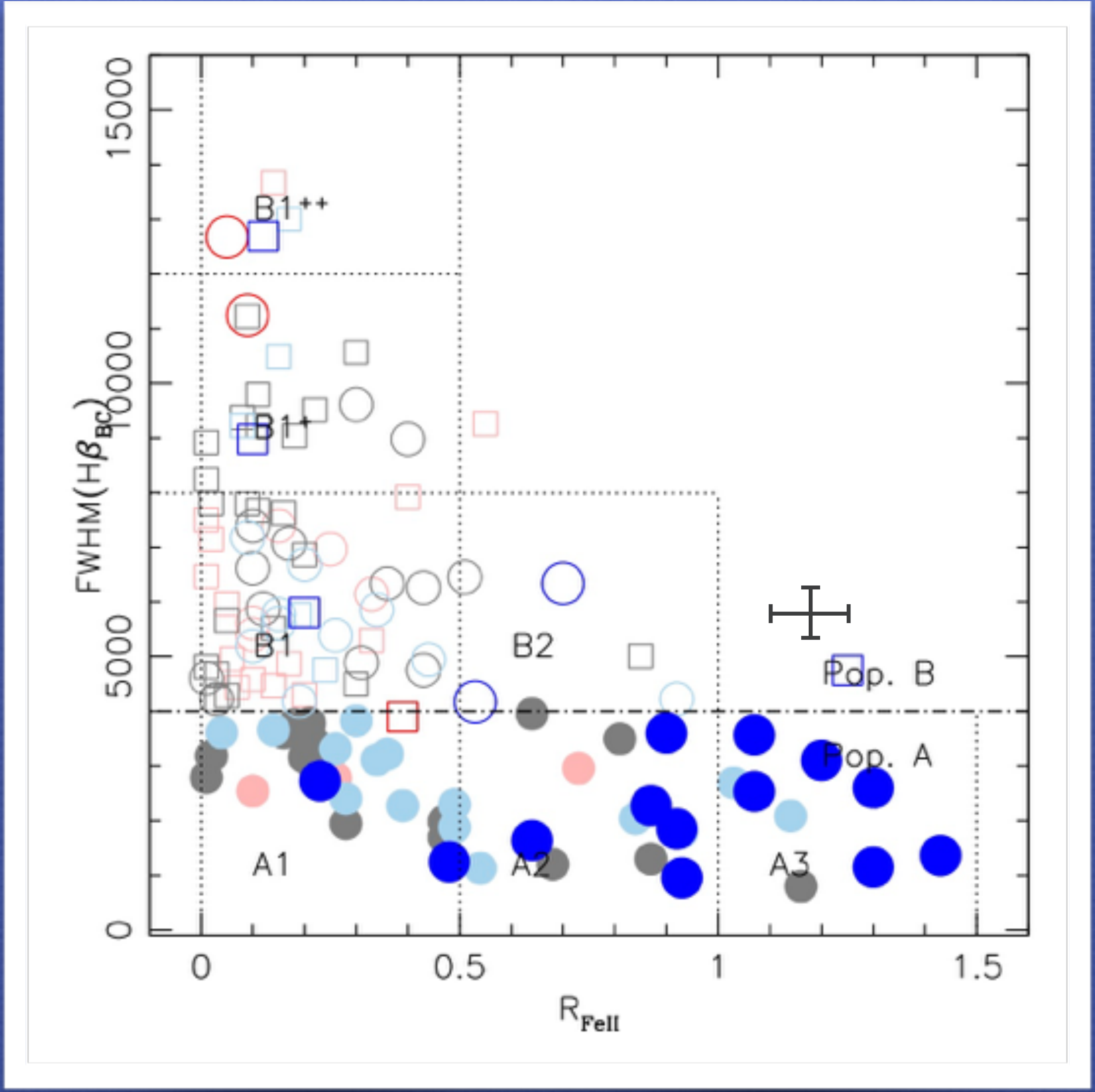

Large shift are found for FWHM(Hβ)< 4000 km/s

low *z* sample UV FOS data

Filled: Pop. A
Open: Pop. B
Circles: RQ
Squares: RL

c(1/2)≤-1000
-300 ≥c(1/2) > -1000
-300 < c(1/2) ≤ 300
300 < c(1/2) ≤ 1000
c(1/2) > 1000

LIL resonance line MgIIλ2800: Low ionization outflows

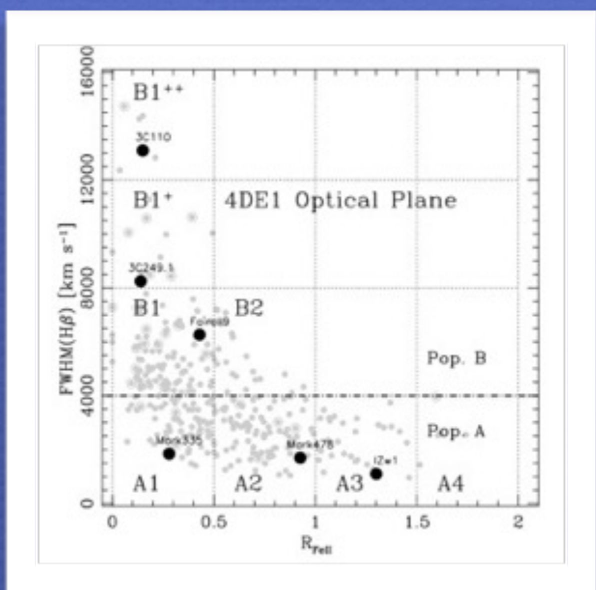

SDSS sample covering both Hβ and MgII
0 .4 < z <0.7; Marziani et al. 2013a,b

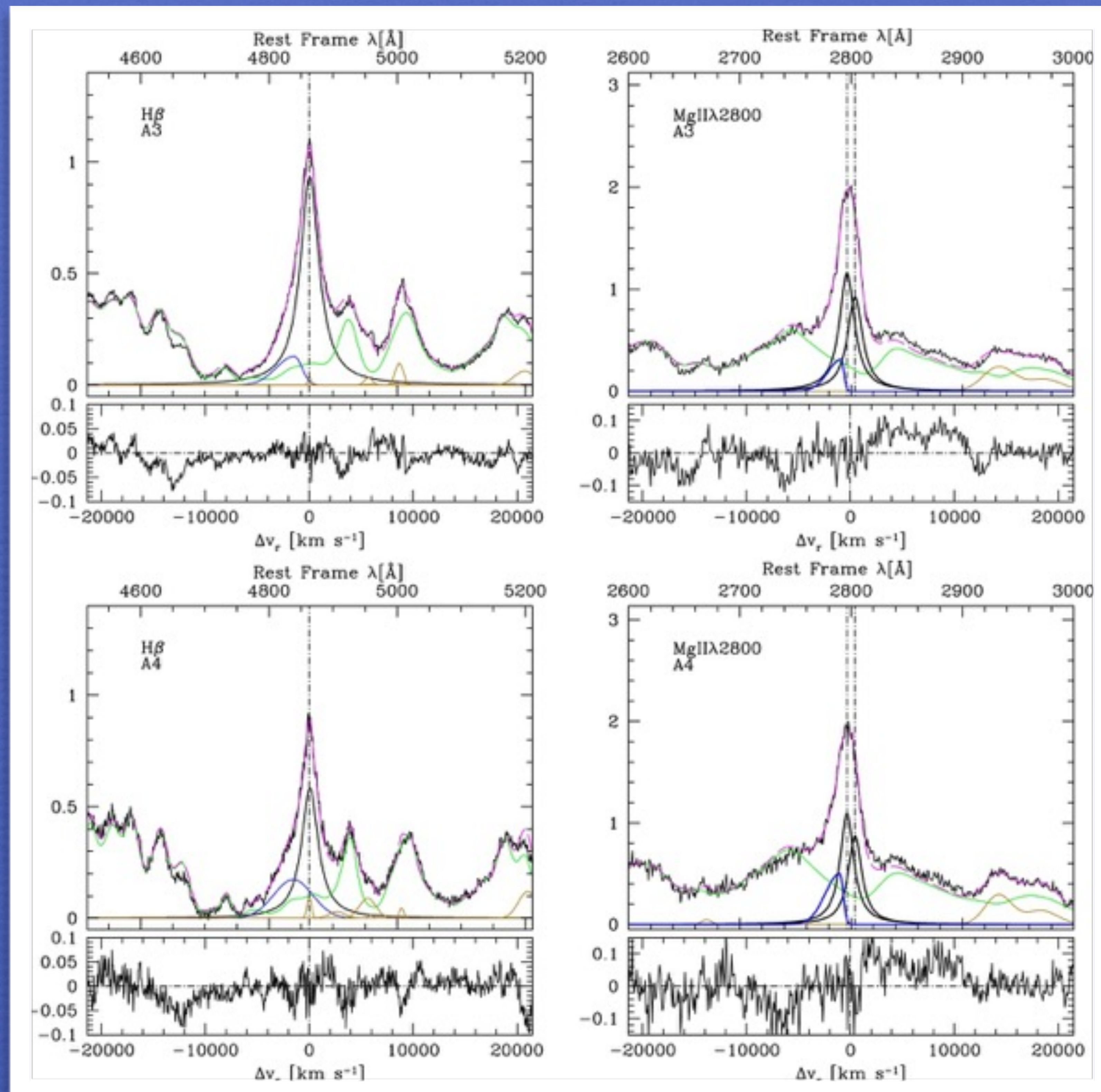

Lower radial velocities involved in MgII λ2800 than in CIVλ 1549

CIV λ1549 blueshift distributions for RQ and RL quasars

RL (mainly Pop. B) show smaller CIVλ 1549 blueshift and often redshifted CIVλ 1549

All and Pop. A; FOS + HE

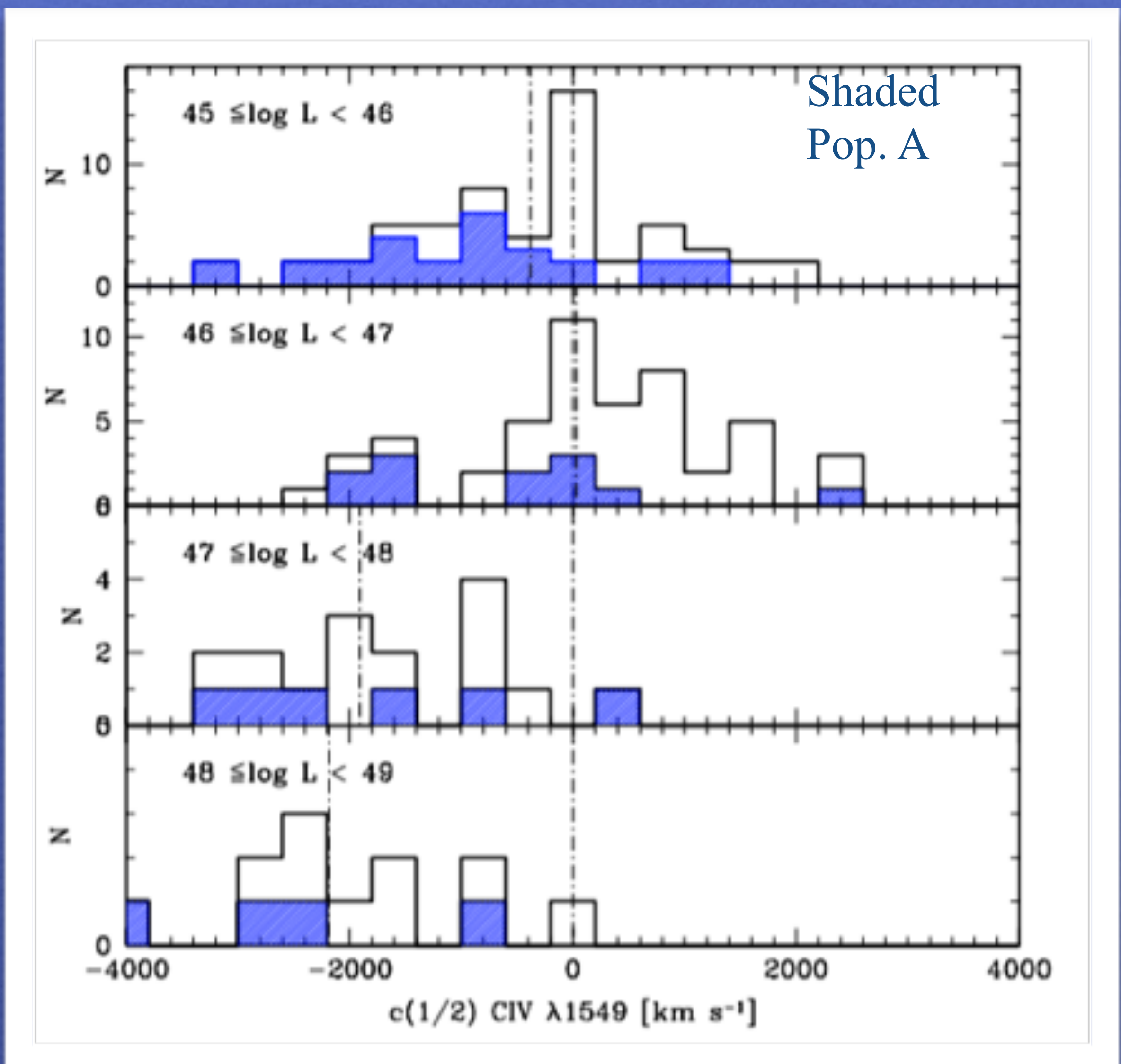

All and RL; FOS + HE

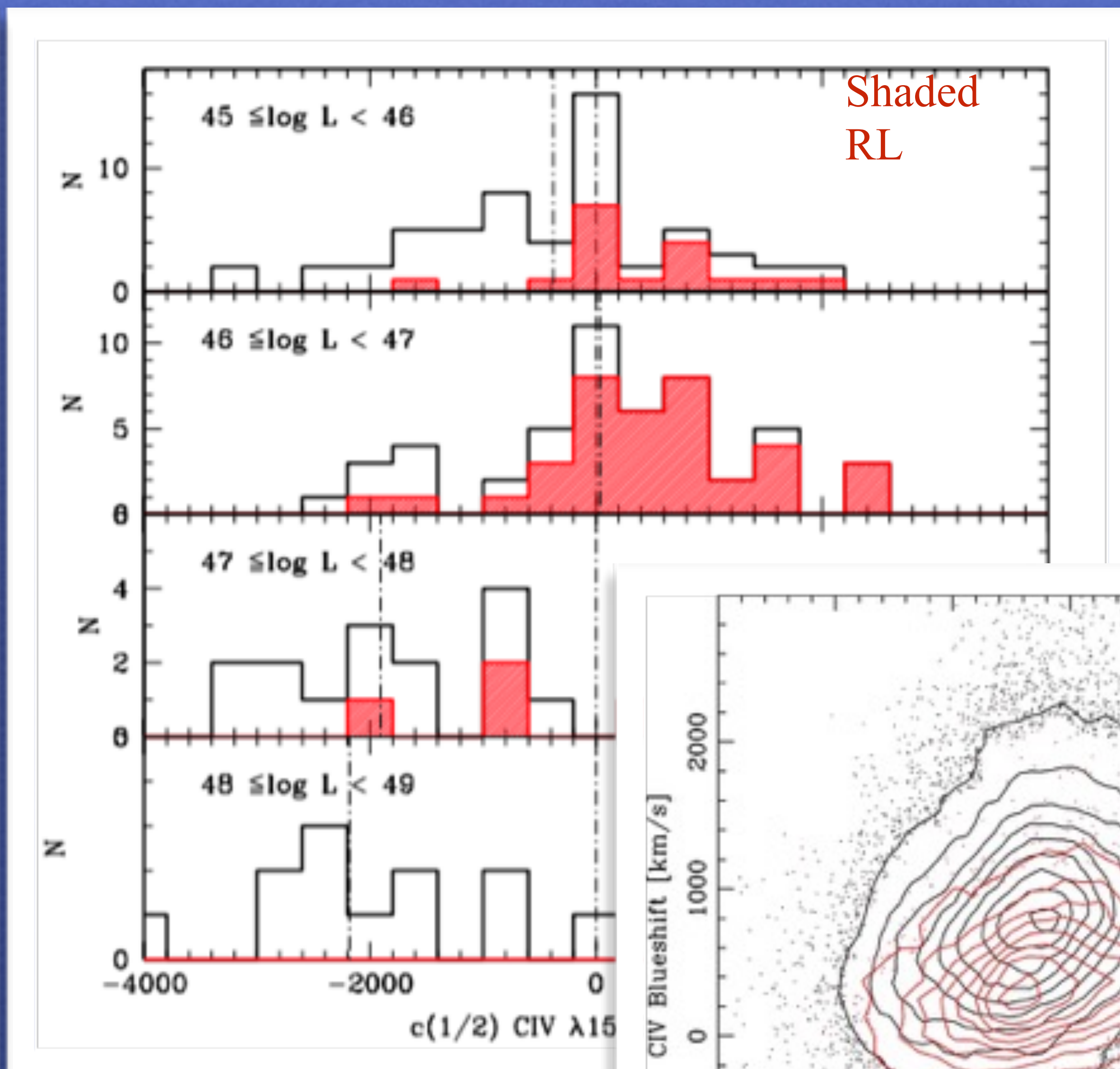

Consistent with result from SDSS

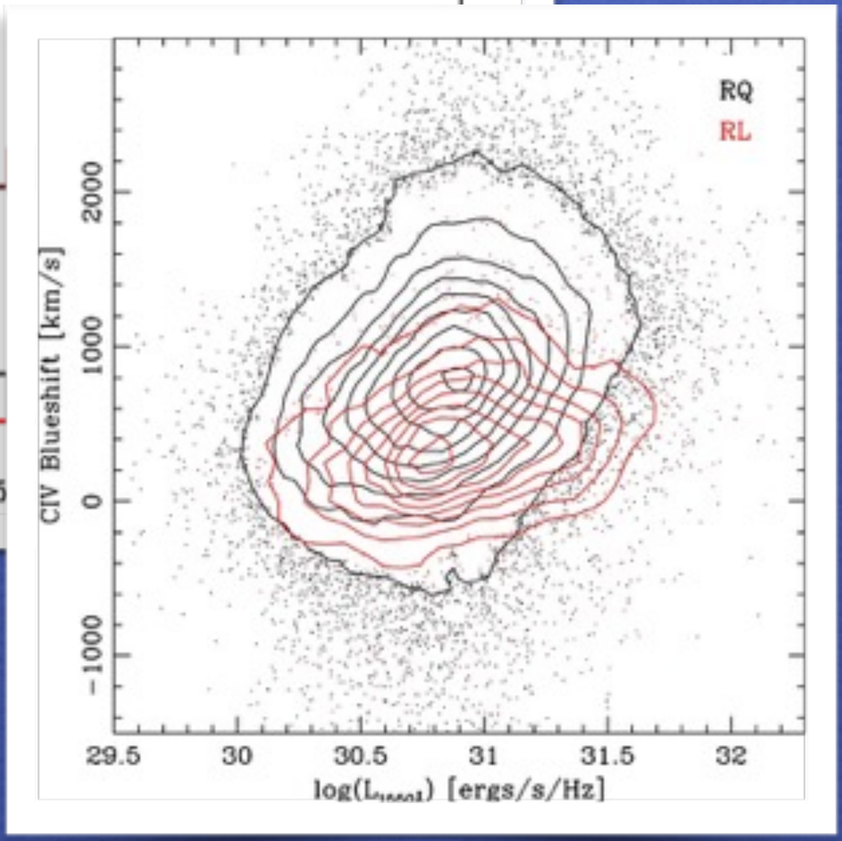

Richards et al. 2011

Contextualization for High Ionization Lines

HIL < Pop. A, Pop. B

Pop. B < RQ, RL

LIL < Pop. A, Pop. B

No strong effect of Radio Loudness on LIL profiles, only on HILs.

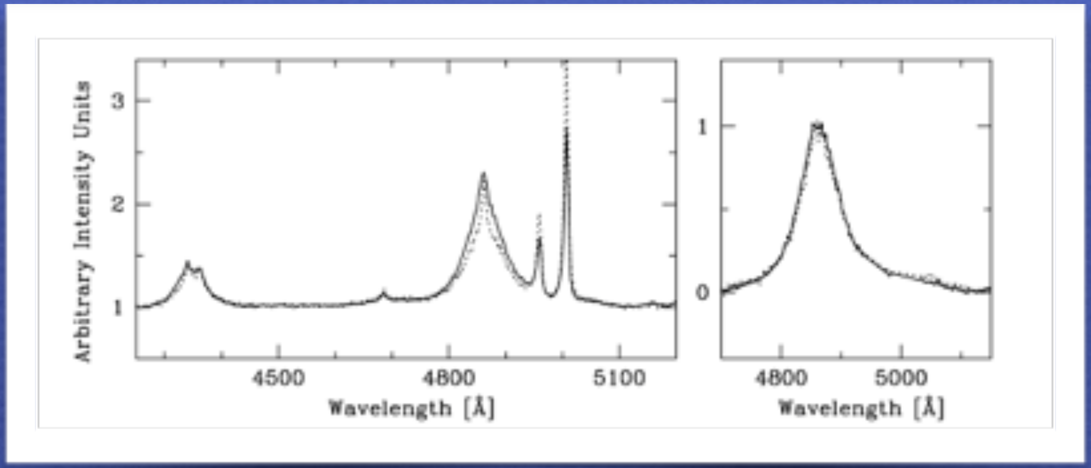

Hβ RL vs RQ
Pop. B

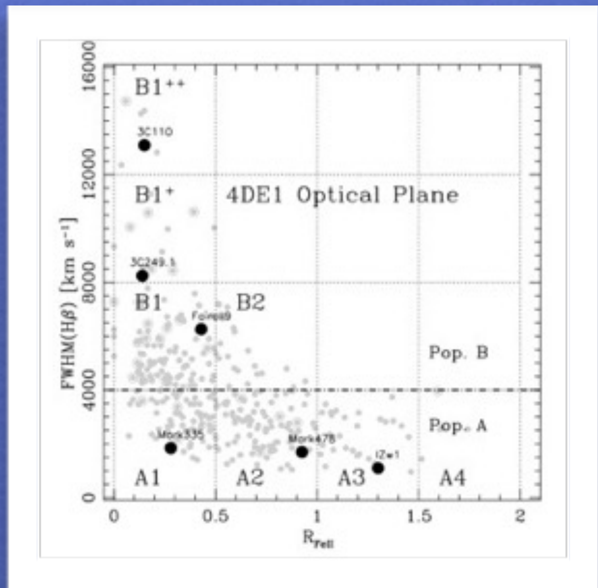

UV spectral changes along 4DE1

Metallicity and density sensitive emission line ratios

Bachev et al. 2004; Negrete et al. 2012

Imply growth of density and metallicity toward A4

HST/FOS composite spectra of quasars at z<0.7

Along the sequence (A4 → B1++)

NVλ1240 ↘

AlIIIλ1860 ↘

CIII]λ1909 ↗

NIII]1750 ↘

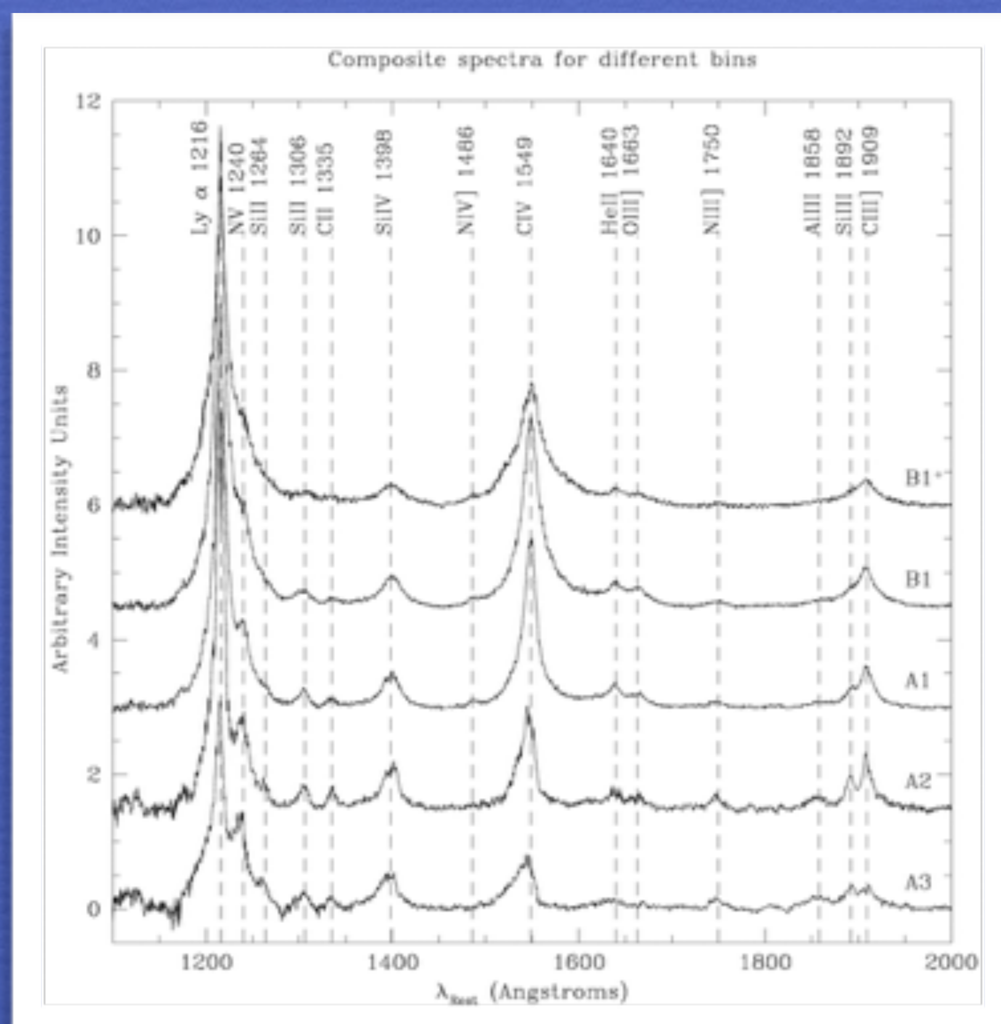

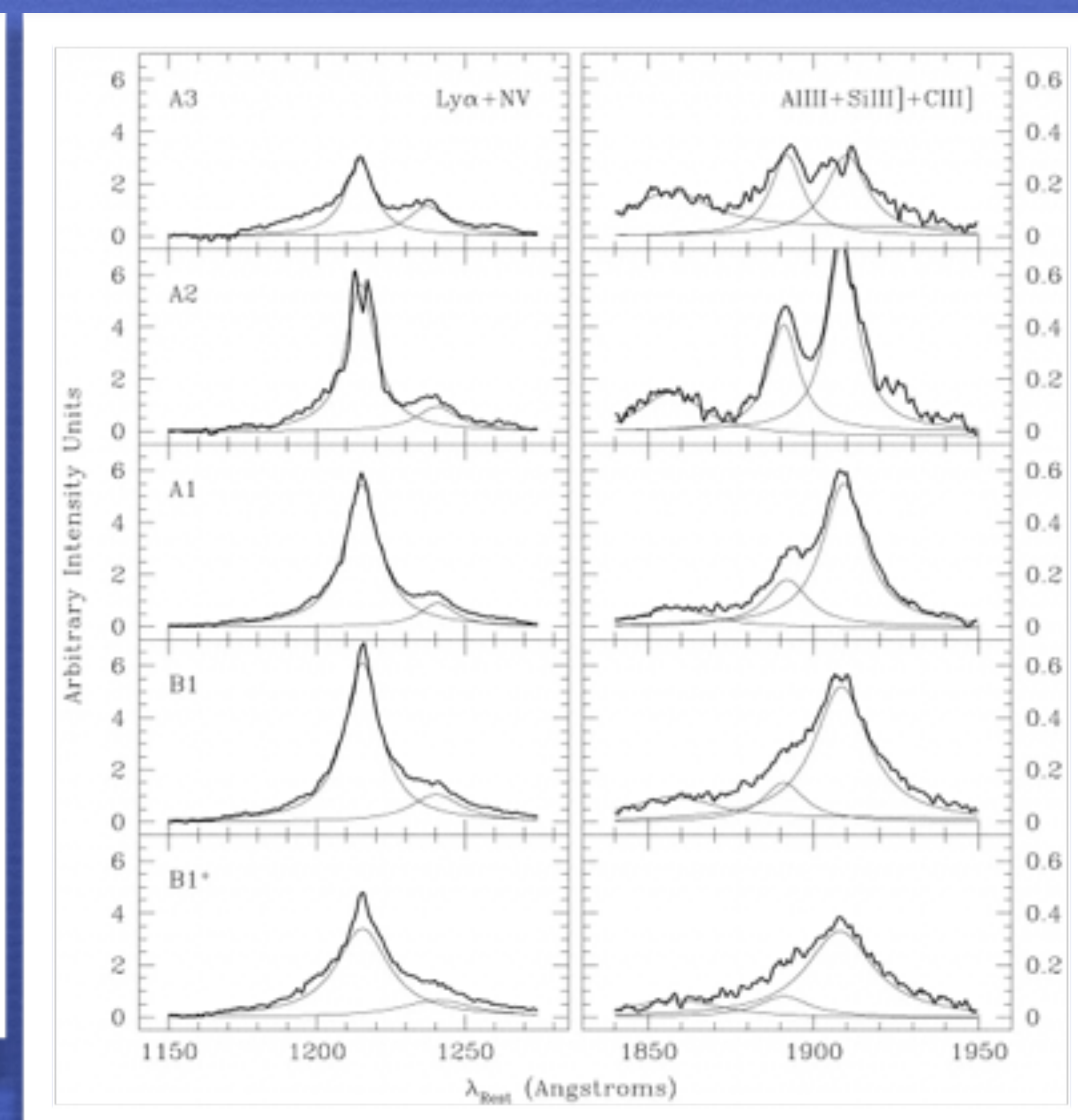

Optical plane of 4DE1: a sequence of Eddington ratio

with significant orientation and black hole mass effects

Ionization parameter $U = \frac{\int_{\nu_0}^{+\infty} \frac{L_\nu}{h\nu} d\nu}{4\pi r_{\rm BLR}^2 n_{\rm e} c}$ written as a function of $L/M_{\rm BH}$ and $M_{\rm BH}$

assuming flattened geometry, FeII and line width orientation dependence, $r \propto L^a$

Fixed black hole mass

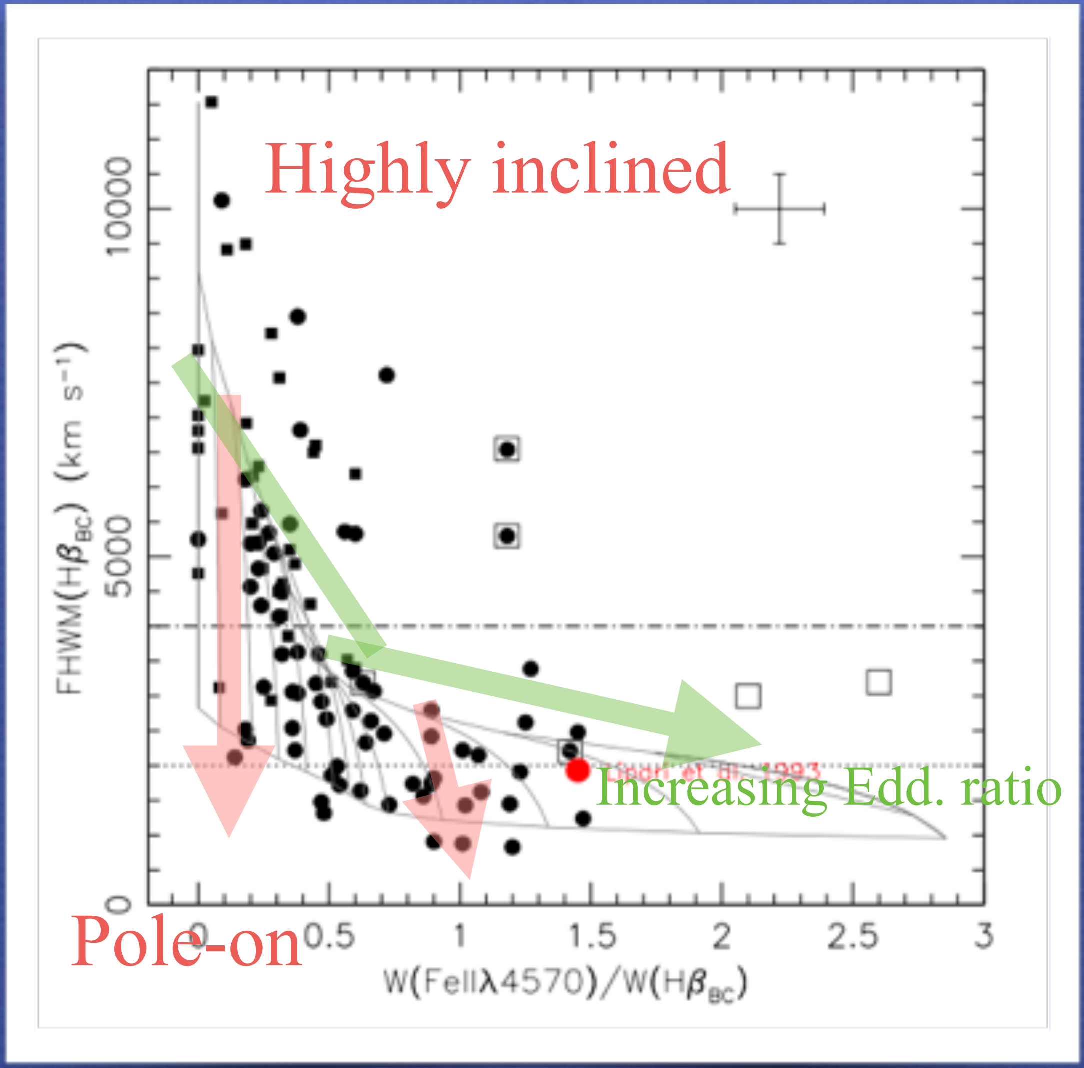

Varying black hole mass, average orientation

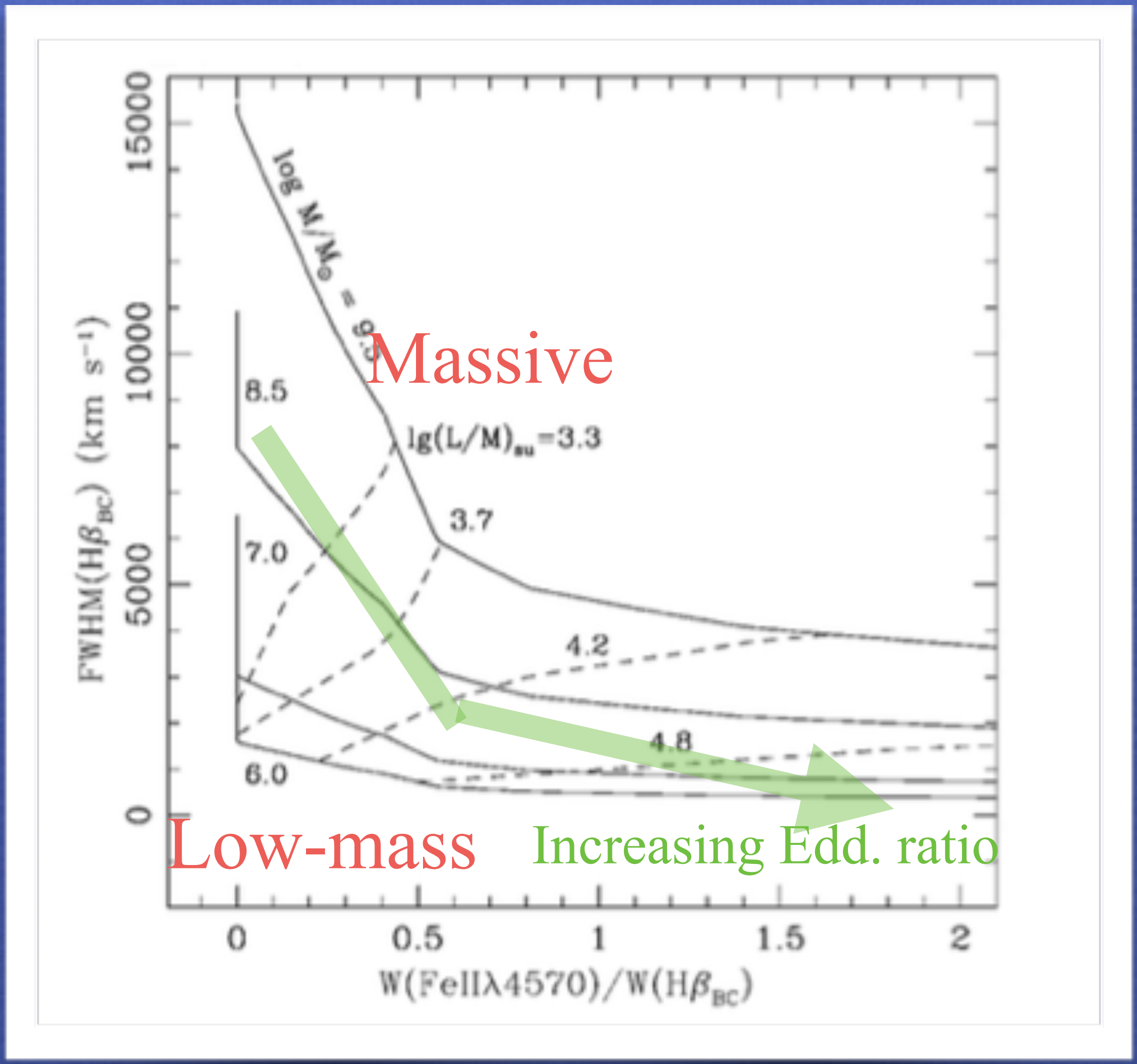

Marziani et al. 2001; Zamanov & Marziani 2002, cf. Shen & Ho 2014, Sun & Shen 2015

Virial Black Hole Mass & Eddington ratio

geometry
dynamics

$$M_{\rm BH} = \frac{f r (\delta v)^2}{G}$$

$r_{\rm BLR}$

FHWM
σ
FWZI

Keplerian velocity field: the BLR dynamics dominated by the gravity of a central mass; $v \propto r^{-1/2}$

$$M_{\rm BH}(H\beta) = 1.05 \times 10^8 \left[\frac{L_{5100}}{10^{46}\,\mathrm{ergs\,s^{-1}}}\right]^{0.65} \left[\frac{\mathrm{FWHM}(H\beta)}{10^3\,\mathrm{km\,s^{-1}}}\right]^2 M_\odot.$$

valid for low-ionization lines Hβ and MgII λ2800

scaling laws for large samples: $r \propto L^{1/2} \longrightarrow M_{\rm BH} = M_{\rm BH}(L, \mathrm{FWHM})$

(Vestergaard & Peterson 2006; Trakhtenbrot & Netzer 2012; Shen & Liu 2012)

$$\mathrm{Eddington\ \ ratio} = \frac{L_{\rm bol}}{L_{\rm Edd}} \propto \frac{\lambda L_\lambda \times \mathrm{B.C.}}{M_{\rm BH}}$$

Bolometric correction B.C. not trivial especially at high L

(Richards et al. 2006; Runnoe et al. 2013)

Influence of Eddington Ratio (and M_{BH}) on the Hβ profile: Eddington Ratio matters more

Low *z* Hβ sample: Marziani et al. 2003b

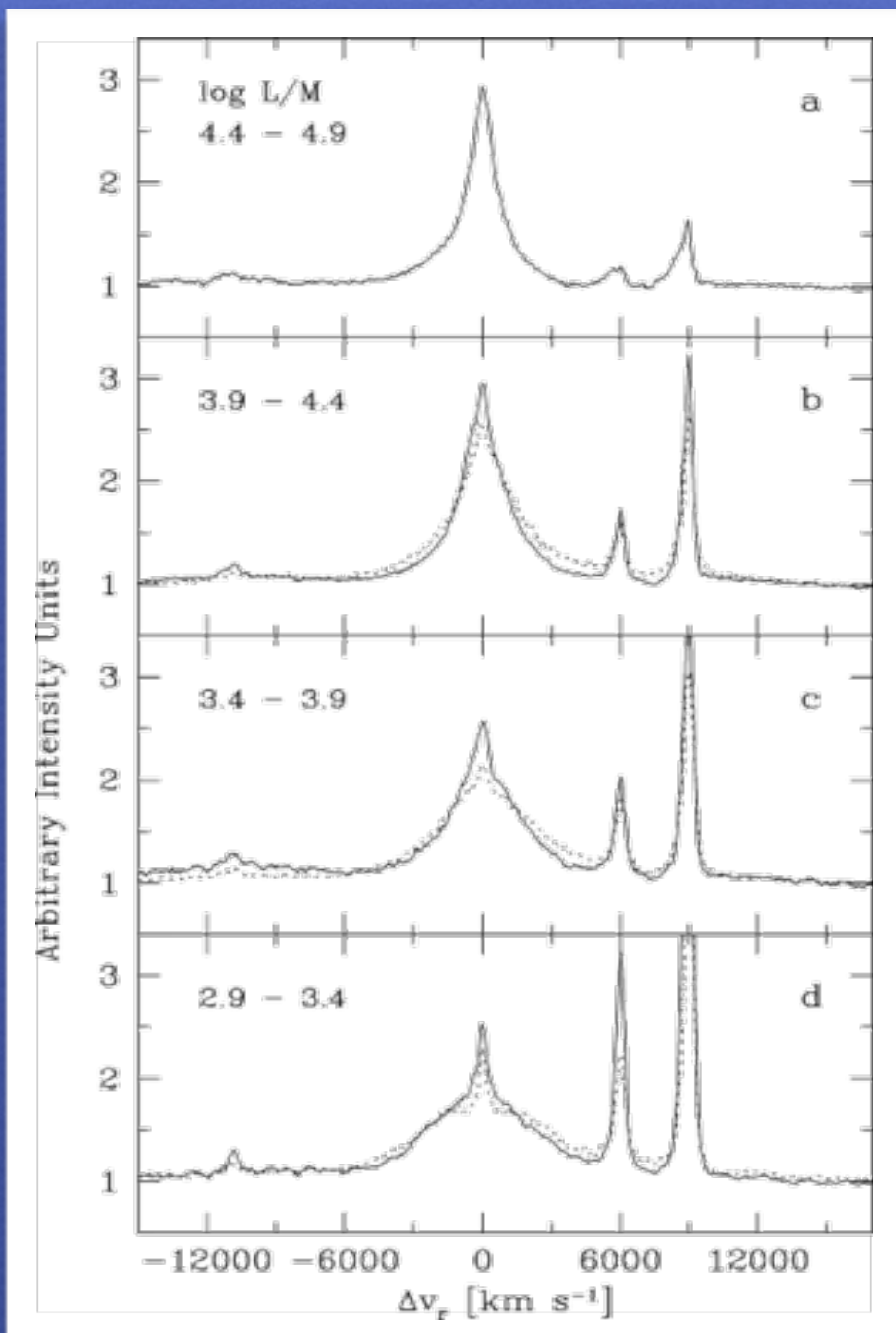

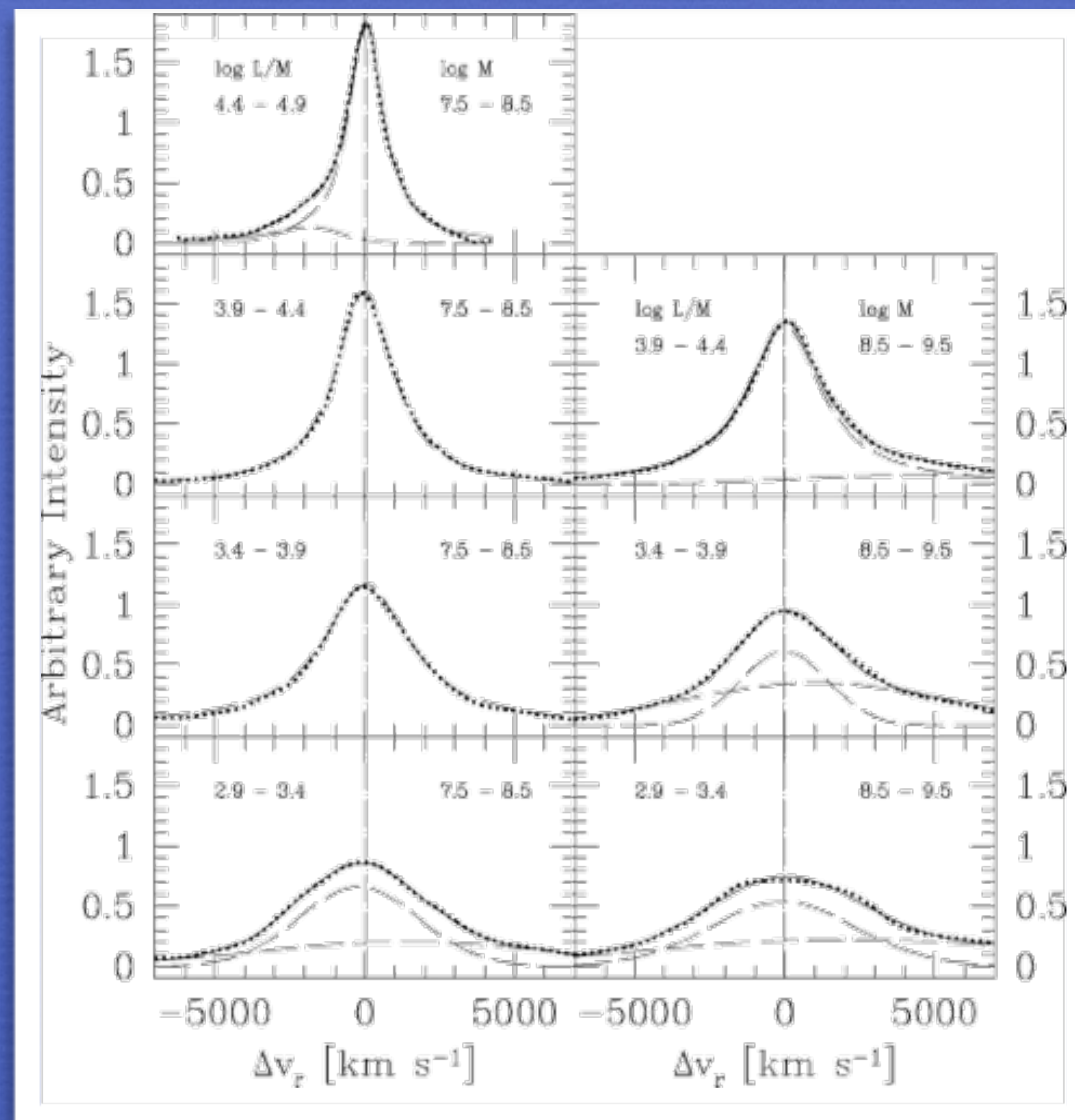

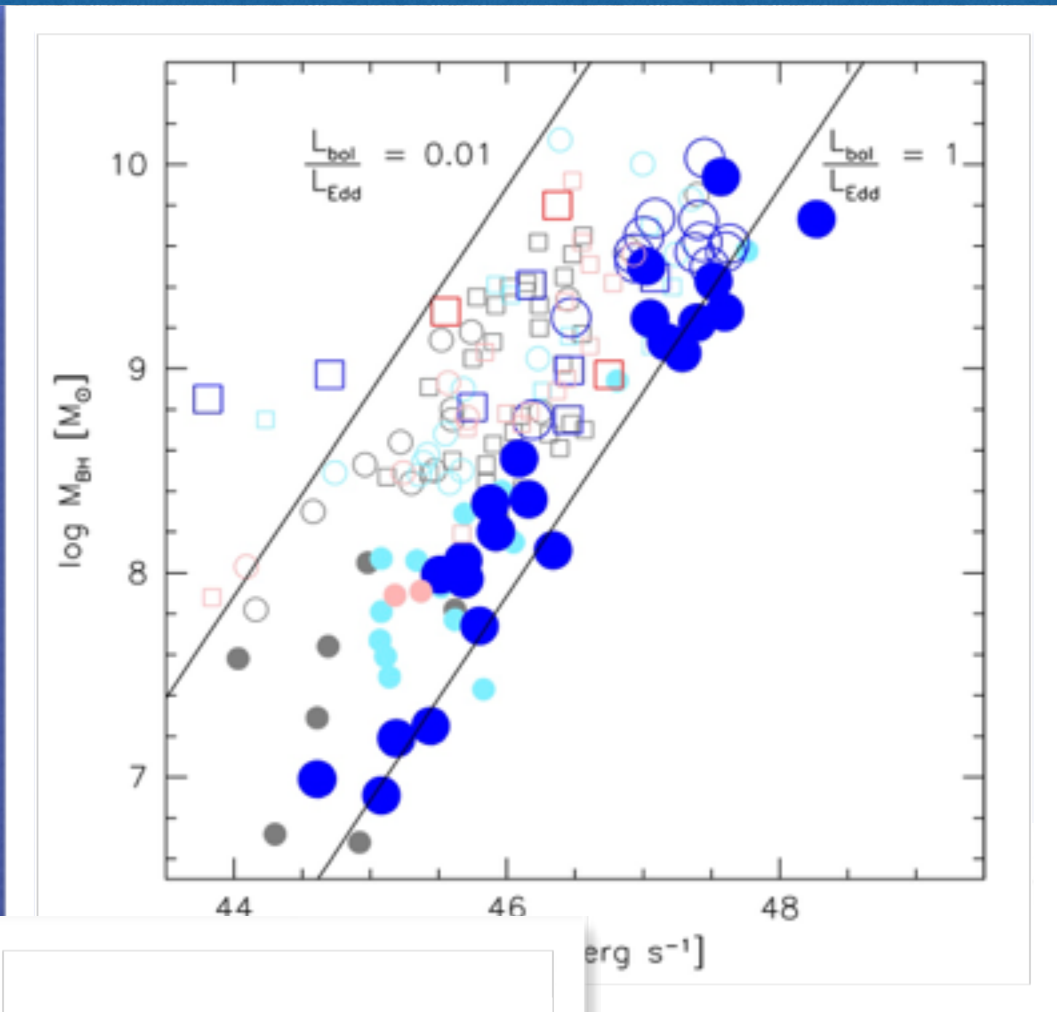

Largest CIVλ1549 blueshifts are observed at high L/L_{EDD} but not necessarily at high M_{BH} or high L

c(1/2)≤-1000
-300 ≥c(1/2) > -1000
-300 < c(1/2) ≤ 300
300 < c(1/2) ≤ 1000
c(1/2) > 1000

Filled: Pop. A
Open: Pop. B
Circles: RQ
Squares: RL

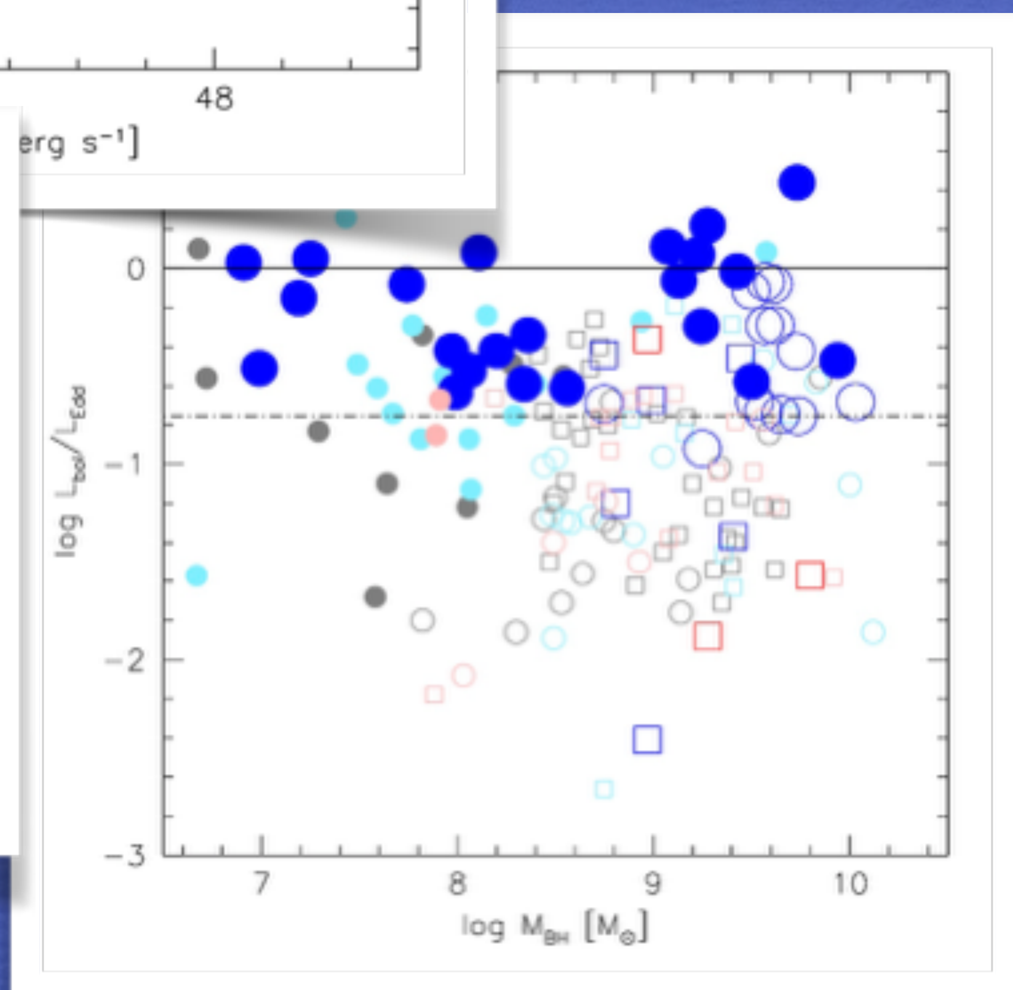

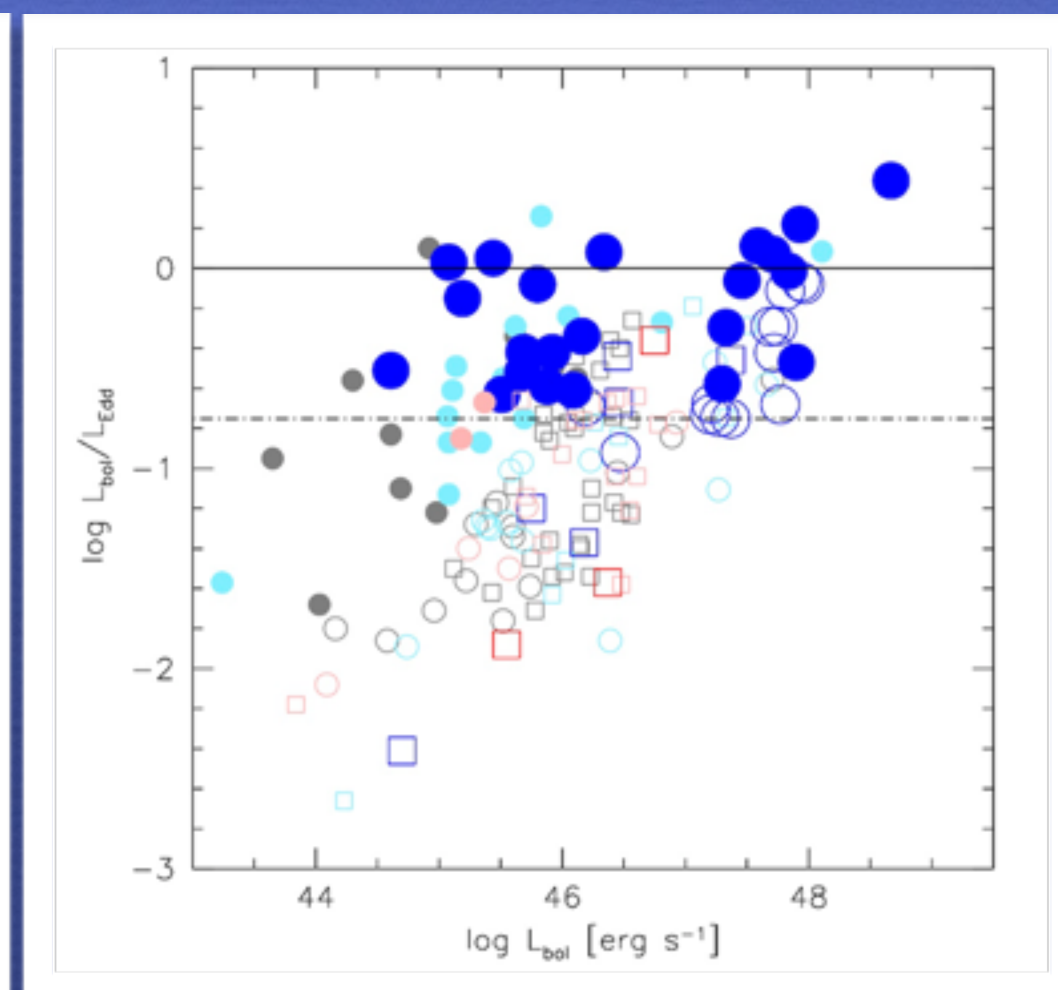

Low Ionization Outflows

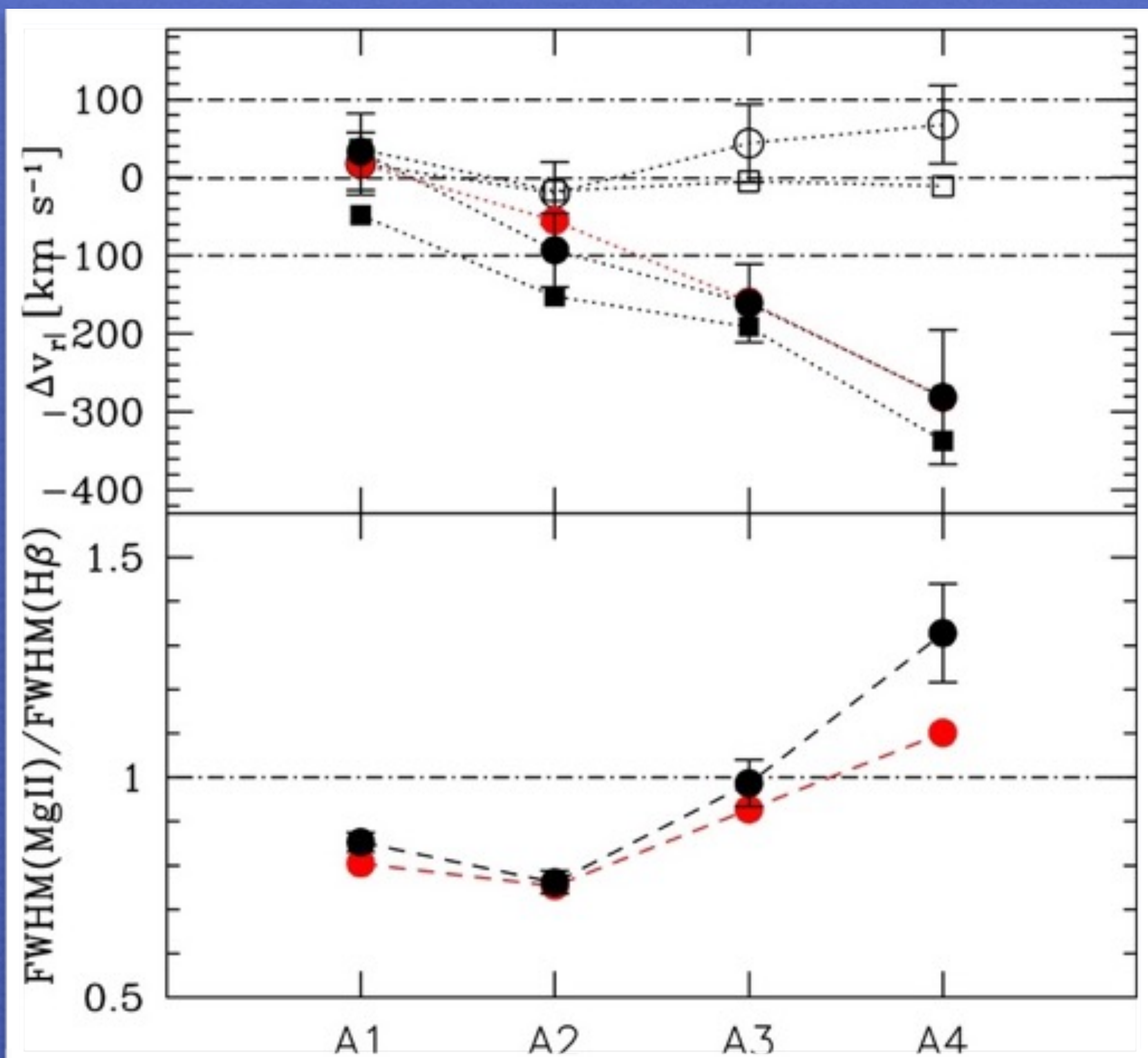

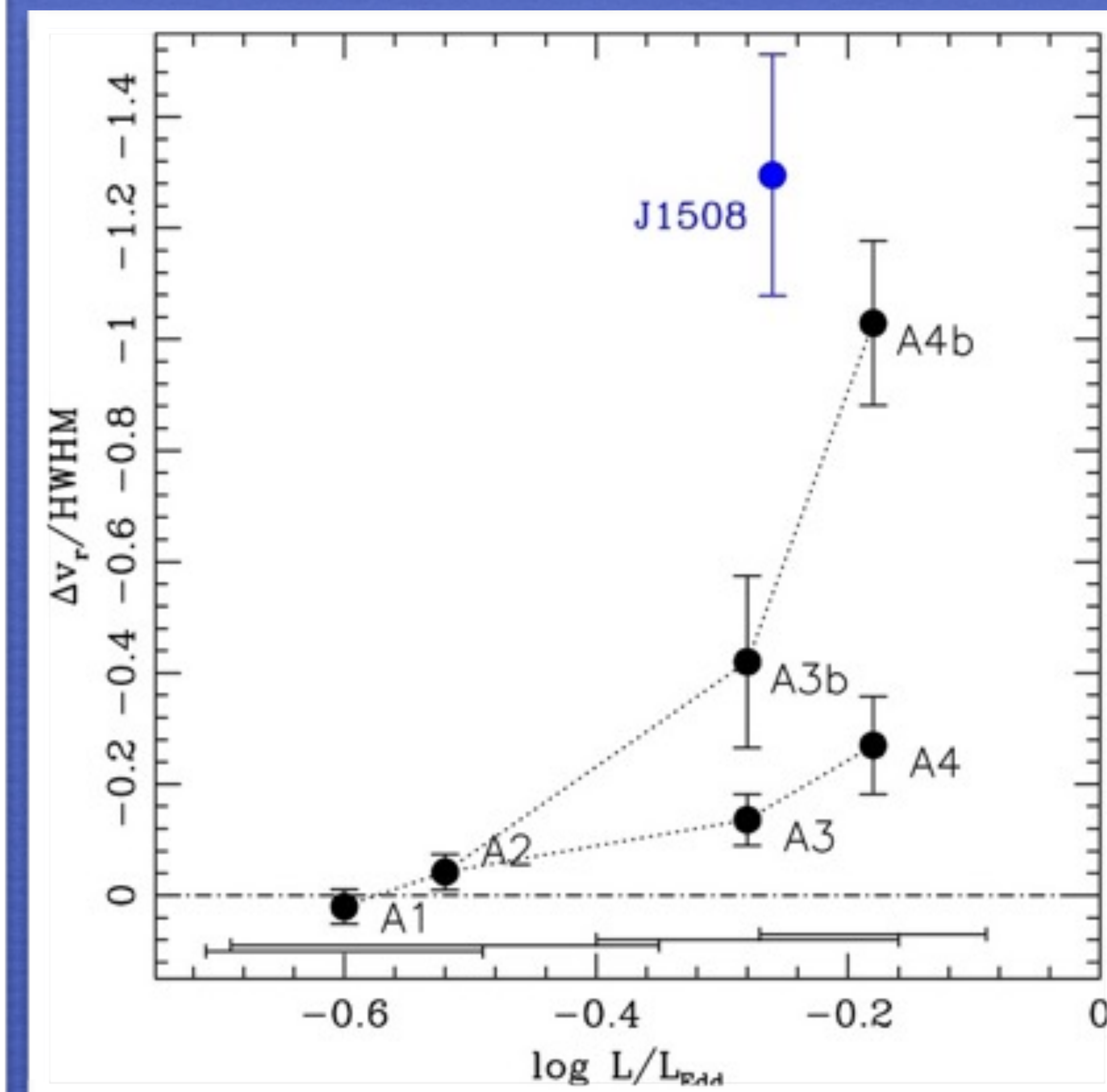

Strongly influenced by Eddington ratio

Marziani et al. 2012; 2013

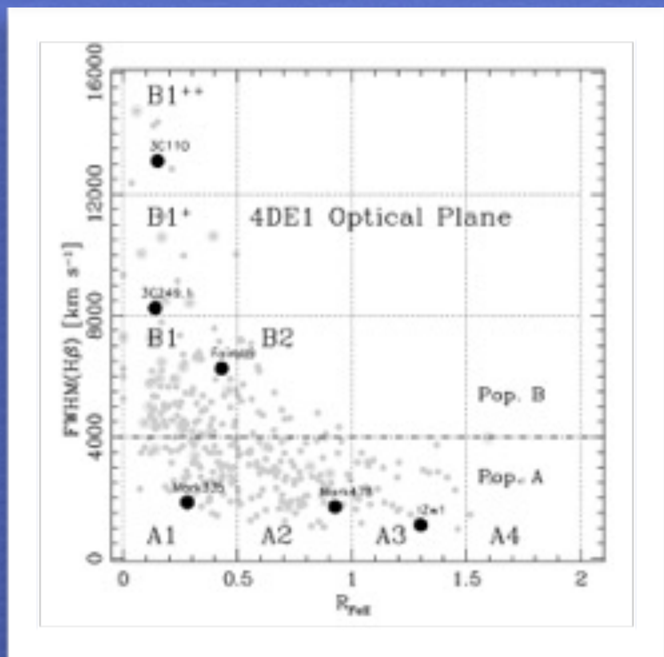

Strongest emission lines along the 4DE1 sequence can be empirically reproduced by three components

Marziani et al. 2010

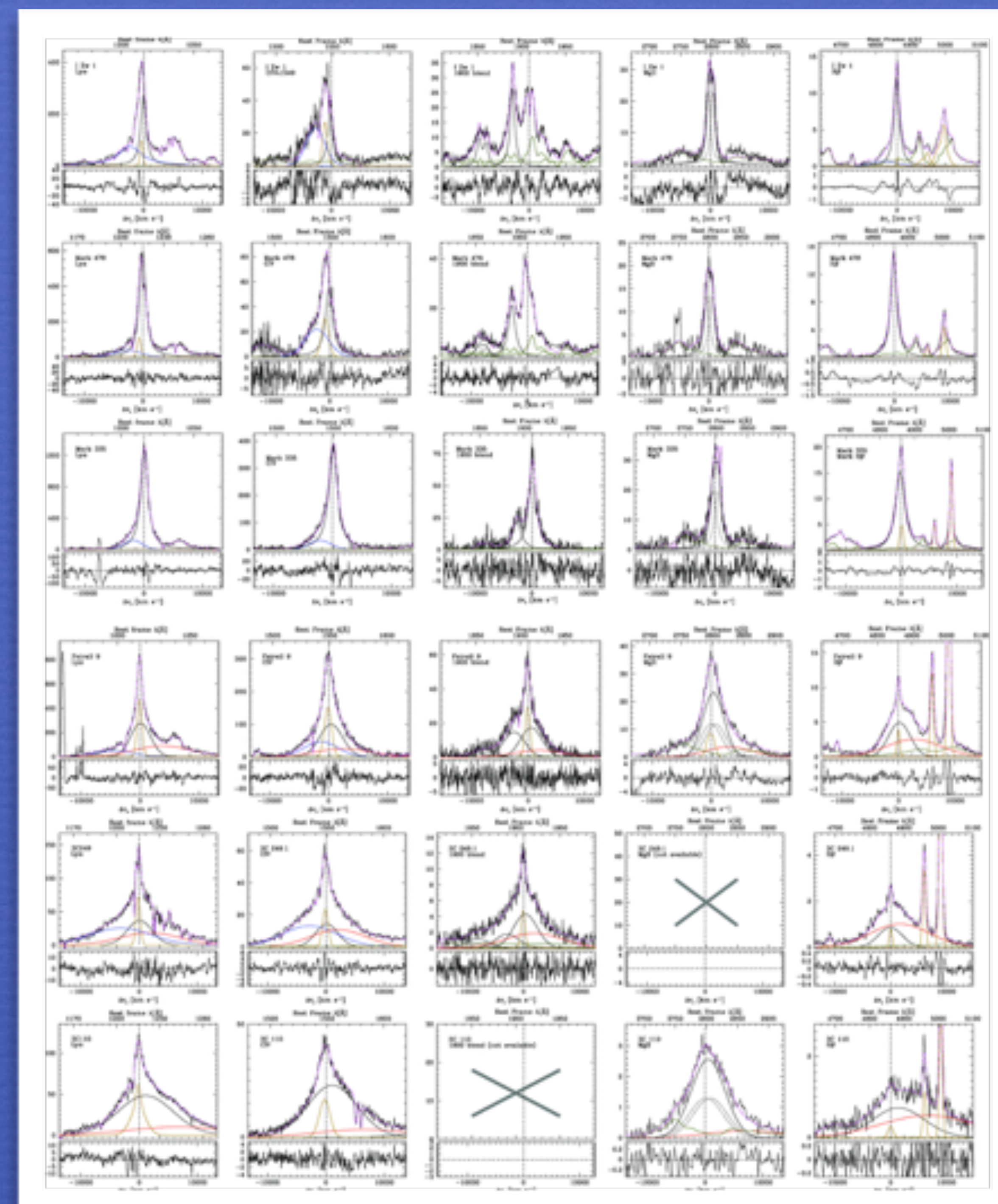

Blueshifted component (BLUE): strong in Lyα, CIVλ1549, HeIIλ1640

"Broad Component"(BC) strong in all low ionization lines: FeII, MgIIλ2800, Hβ

"Very Broad Component" (VBC FWHM~10000 km s^{-1}) redshifted: strong in Lyα, CIVλ1549, HeII, Balmer lines absent in FeII

A very broad component in Population B

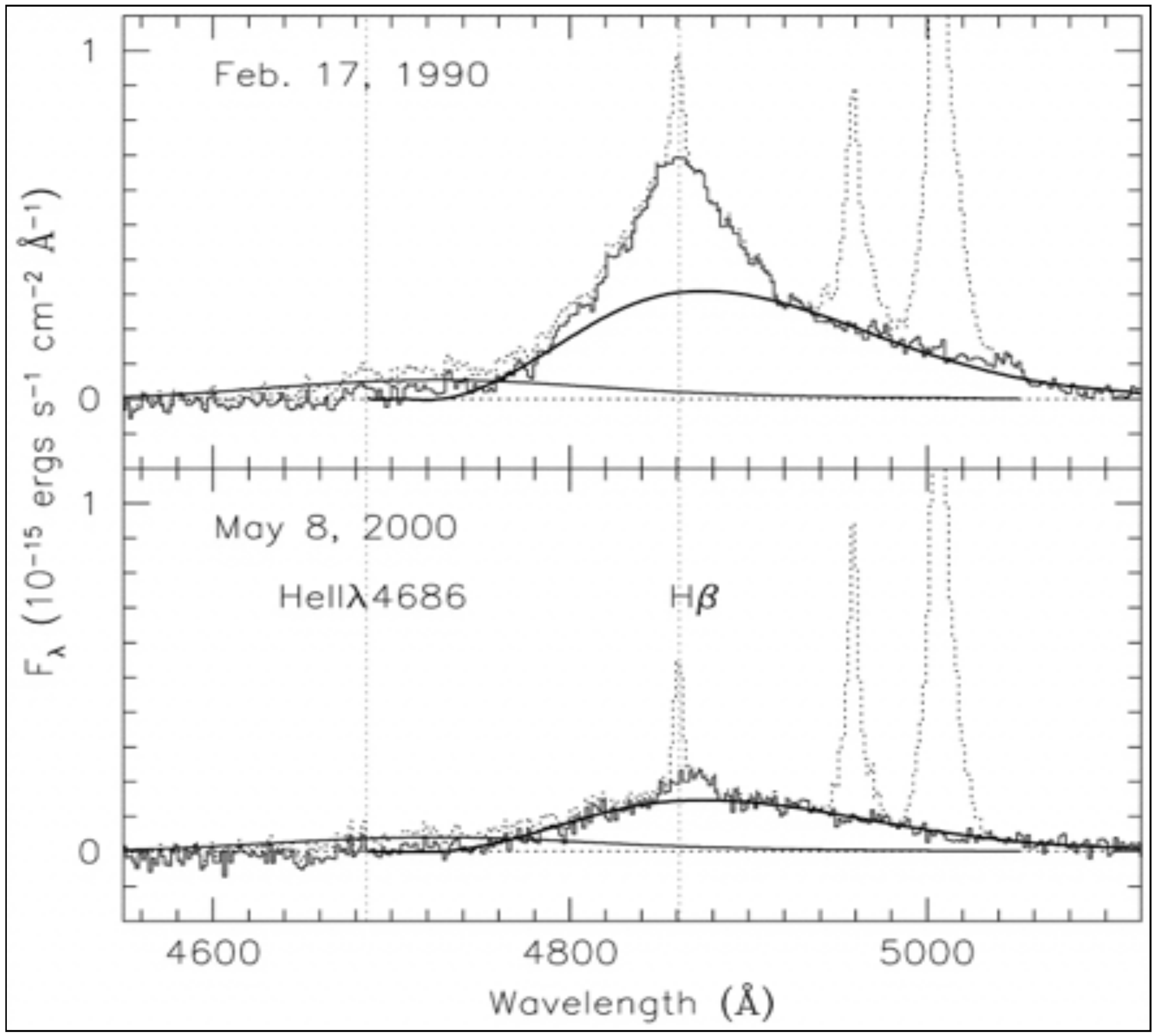

TABLE 2
PG 1416−129 Hβ Emission-Line Variability

	1990 February 17[a]			2000 May 8[b]		
Line Identification	Flux	W (Å)	FWHM (km s^{-1})	Flux	W (Å)	FWHM (km s^{-1})
$H\beta_{BC+VBC}$	86.0	160	6000	40.0	300	9000
$H\beta_{BC}$	23.0	47	4000	2.0	13	1450
$H\beta_{VBC}$	63.0	110	13000	38.0	220	13000

[a] Specific flux at 4500 Å, $F_\lambda \approx 7.5 \times 10^{-16}$ ergs s^{-1} cm^{-2} Å^{-1}.
[b] Specific flux at 4500 Å, $F_\lambda \approx 1.9 \times 10^{-16}$ ergs s^{-1} cm^{-2} Å^{-1}.

Sulentic et al. 2000

PG 1416-129 It is the “core” broad component that seems (in some cases) to respond more strongly to continuum changes.

Typical behavior of reverberating sources
Peterson et al. 2004

A Very Broad Line Region (VBLR?)
A long history (e.g., Peterson & Ferland 1986; Brotherton 1996; Corbin 1997)

Optically thin gas seems unlikely (pro: Morris & Ward 1989; Shields et al. 1995; against: Korista & Goad 2004; Snedden & Gaskell 2007).

VBLR suggested by the double Gaussian decomposition of Hβ in Pop. B sources

There is no evidence of FeII emission associated with the VBLR

Diagnostic Intensity Ratios

(SIV+OIV])λ1400/Si III] λ1892 Si II 1814/Si III] λ1892	*weakly dependent on metallicity* *sensitive to ionization*
CIV λ1549/(Si IV+OIV])λ1400	*sensitive to metallicity*
Al III λ1860/Si III] λ1892 Si III] λ1892/CIII] λ1909	*sensitive to density*
C IV λ1549/Al III λ1860 C IV λ1549/Si III] λ1892	*sensitive to ionization* *dependent on metallicity*
NVλ1240/CIV λ1549 NVλ1240/HeIIλ1640	*sensitive to metallicity*

The 4DE1 approach UV diagnostics

TABLE 1
Lines in the 1350–2000 Å Spectral Range

Ion	λ [Å]	X [eV]	$E_l - E_u$ [eV]	Transition	A_{ki} [s^{-1}]	n_c [cm^{-3}]	Note
Si IV	1393.755	45.20	0.000 - 8.896	$^2P^o_{3/2} \rightarrow {}^2S_{1/2}$	$8.80 \cdot 10^8$	⋯	1
Si IV	1402.770	45.20	0.000 - 8.839	$^2P^o_{1/2} \rightarrow {}^2S_{1/2}$	$8.63 \cdot 10^8$	⋯	1
C IV	1548.202	47.89	0.000 - 8.008	$^2P^o_{3/2} \rightarrow {}^2S_{1/2}$	$2.65 \cdot 10^8$	⋯	1
C IV	1550.774	47.89	0.000 - 7.995	$^2P^o_{1/2} \rightarrow {}^2S_{1/2}$	$2.64 \cdot 10^8$	⋯	1
Si II	1808.00	8.15	0.000 - 6.857	$^2D^o_{3/2} \rightarrow {}^2P_{1/2}$	$2.54 \cdot 10^6$	⋯	1
Si II	1816.92	8.15	0.036 - 6.859	$^2D^o_{5/2} \rightarrow {}^2P_{3/2}$	$2.65 \cdot 10^6$	⋯	1
Al III	1854.716	18.83	0.000 - 6.685	$^2P^o_{3/2} \rightarrow {}^2S_{1/2}$	$5.40 \cdot 10^8$	⋯	1
Al III	1862.790	18.83	0.000 - 6.656	$^2P^o_{1/2} \rightarrow {}^2S_{1/2}$	$5.33 \cdot 10^8$	⋯	1
[Si III]	1882.7	16.34	0.000 - 6.585	$^3P^o_2 \rightarrow {}^1S_0$	0.012	[illegible]	[illegible],2,3
Si III]	1892.03	16.34	0.000 - 6.553	$^3P^o_1 \rightarrow {}^1S_0$	1670	$2.1 \cdot 10^{11}$	[illegible],5
[C III]	1906.7	24.38	0.000 - 6.502	$^3P^o_2 \rightarrow {}^1S_0$	0.0052	[illegible]	1,2,6
C III]	1908.734	24.38	0.000 - 6.495	$^3P^o_1 \rightarrow {}^1S_0$	114	$1.4 \cdot 10^{10}$	[illegible],4,5
Fe III	1914.066	16.18	3.727 - 10.200	$z^7P^o_3 \rightarrow a^7S_3$	$6.6 \cdot 10^8$	⋯	7

Note. — All wavelengths are in vacuum. (1) Ralchenko, Yu., Kramida, A.E., Reader, J., and NIST ASD Team (2008). NIST Atomic Spectra Database (version 3.1.5). Available at: http://physics.nist.gov/asd3. 2: Feibelman & Aller (1987). 3: n_c computed following Shaw & Dufour (1995). 4: Morton (1991). 5: Feldman (1992). 6: Zheng (1988). 7: Wavelength and A_{ki} from Ekberg (1993), energy levels from Edlén and Swings (1942).

CIV (Al III, Si IV,NV)

C III] (Si III])

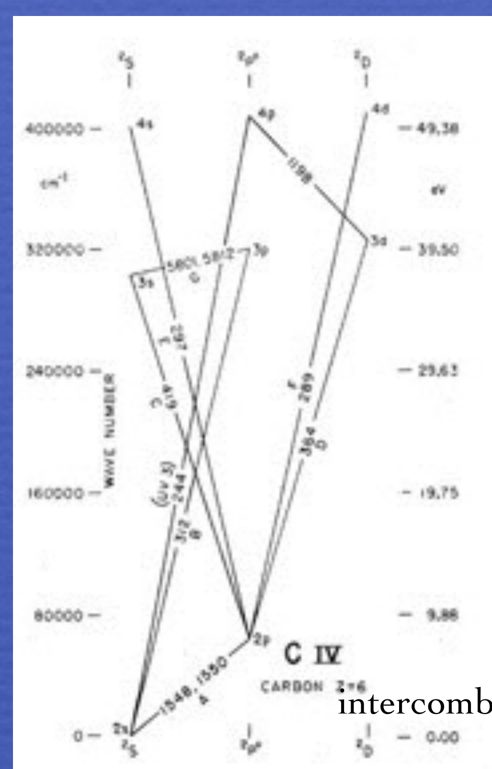

intercombination

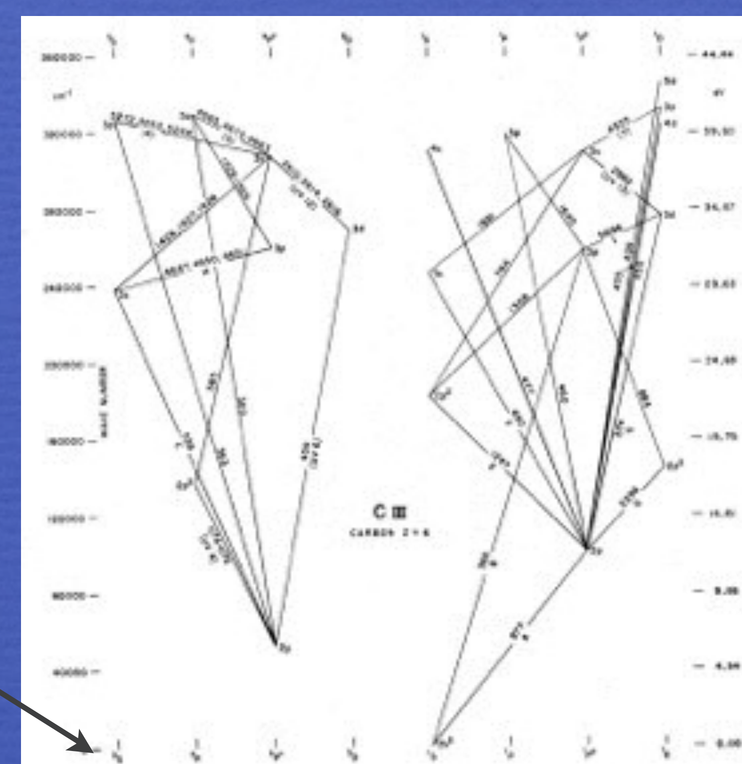

Behavior of diagnostic line ratios in the plane ionization parameter vs. density

Cloudy 08.00 array of simulations (Ferland et al. 2013): constant density, U, solar and 5 times solar abundances, standard quasar continuum, and column density log N_c = 23,24,25, dust free

Maps built on an array of 571 photoionization models for a given Z and N_c n and U evaluated at steps of 0.25 dex

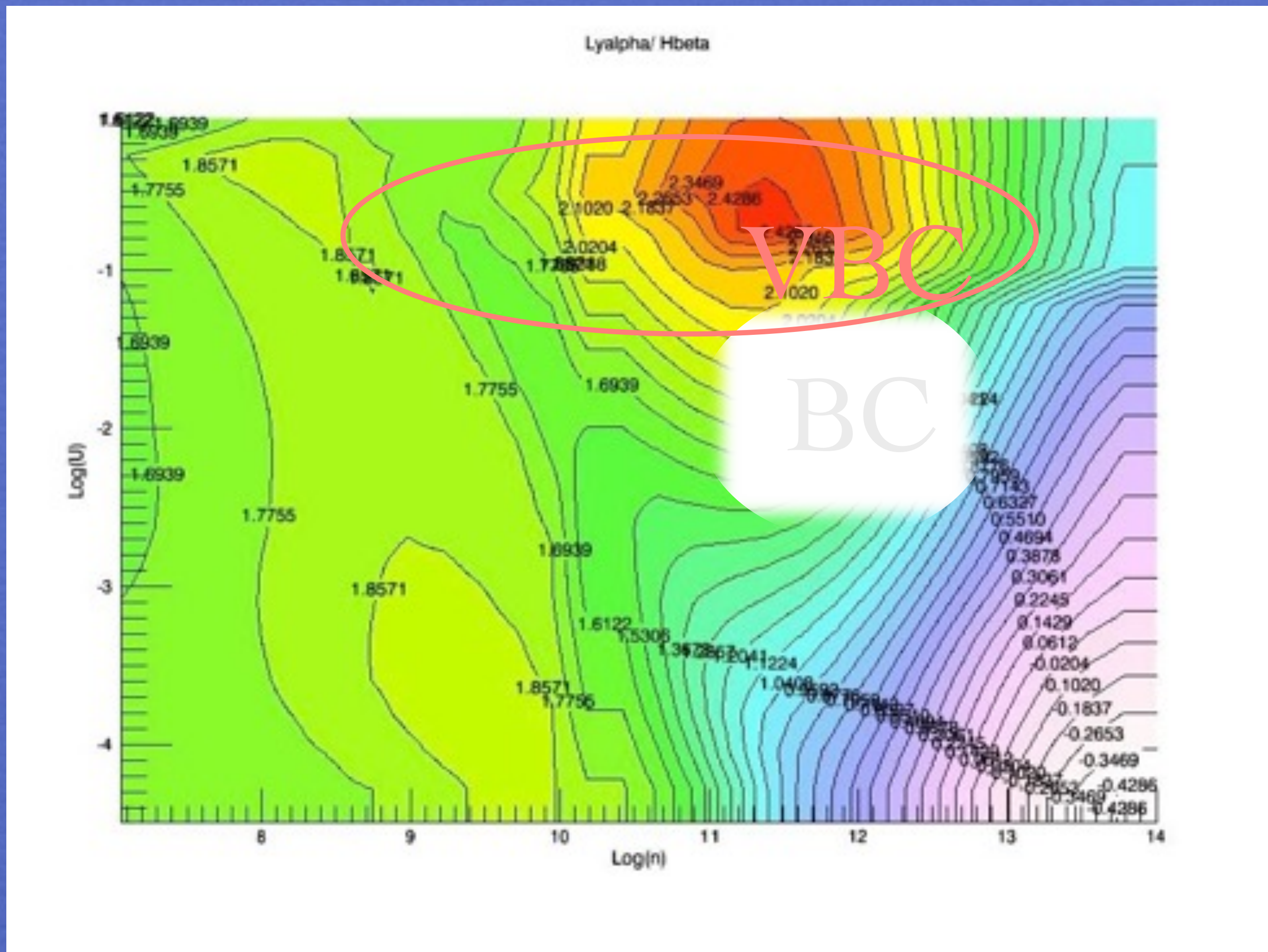
Lyalpha/ Hbeta
VBC
BC
Log(U)
Log(n)

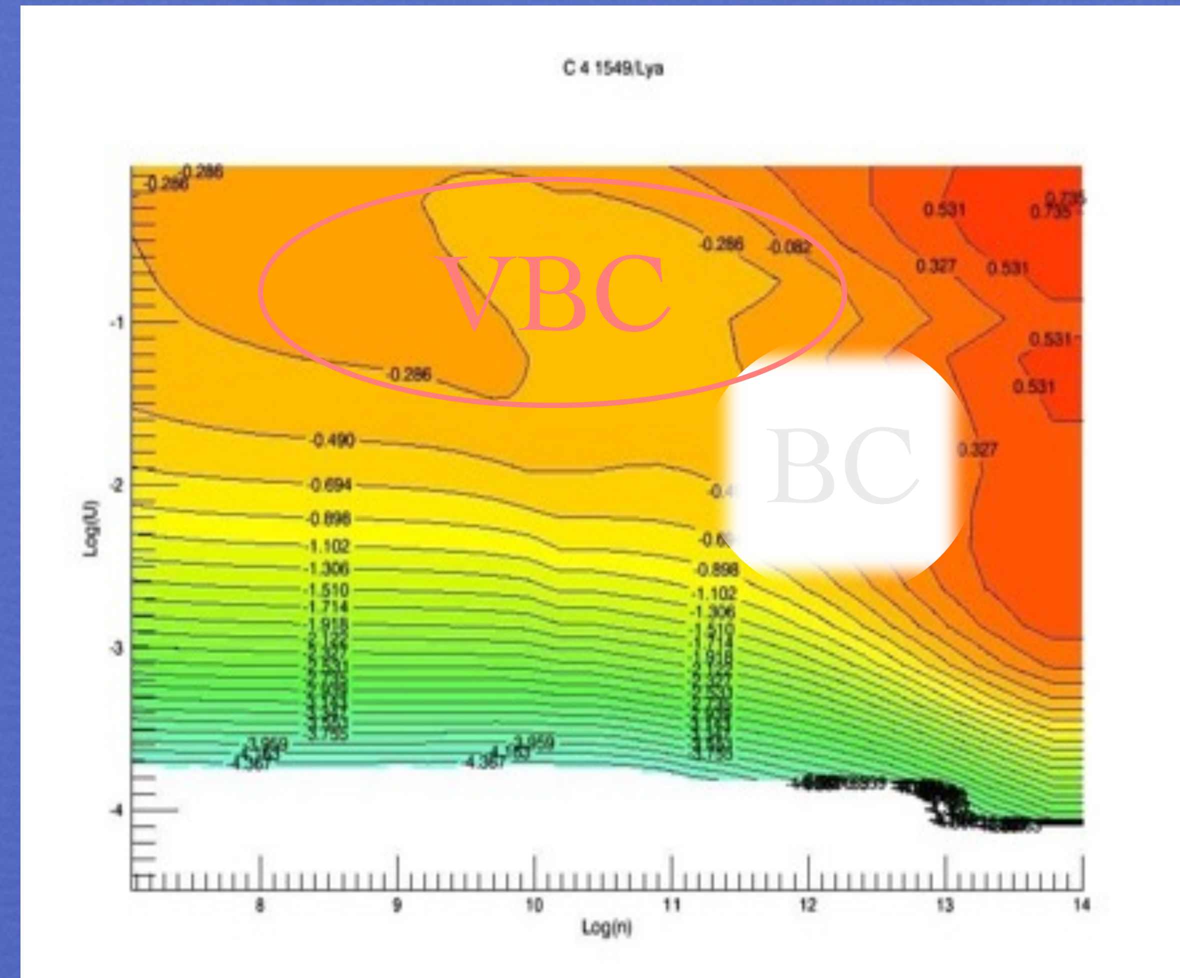
C 4 1549/Lya
VBC
BC
Log(U)
Log(n)

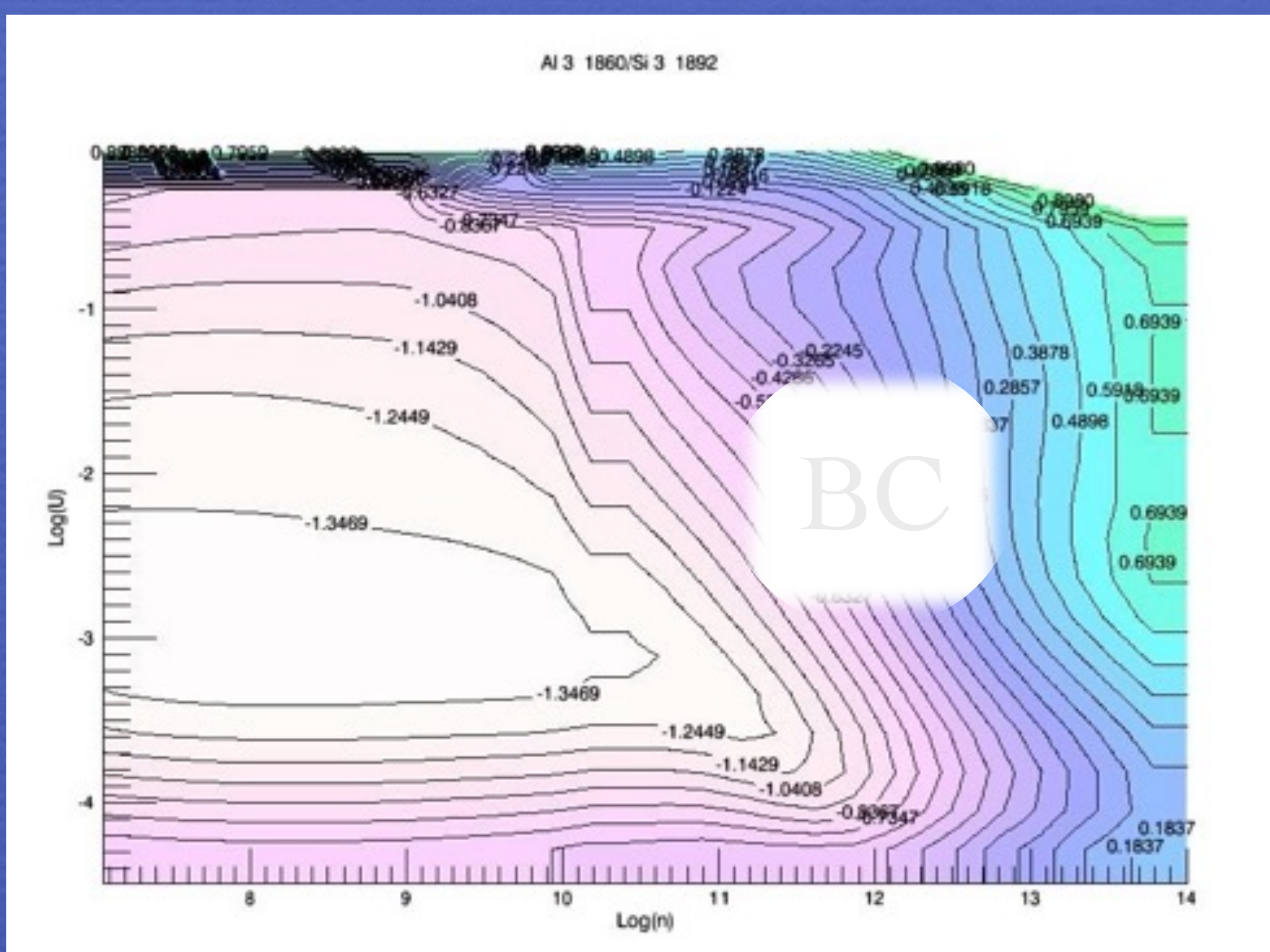
Al 3 1860/Si 3 1892
BC
Log(U)
Log(n)

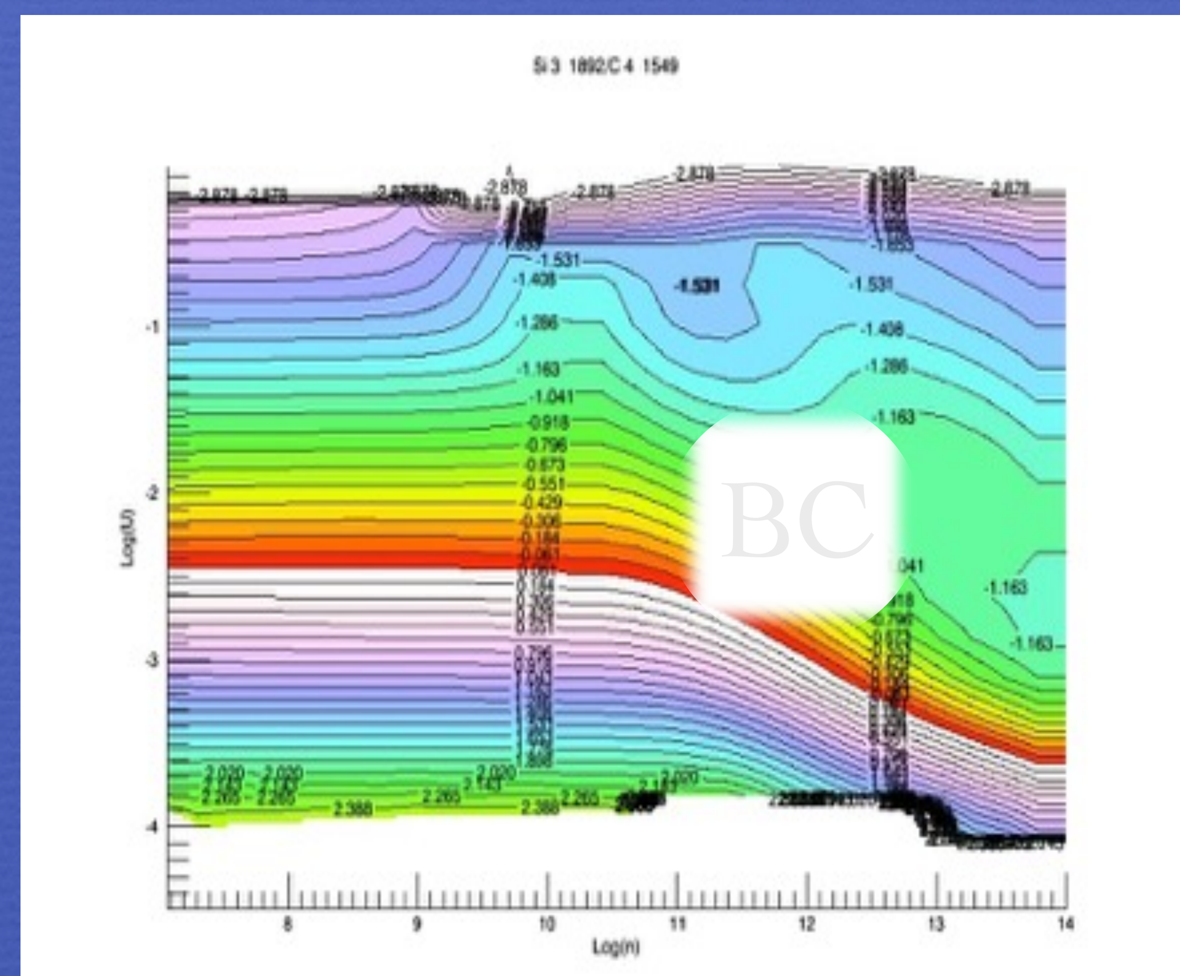
Si 3 1892/C 4 1549
BC
Log(U)
Log(n)

Table 4. BLUE: FWHM ~ 7000 km s^{-1}, Δv_r ~ −3000 km s^{-1}.

Sp. T.	Name	Intensity ratio				W^a
		C IV/ Lyα	He II/ C IV	Hα/ Hβ	Lyα/ Hβ[b]	Lyα
A3	I Zw 1	0.25	0.41	4.2	~18	60
A2	Mrk 478	0.66	0.17	–	≳46	15
A1	Mrk 335	0.45	0.67	–	≳32	16
B1	Fairall 9	1.05	0.14	–	≳46	30
B1$^+$	3C 249.1	0.59	0.17	–	≳32	53
B1^{++}	3C 110[c]	–	–	–	–	0

[a] EW in Å.
[b] Lower limits to Lyα/Hβ are estimated by the maximum contribution expected by a component of the same shift and width if peaking at 3σ the noise level. See the text for a detailed explanation.
[c] Consistent with 0 intensity in all lines.

Blueshifted component physical conditions

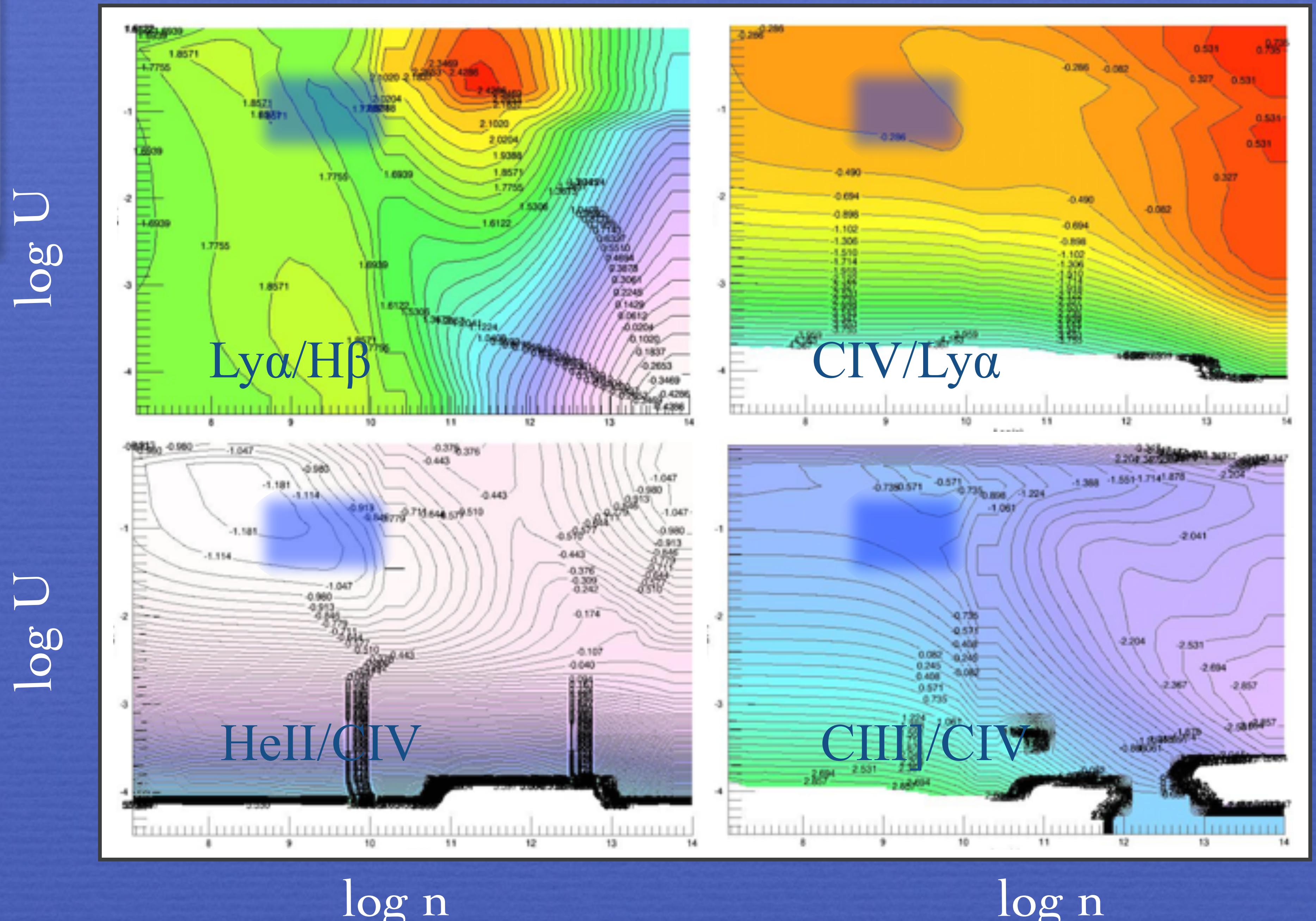

BLUE consistent with high ionization (U~$10^{-1\pm0.5}$) and moderate density (n_H~$10^{9.5\pm0.5}$ cm^{-3})

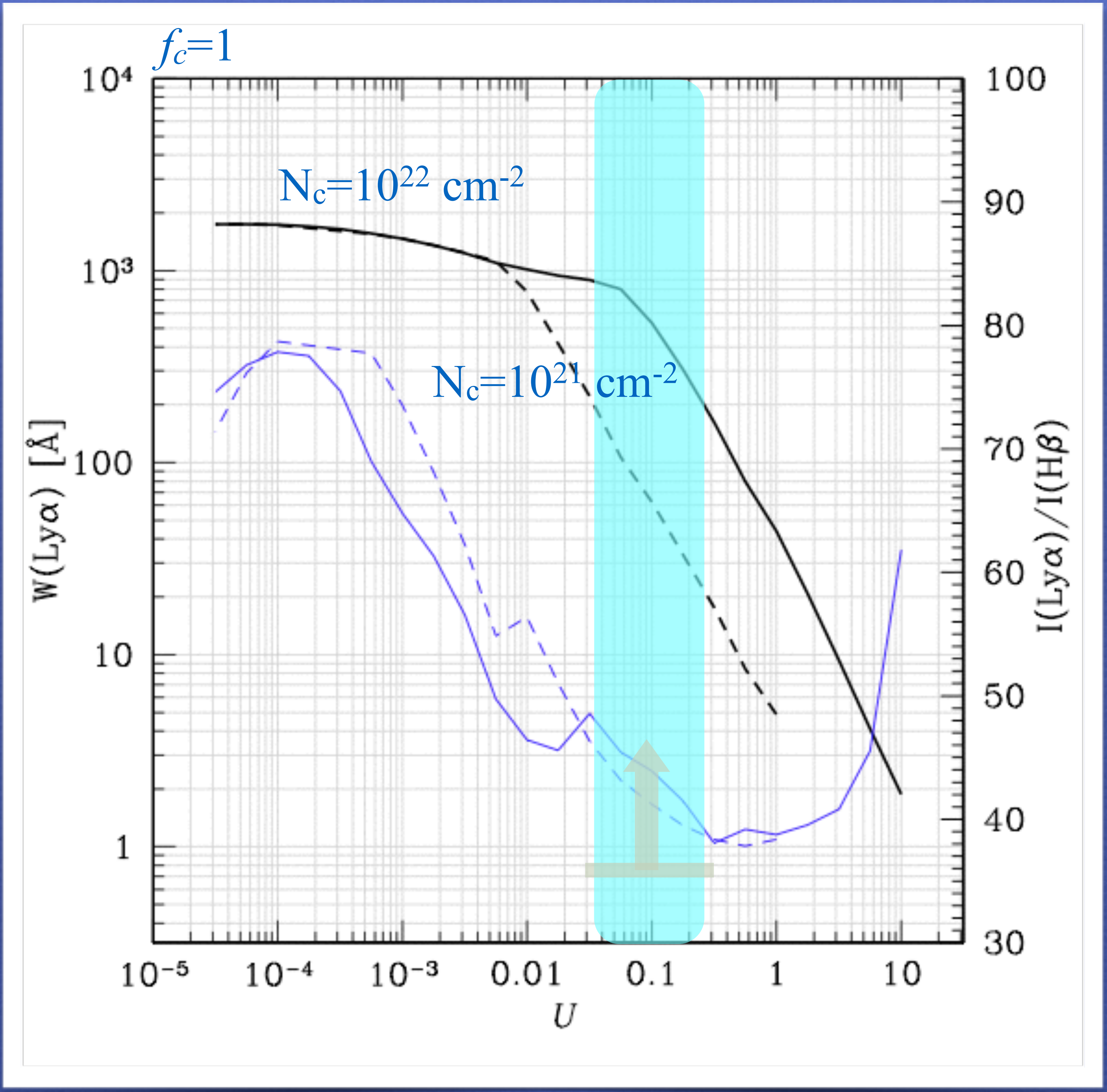

Blueshifted component: large Lyα/Hβ>30

Very different from the other components for which Lyα/Hβ ~ 5 – 10

Matter bounded emitting region?

Interpretation of the heuristic decomposition of the broad profiles: "stratification"

broad component → lower ionization **Broad Line Region**

line broadening predominantly virial; FeII, CaII emission; high density, large column density

very broad component →

high-ionization inner **Very Broad Line Region (VBLR)**

emitting no FeII and showing lower continuuum responsivity

large column density

(Snedden & Gaskell 2007; Goad & Korista 2014).

blueshifted component → outflow/wind

Balance between gravitation and radiation forces

Ferland et al. 2009; Marziani et al. 2010; Netzer & Marziani 2010

$$\frac{a_{\rm rad}}{a_{\rm grav}} \approx 0.088 L_{44} M_{\rm BH}^{-1} N_{\rm c,23}^{-1}$$

$$\frac{a_{\rm rad}}{a_{\rm grav}} \approx 7.2 \frac{L_{\rm bol}}{L_{\rm Edd}} N_{\rm c,23}^{-1}$$

gas cloud trajectories

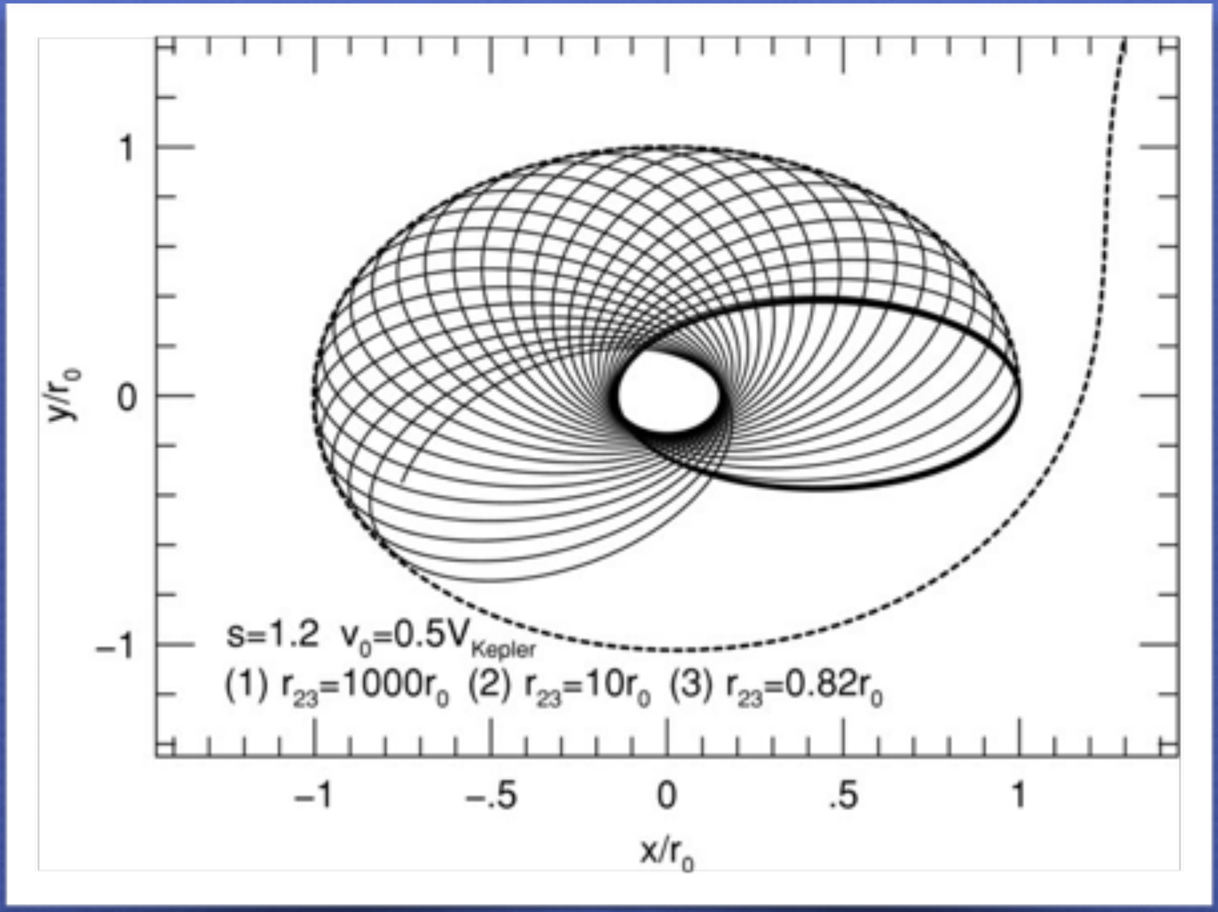

Blueshifted component outflowing: low N_c gas may become unbound

Broad Component stable (virial)

Very Broad Component partly infalling

The 4DE1 approach BLR structure along the MS

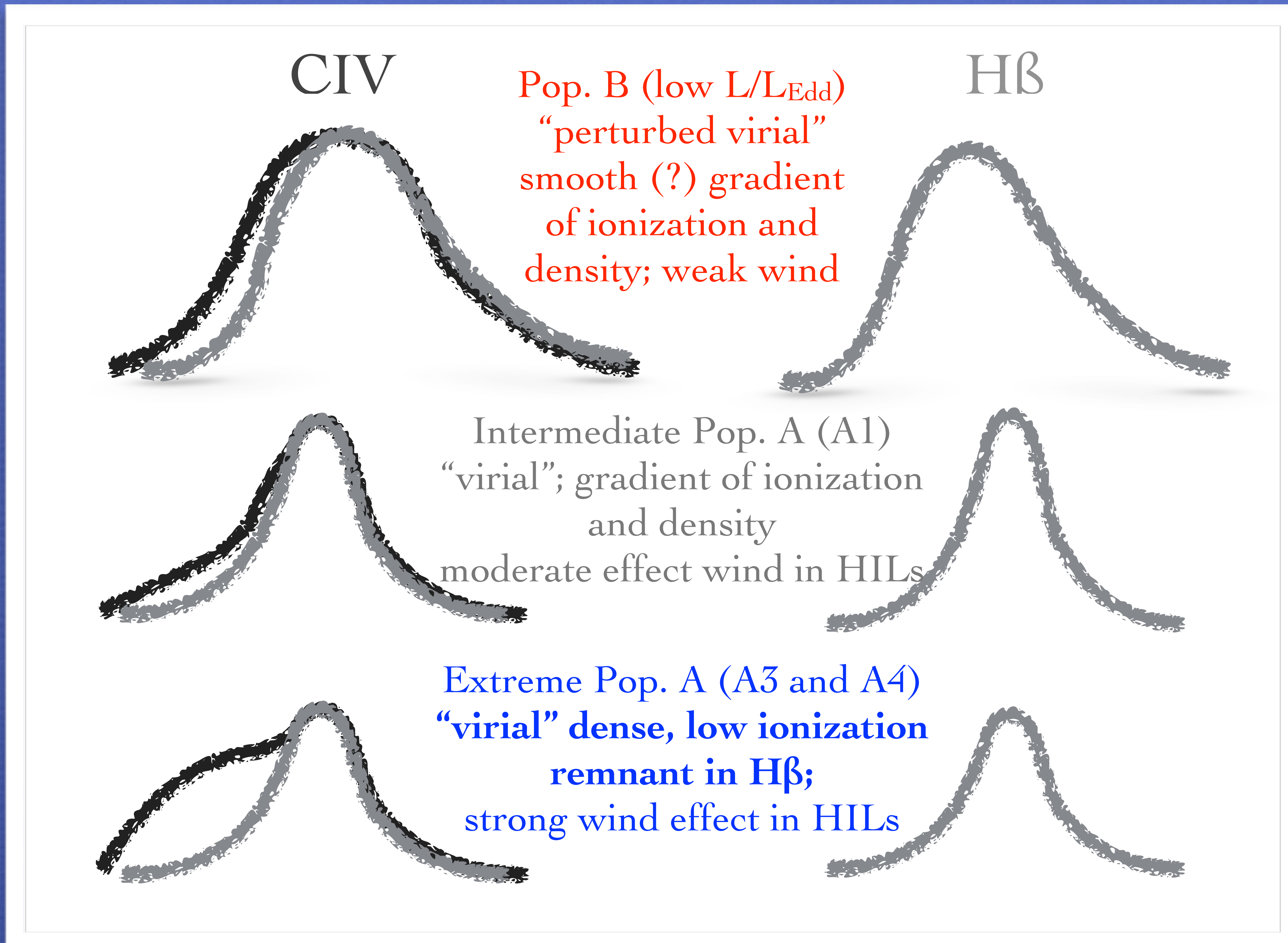

Including non virial components:

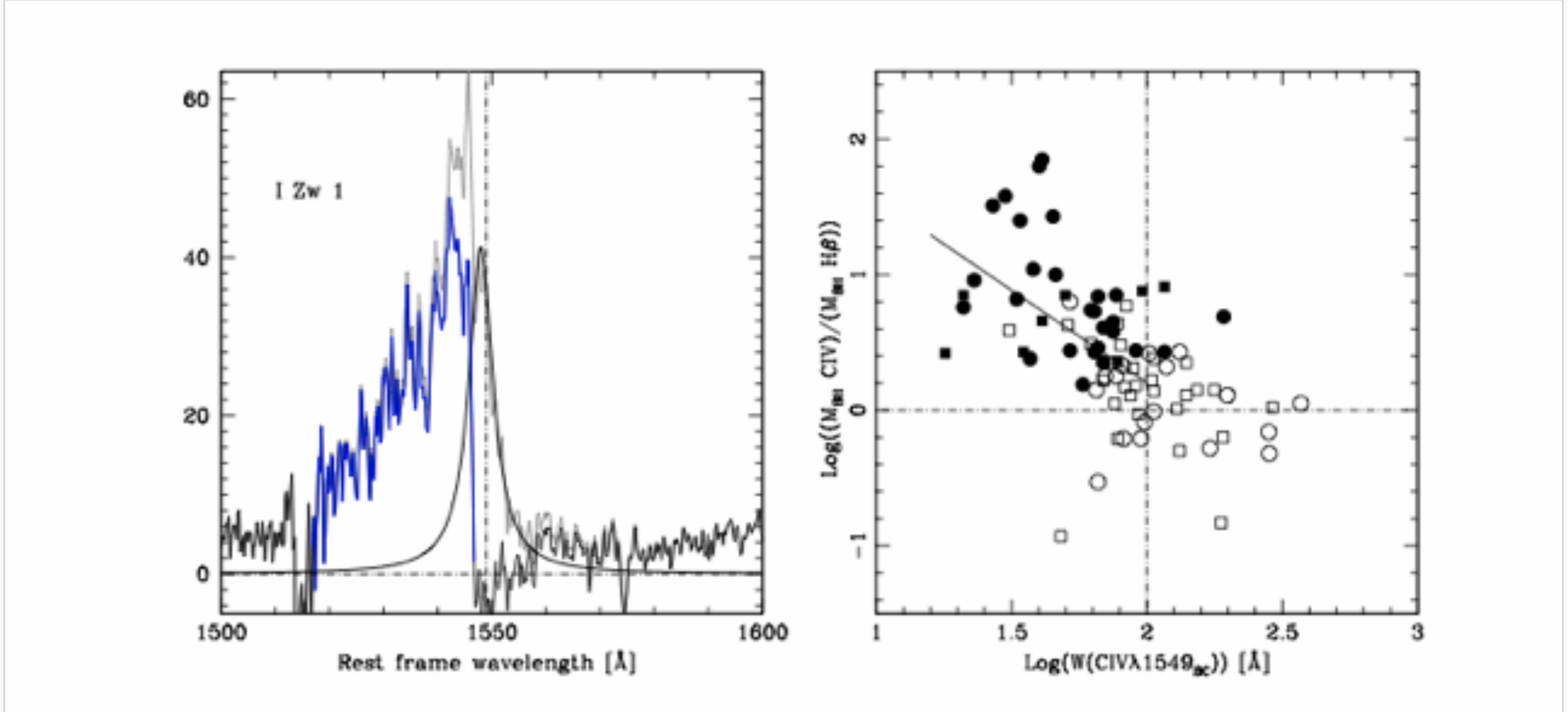

Table 5. Conversion factors.

	$\xi(\mathrm{H}\beta)^{a}$	$\xi(\mathrm{Mg\,II}\lambda2800)^{a}$	Mg II$\lambda2800_{\mathrm{BC}}$/ H$\beta$ obs	Mg IIλ2800 obs/ Hβ_{BC}
A2	1.00	1.00	0.76	0.90
A1	1.00	1.00	0.85	0.96
B1	0.81	0.87	0.66	0.93
B1 CD	0.75	0.82	0.66	1.07
B1 FRII	0.79	0.87	0.71	1.02
B1^{+}	0.82	0.85	0.67	0.97
B1^{++}	0.77	0.95	0.68	0.93

Notes. [a] Conversion factor ξ is the FWHM of BC divided by the FWHM of the full ("observed") profile. The Mg IIλ2800 doublet is treated as a single feature.

Sulentic et al. 2007
Marziani et al. 2013a,b

Dramatic effect for HILs; moderate for LILs such MgII and Hβ

Heuristic models

line-of-sight

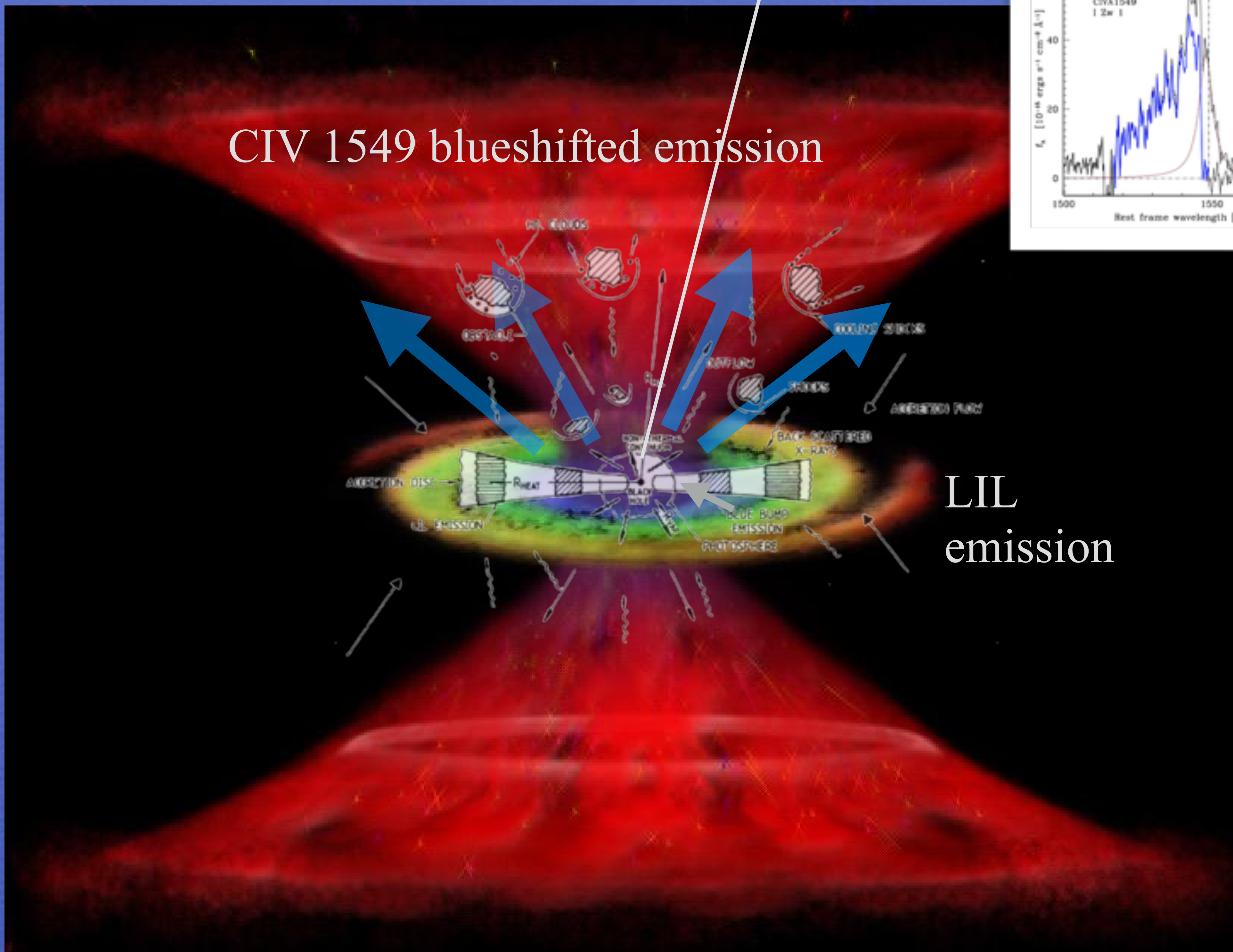

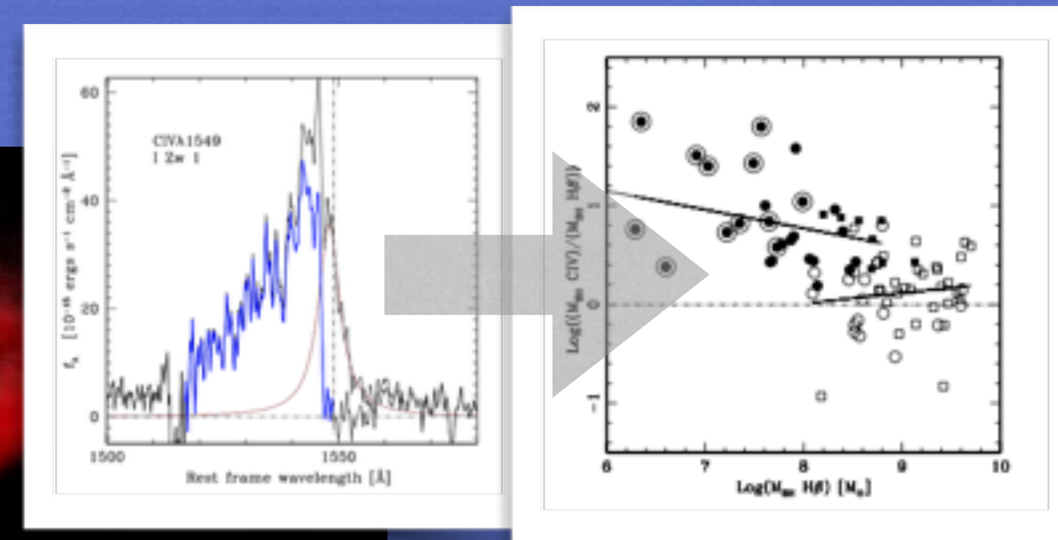

Explain most striking observations of blueshifts in Pop. A sources

Elvis 2000; Collin-Souffrin et al. 1986

The 4DE1 approach Main sequence correlates

At low z(<0.7) Pop. A low mass highly accreting Pop. B high mass accreting at low rate

a reflection of "downsizing" of nuclear activity

Table 1. Main trends along the 4DE1 sequence.

Parameter	Pop. A	Pop. B	References
FWHM(Hβ_{BC})	800–4000 km s^{-1}	4000–10000 km s^{-1}	1,2
$R_{Fe II}$	0.7	0.3	1
c($\frac{1}{2}$) C IV λ1549$_{BC}$	–800 km s^{-1}	zero	3,4
Γ_S	often large	rarely large	1,5
W(Hβ_{BC})	$\sim$80 Å	$\sim$100 Å	1
Hβ_{BC} profile shape	Lorentzian	double Gaussian	6,7,9
c($\frac{1}{2}$) Hβ_{BC}	$\sim$zero	+500 km s^{-1}	7
Si III / C III]	0.4	0.2	10,11
FWHM C IV λ1549$_{BC}$	(2–6) $\cdot 10^3$ km s^{-1}	(2–10) $\cdot 10^3$ km s^{-1}	3
W (C IV λ1549$_{BC}$)	58 Å	105 Å	3
AI (C IV λ1549$_{BC}$)	–0.1	0.05	3
X-ray variability	extreme/rapid common	less common	12,13
Optical variability	possible	more frequent/higher amplitude	14
Probability radio loud	$\sim$3–4%	$\sim$25%	15
Broad absorption lines (BALs)	extreme BALs	less extreme BALs	16,17
log density[1]	> 11	$\sim$9.5–10	10
log U[1]	–2.0/–1.5	–1.0/–0.5	10
log M_{BH}	6.5–8.5	8.0–10.0	7,8
L/L_{Edd}	0.1–1.0	0.01–0.5	7,8

1. Sulentic et al. 2000a; 2. Collin et al. 2006; 3. Sulentic et al. 2007; 4. Baskin & Laor 2005; 5. Wang et al. 1996 6. Veron-Cetty et al. 2001; 7. Marziani et al. 2003; 8. Peterson et al. 2004; 9. Sulentic et al. 2002; 10. Marziani et al. 2001; 11. Wills et al. 1999; 12. Turner et al. 1999 13. Grupe et al. 2001; 14. Giveon et al. 1999; 15. Zamfir et al. 2008; 16. Reichard et al. 2003; 17. Sulentic et al. 2006.

Sulentic et al. 2011

Pop. A/B transition: geometrically thick/thin disk?

Abramowicz et al. 1988, Shakura & Sunyaev 1973

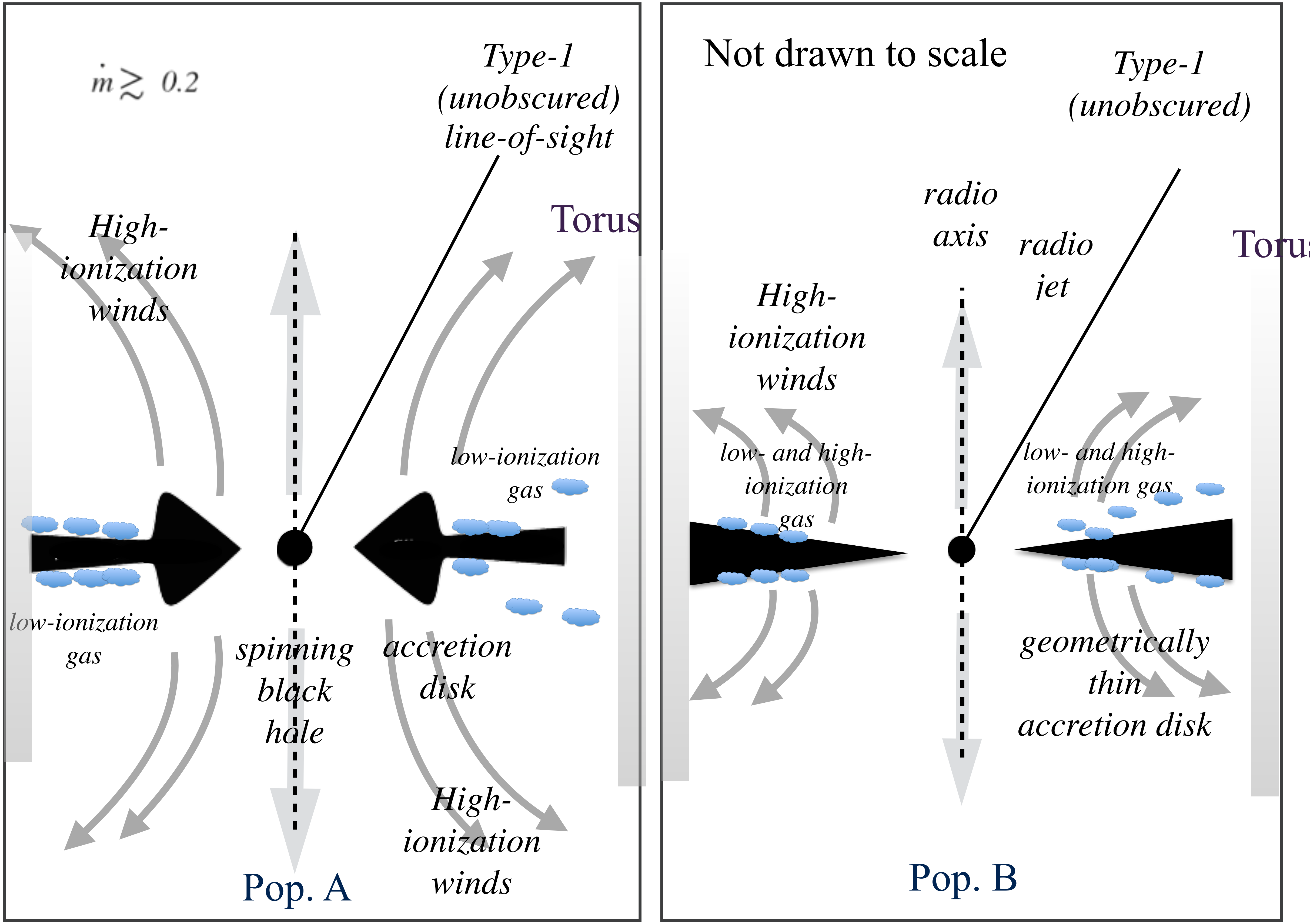

Summary

An MS has been defined in the optical plane of 4DE1 (FWHM Hβ vs. R_{FeII}
constraints if analyzed along the sequence for at least one representative low- and high-ionization line. An outflow component strongly varies along the sequence.

The main governing factor is apparently
of orientation. High
affects the relative prominence of high- and low- ionization "virialized" components.

There is evidence favoring a discontinuity in properties at FWHM Hβ 4000 km/s: Pop. A / Pop. B ("virial /disk"or "outflow/ wind" dominated). This limit may be associated with a structure change in the accretion disk at dimensionless accretion rate 0.1 - 0.2. NLSy1s should be considered as part of Pop. A.

Luminosity effects

Luminosity trends: median composite spectra

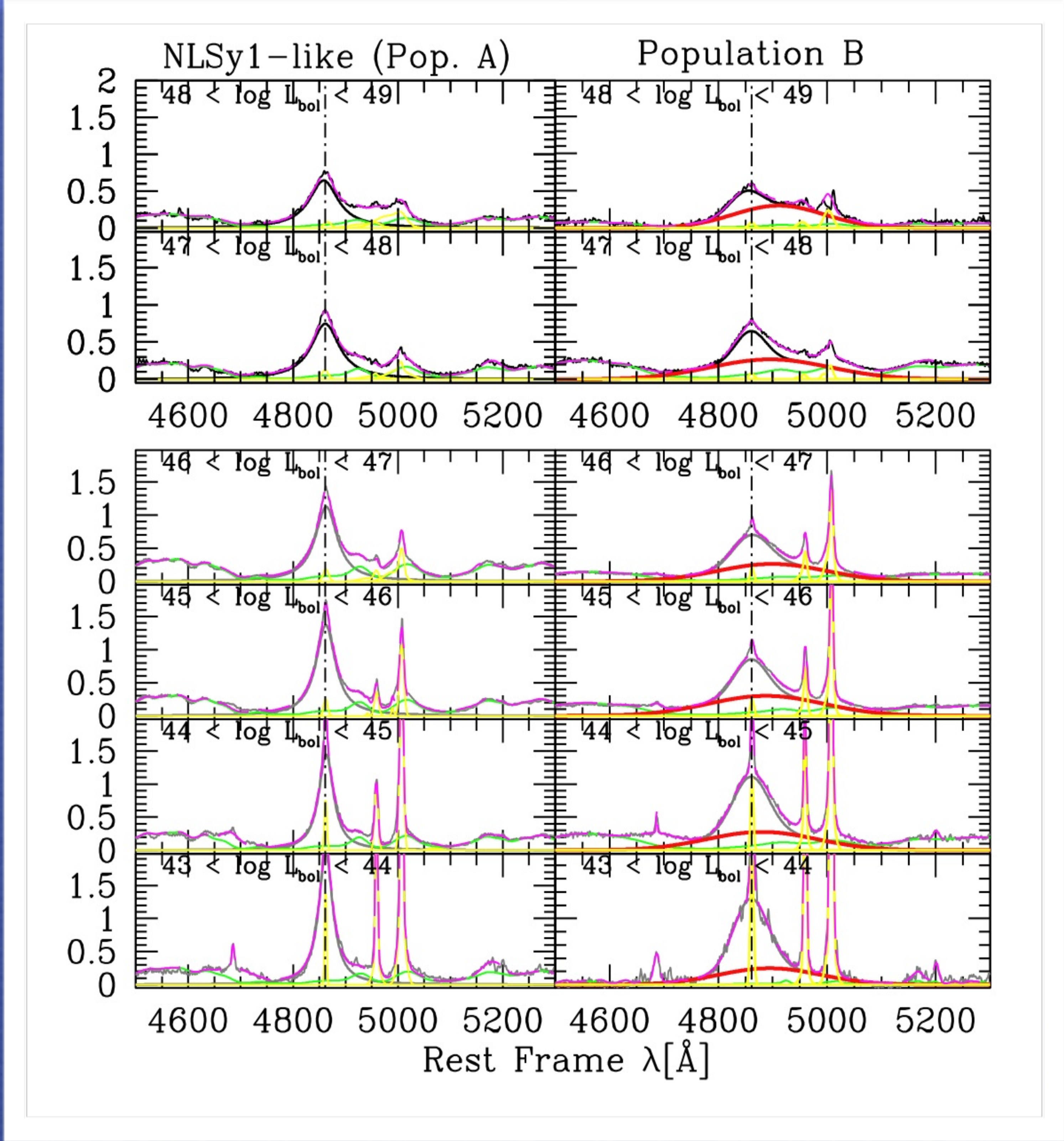

HE/
VLT
ISAAC

The A/B distinction is preserved over a very wide luminosity range

A "Baldwin effect" in [OIII] is evident in both Pop. and B sources.

SDSS,
Zamfir et al. 2010

Luminosity effects Low Ionization Lines

Hb becomes less prominent and broader with *L*

Pop. A Pop. B

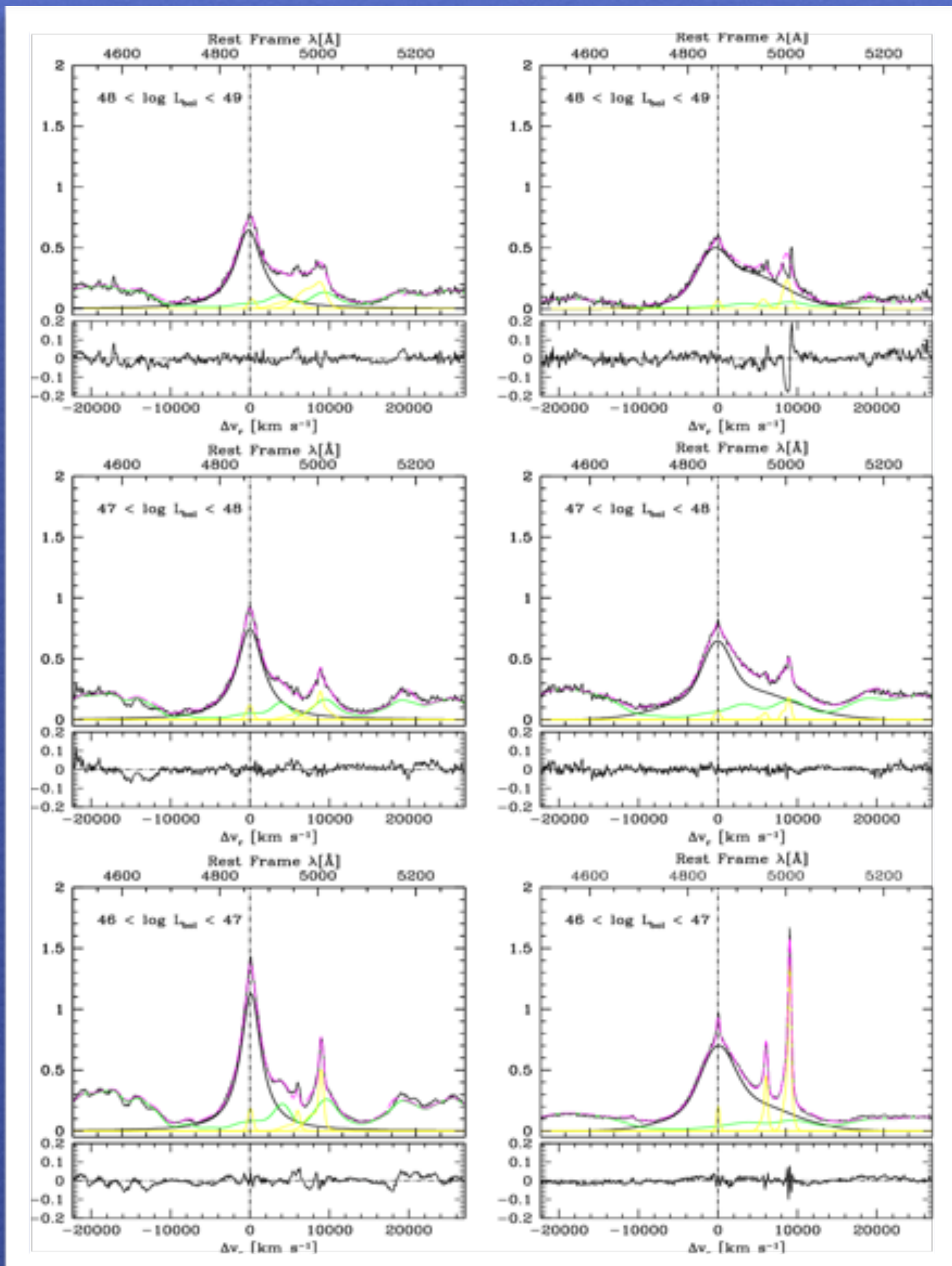

Pop. A Pop. B

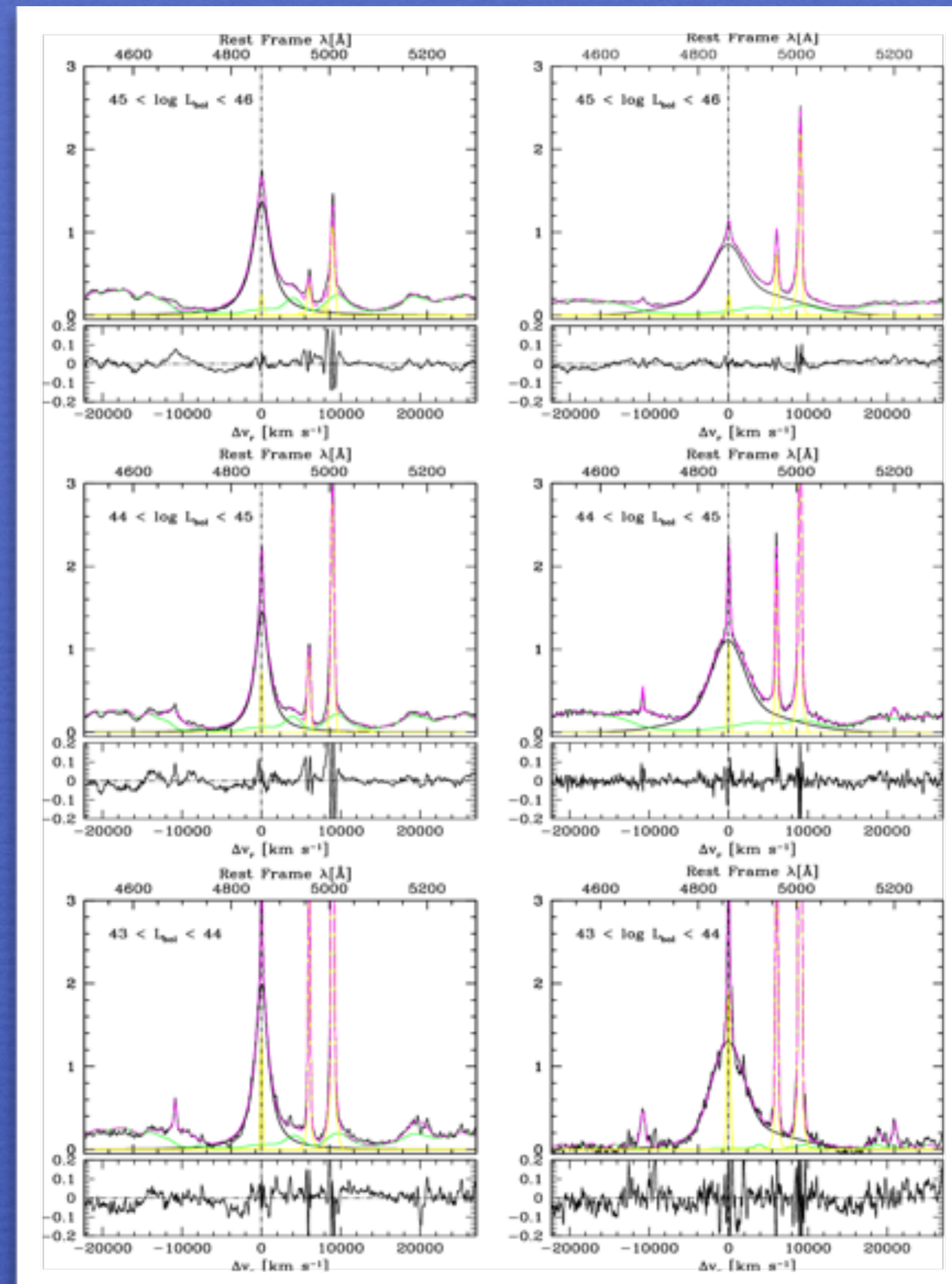

Luminosity effects Low Ionization Lines

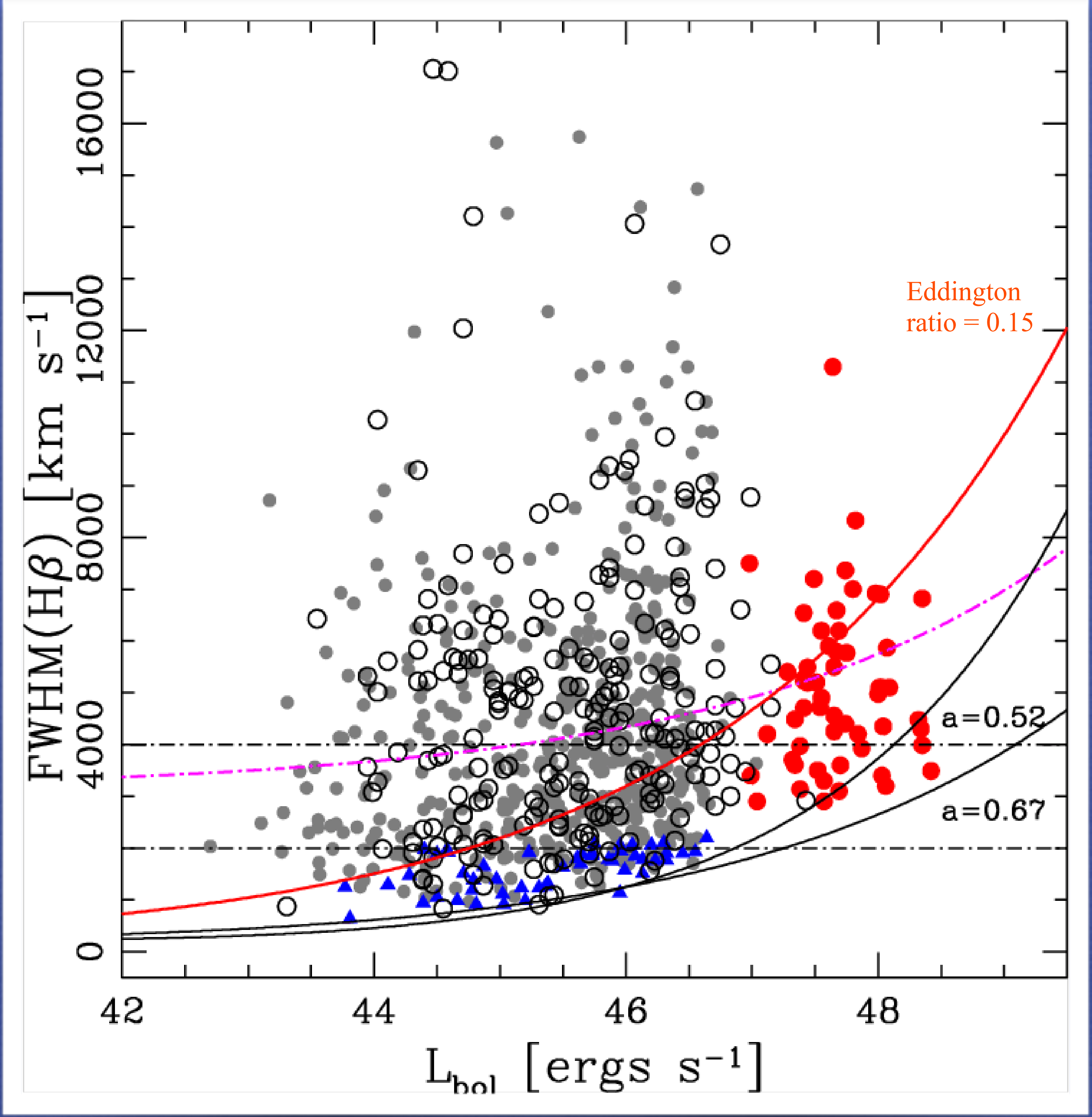

Minimum FWHM(Hβ) consistent with virial assumption and maximum luminosity ad Eddington Limit

The Pop. A limit is luminosity dependent

Curves assume virial relationship with $r \propto L^a$

Marziani et al. 2009

The “Baldwin effect” in CIVλ

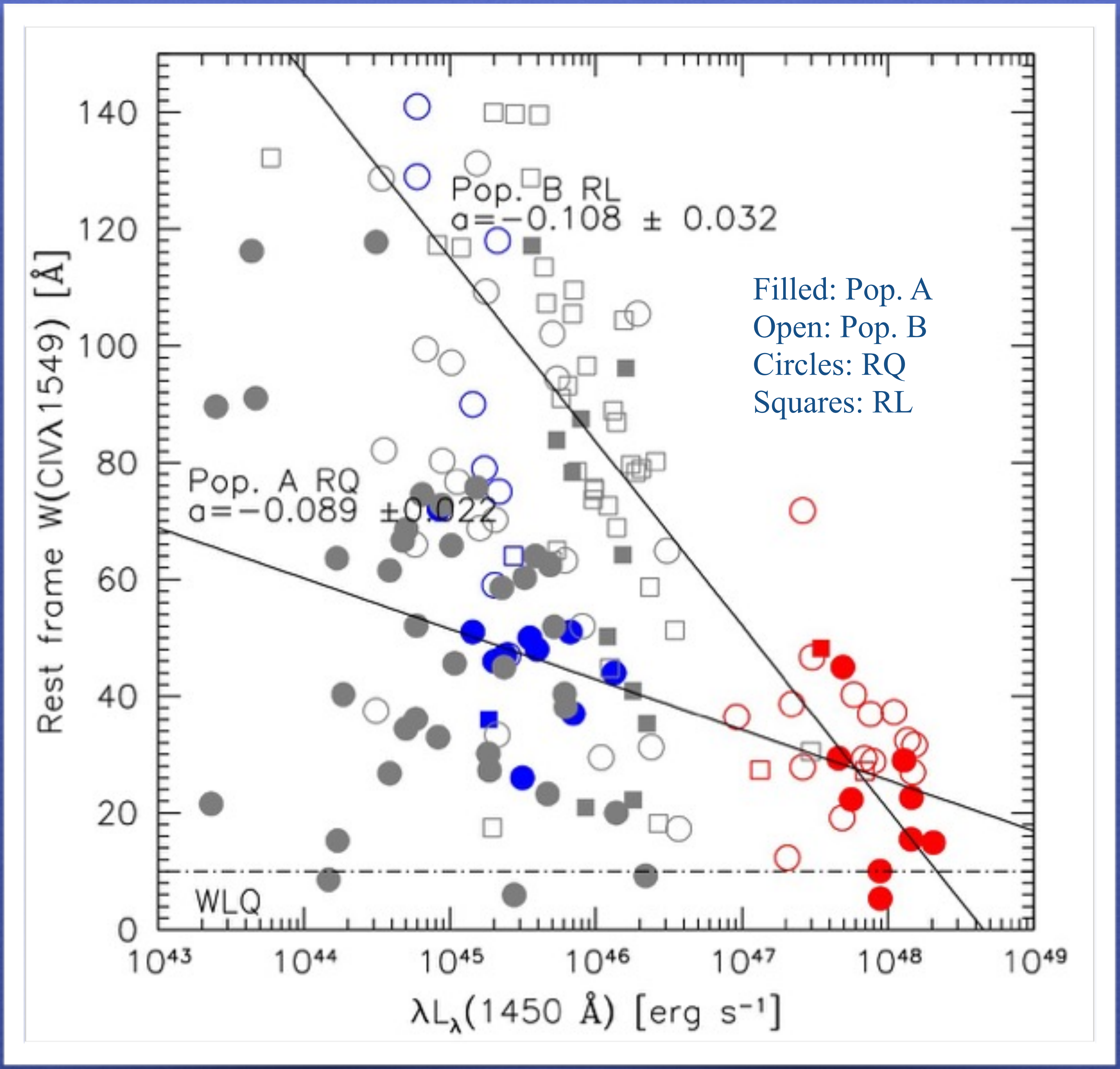

Our samples provide a view consistent with the one of Bian et al. (2005) who used SDSS data

BE explainable by a dependence on Eddington ratio and selection effects

Bachev et al. 2004; Baskin & Laor 2005
Sulentic et al. 2007; Marziani et al. 2008

Luminosity effects High Ionization Lines

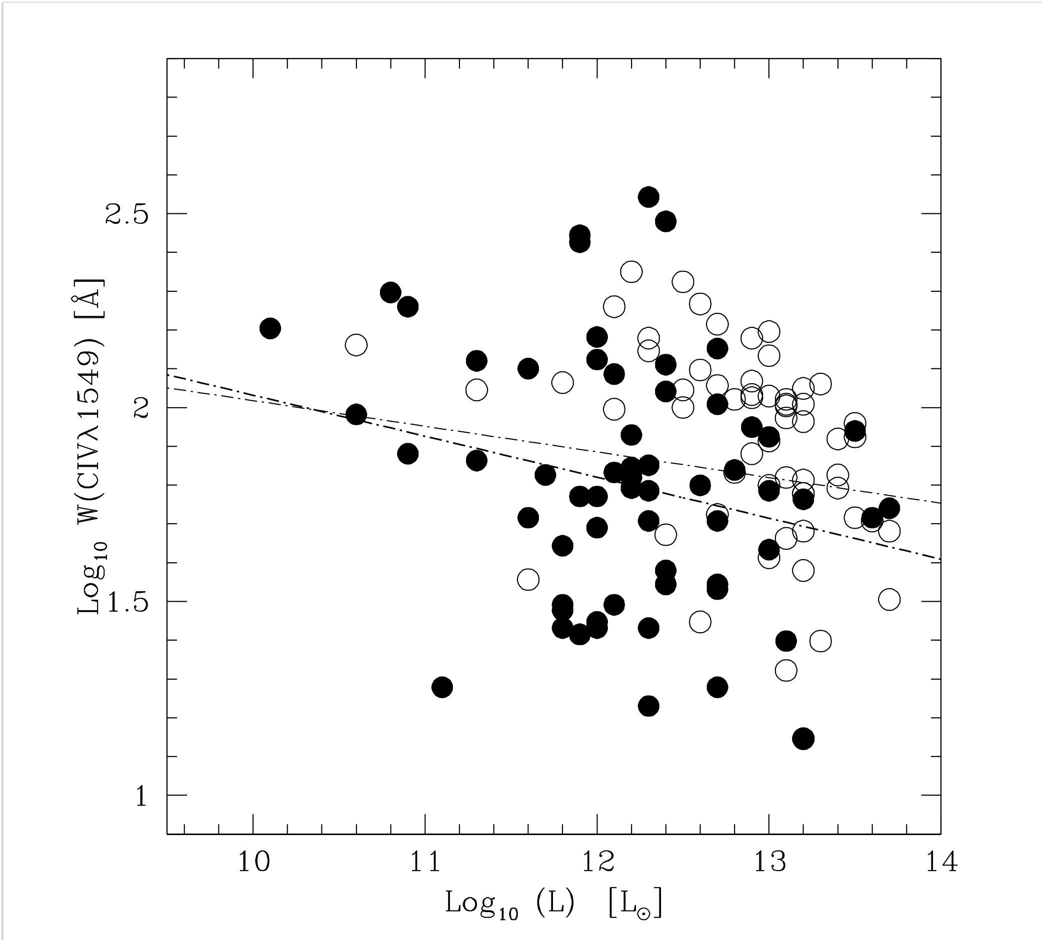

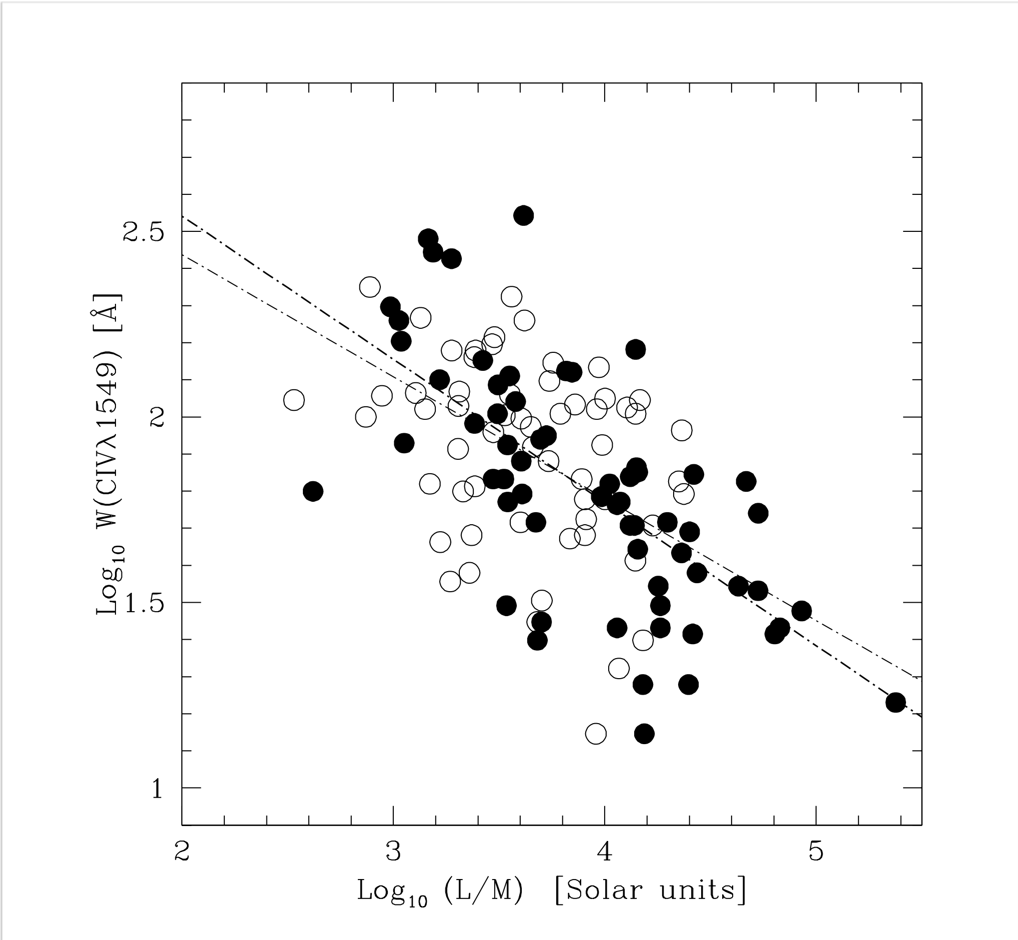

Table 2. The main C IV EW correlations.

Variable Name[a]	r_s[b]	Pr[b]
νL_ν(3000Å)	−0.154	1.71×10^{-01}
	−0.018	9.08×10^{-01}
L/L_{Edd}	−0.581	1.31×10^{-08}
	−0.642	1.53×10^{-06}
α_{ox}	0.525	4.87×10^{-07}
	0.463	1.18×10^{-03}
[O III] λ5007 EW	0.624	4.71×10^{-10}
	0.708	3.67×10^{-08}
Fe II EW	−0.518	7.49×10^{-07}
	−0.536	1.24×10^{-04}
Hβ FWHM	0.427	7.03×10^{-05}
	0.510	2.92×10^{-04}
R [O III] λ5007 peak height	0.624	4.78×10^{-10}
	0.647	1.20×10^{-06}
R Fe II EW	−0.626	4.02×10^{-10}
	−0.698	6.94×10^{-08}
R [O III] λ5007 EW	0.471	9.23×10^{-06}
	0.494	4.89×10^{-04}

Bachev et al. 2004; Baskin & Laor 2005; Sulentic et al. 2007; Marziani et al. 2008

Baldwin effect: dependence on Eddington ratio is stronger

Luminosity effects: High Ionization Lines

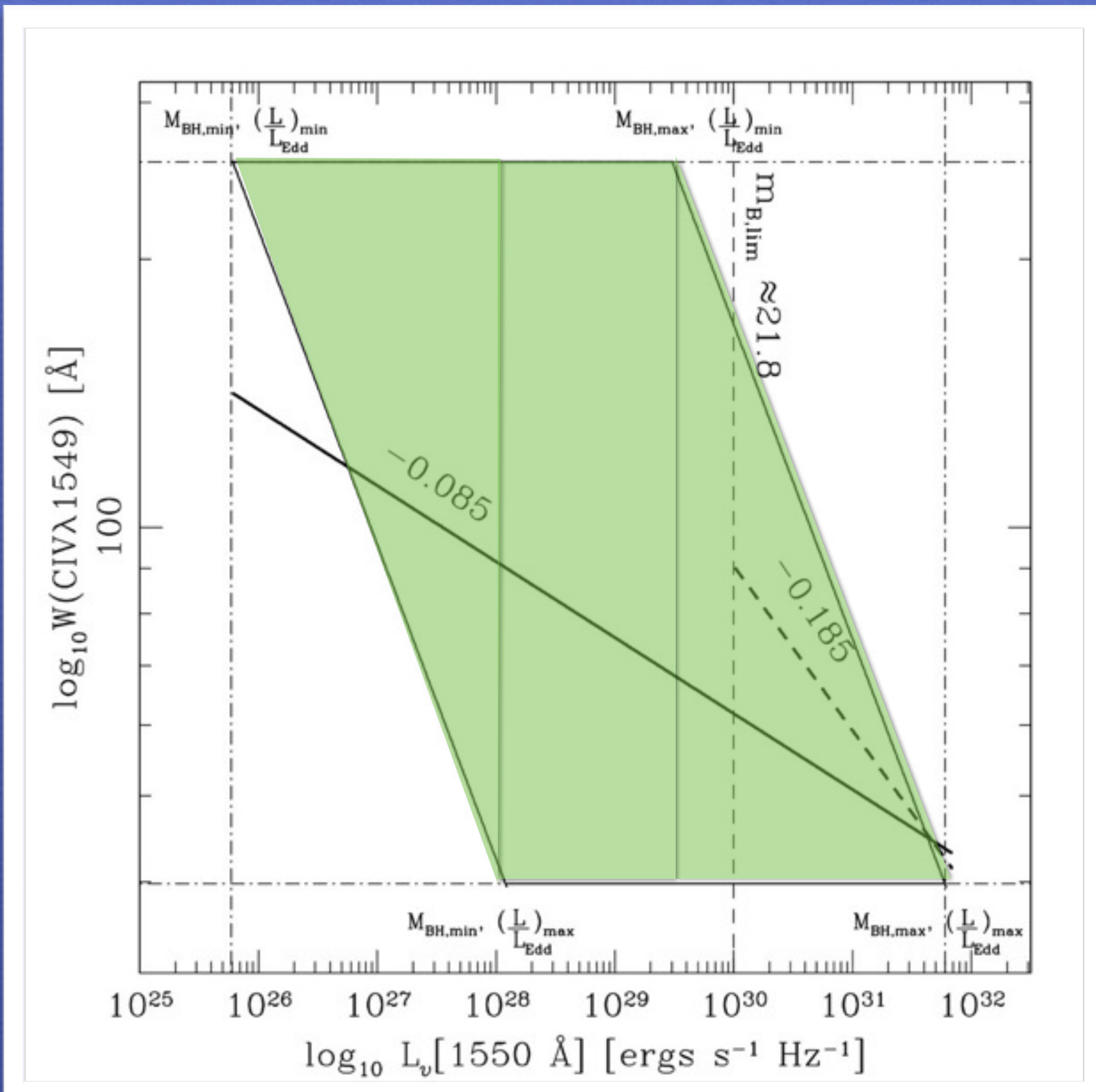

The Baldwin effect can be accounted for assuming an L/M distribution as observed for low-*z* quasars and the relation between L/M and W(CIVλ1549)

A slight anticorrelation is expected even in a volume limited sample; it becomes steeper if the sample is flux limited

Large blueshifts are apparently more frequent at high L but shift amplitudes at lower L are comparable

$\frac{c\left(\frac{1}{2}\right)}{HWHM(H\beta)}$ "Dynamical relevance" of CIVλ1549 shift

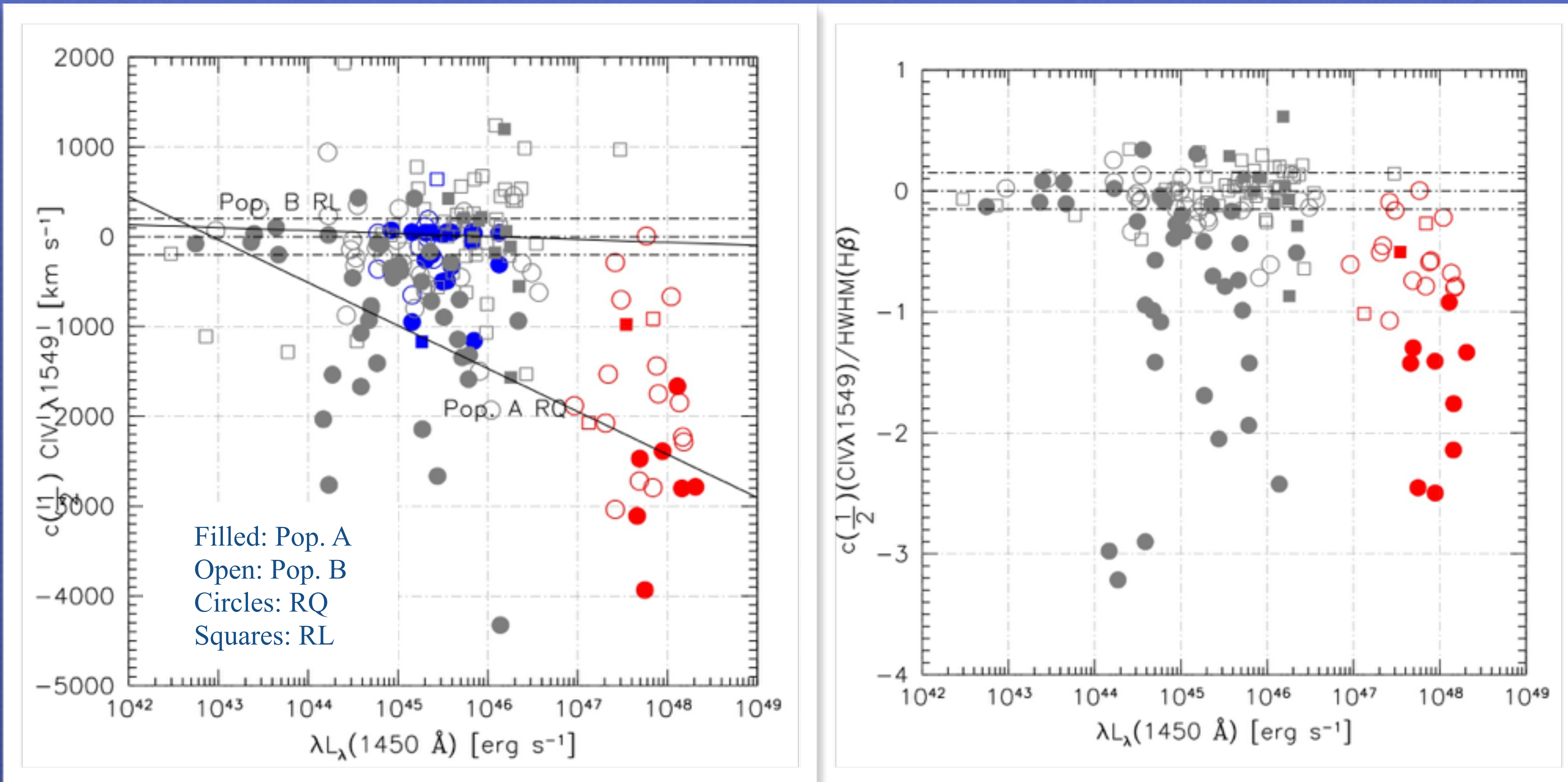

High-L HE quasars in the optical plane of the 4DE1

Luminosity (Mass) effect visible in a systematic increase of the minimum FWHM possible for a sub-Eddington radiator

FOS

c(1/2)≤-1000
-300 ≥c(1/2) > -1000
-300 < c(1/2) ≤ 300
300 < c(1/2) ≤ 1000
c(1/2) > 1000

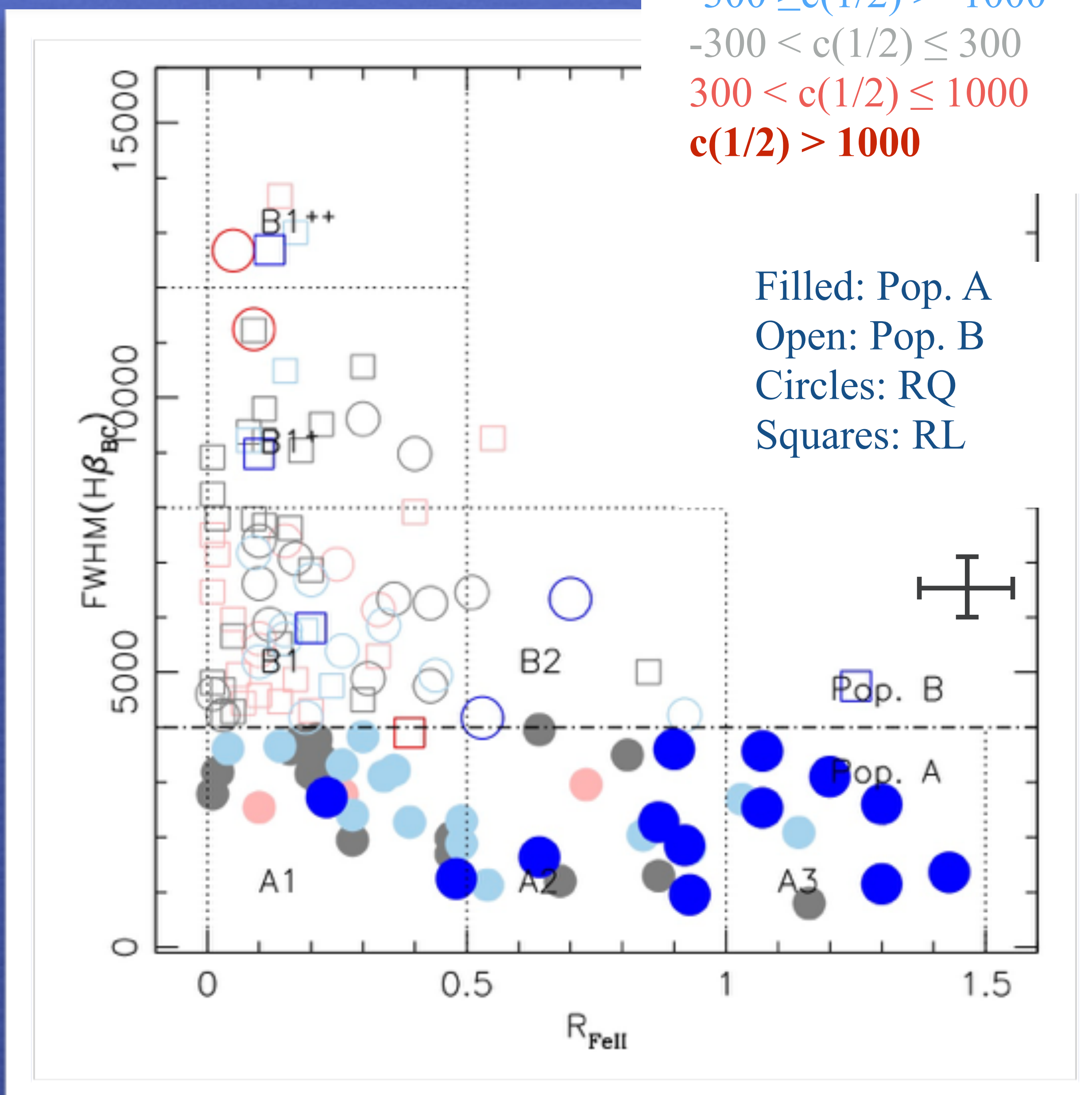

HE

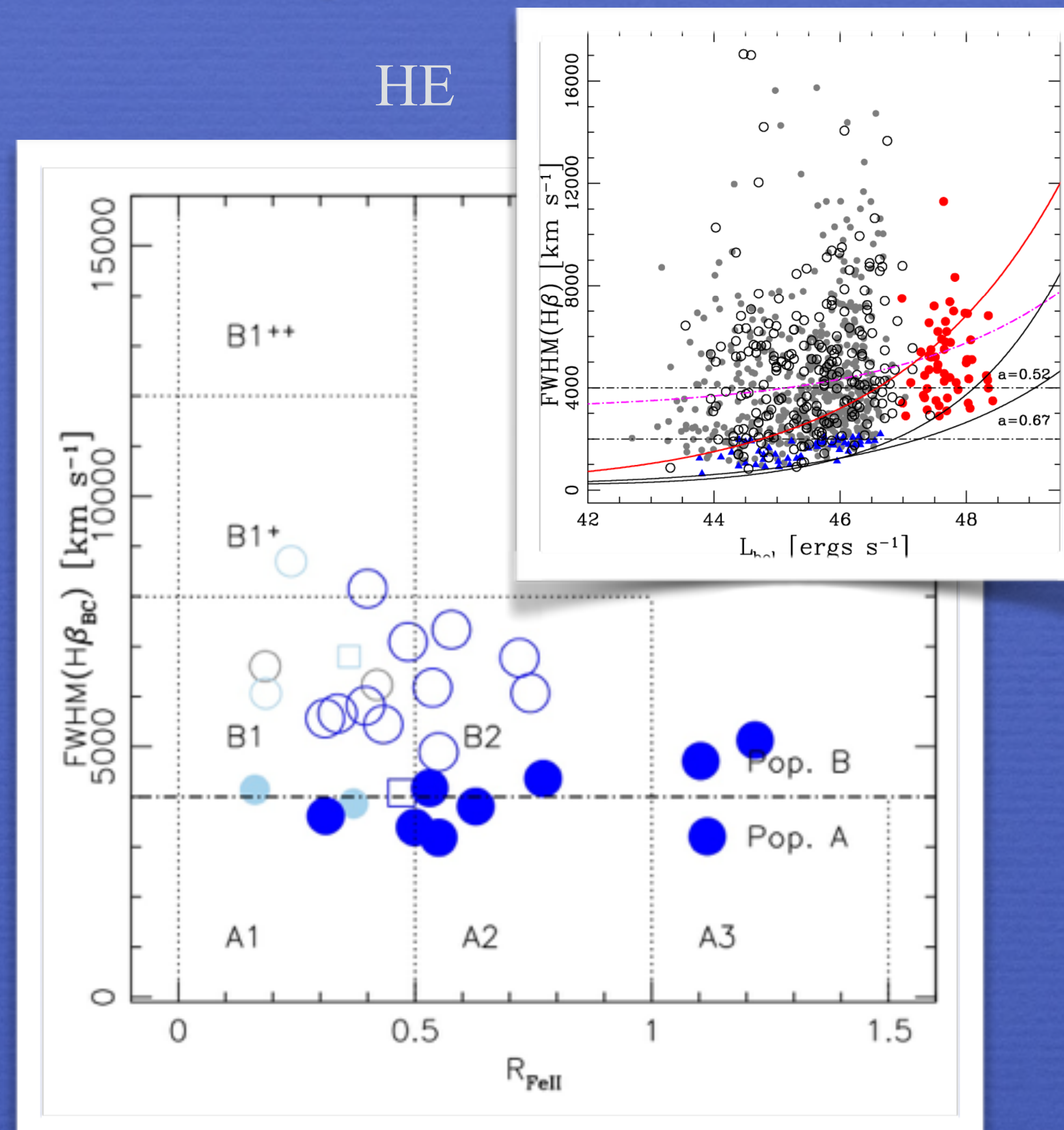

Outflows appear to be a self similar phenomenon over a wide range in L

Larger L implies a displacement of the MS toward larger FWHM(Hβ) i.e., larger masses

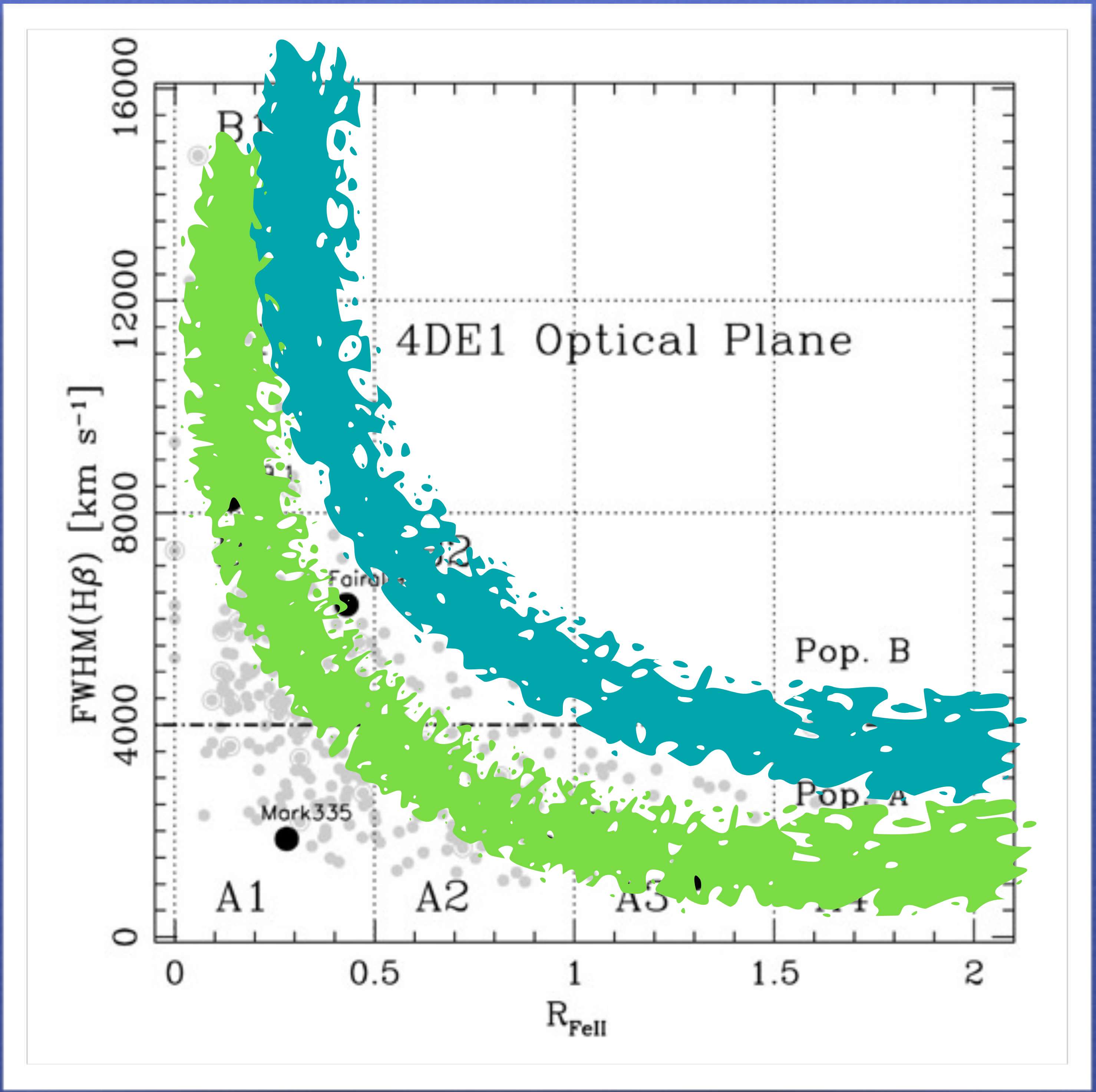

The 4DE1 approach: Weak Line Quasars

Weak Lined Quasars (WLQs)

Low equivalent width of CIVλ1549 (≤10 Å) and Lyα (≤16 Å)

Diamond-Stanic et al. 2009

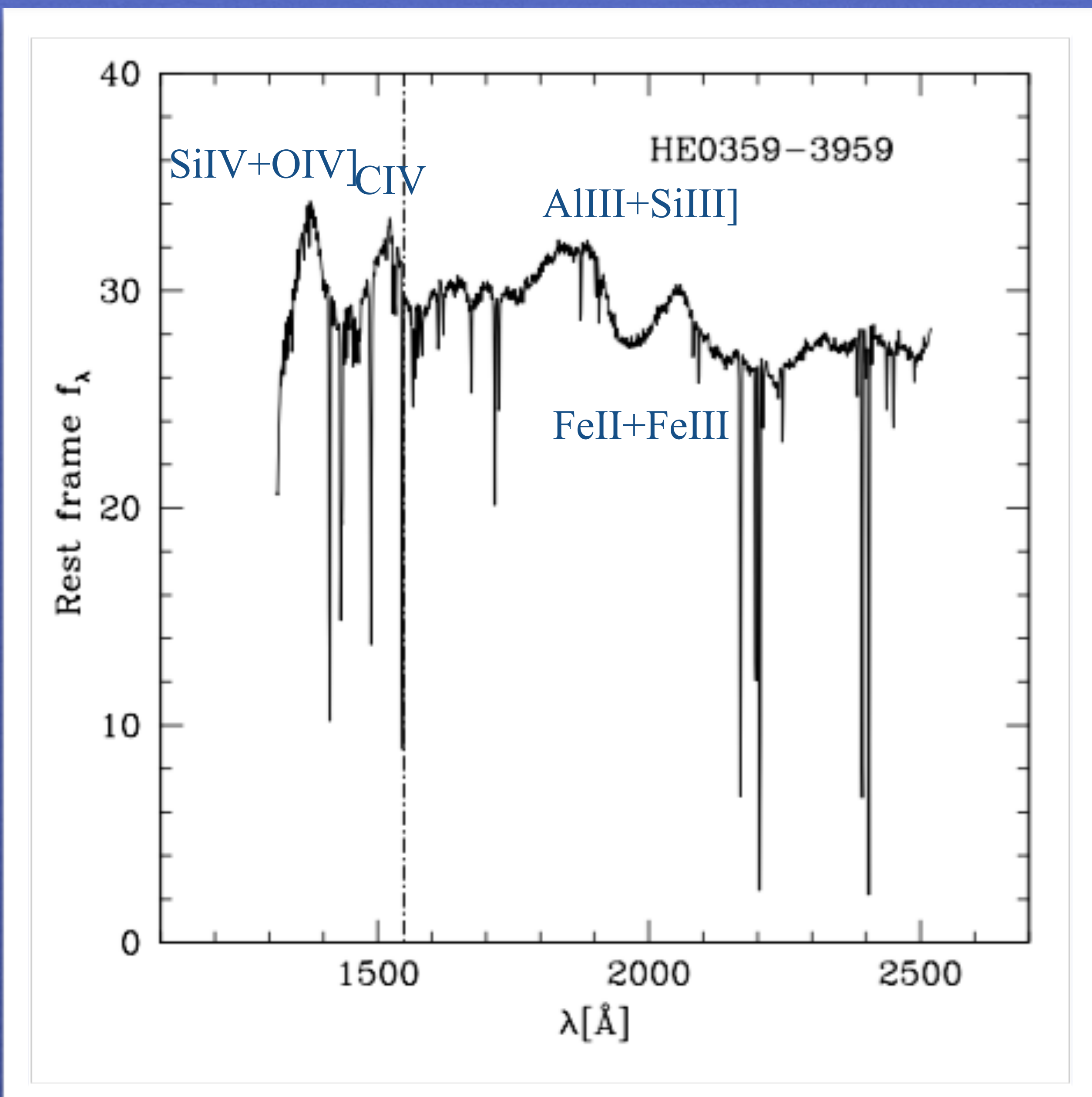

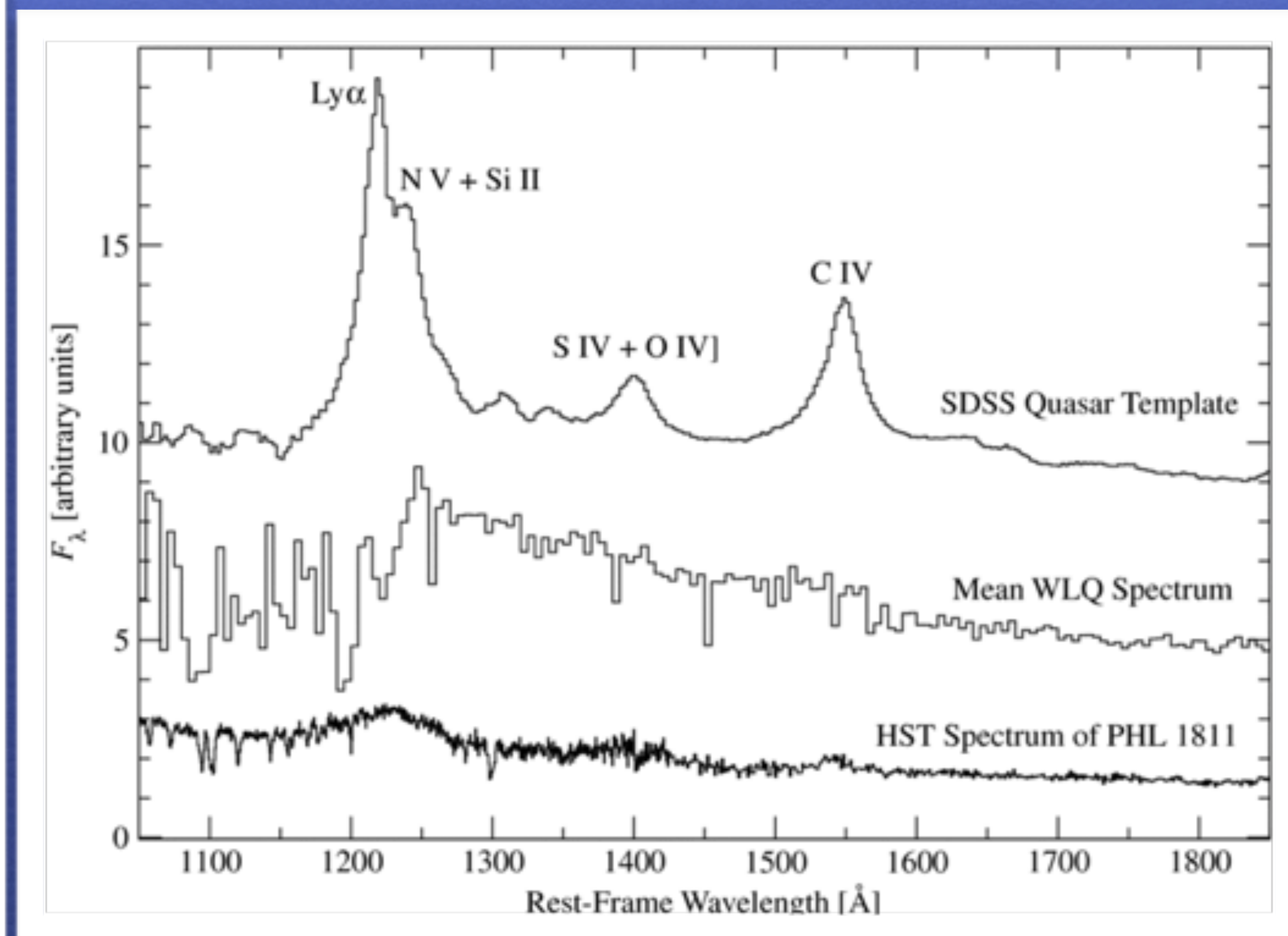

Shemmer et al. 2009

The 4DE1 approach: WLQs

CIVλ1549 profiles show extreme blueshifts

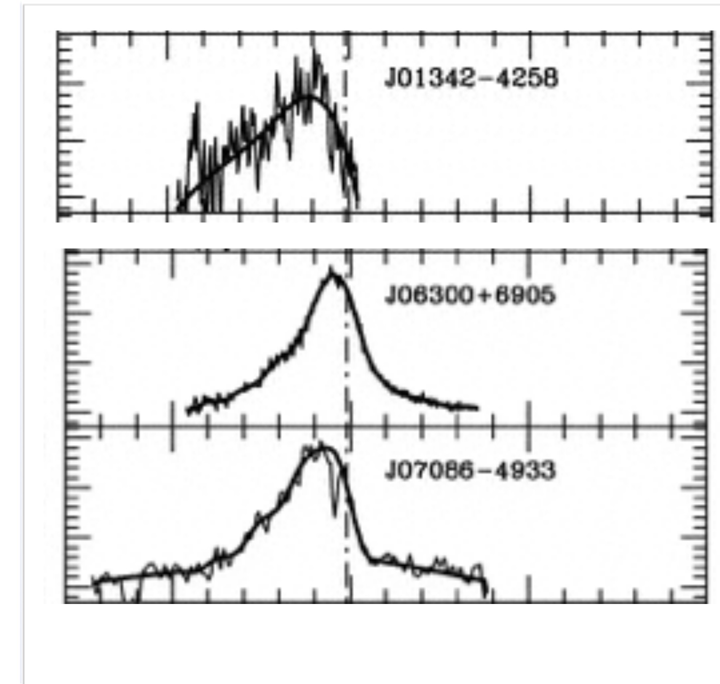

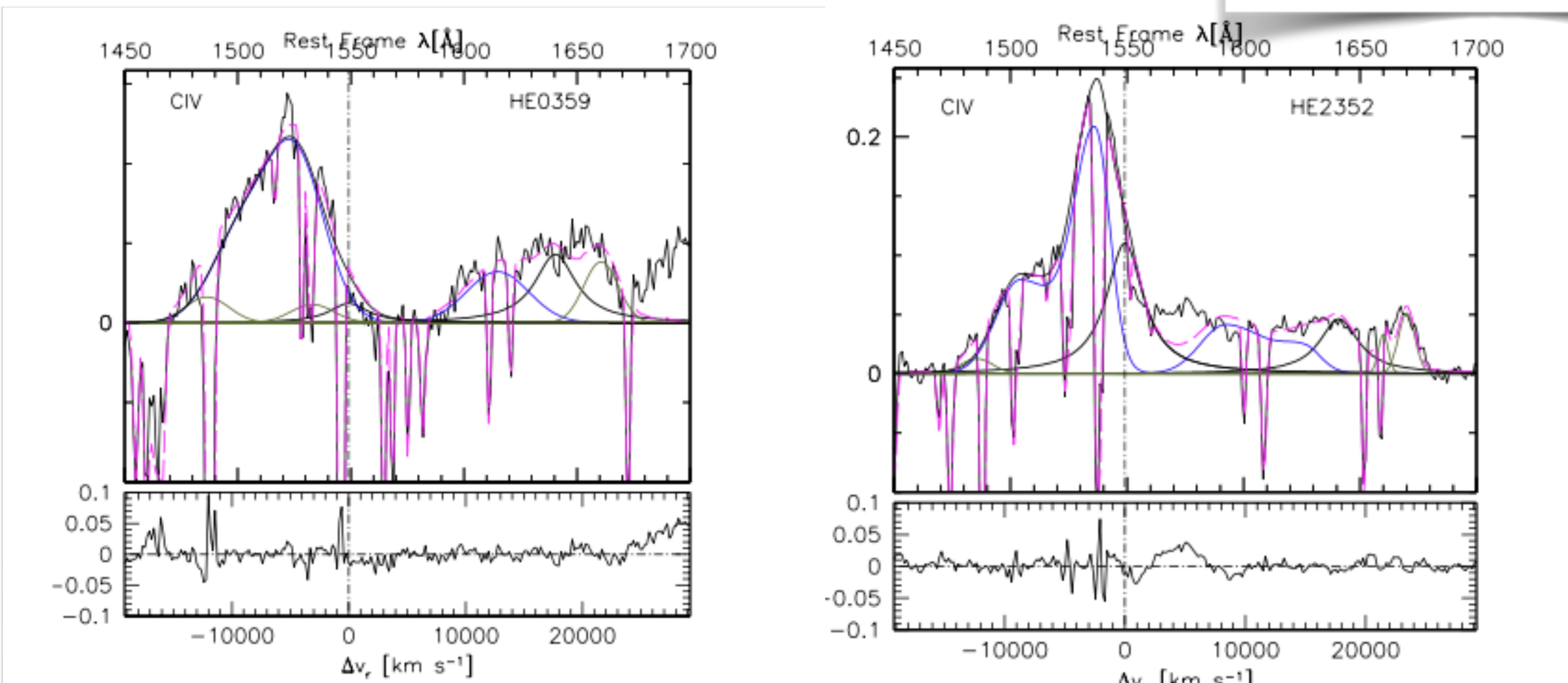

The 4DE1 approach: WLQs

W(CIVλ1549) vs CIV shift

W(CIV) vs CIV shif

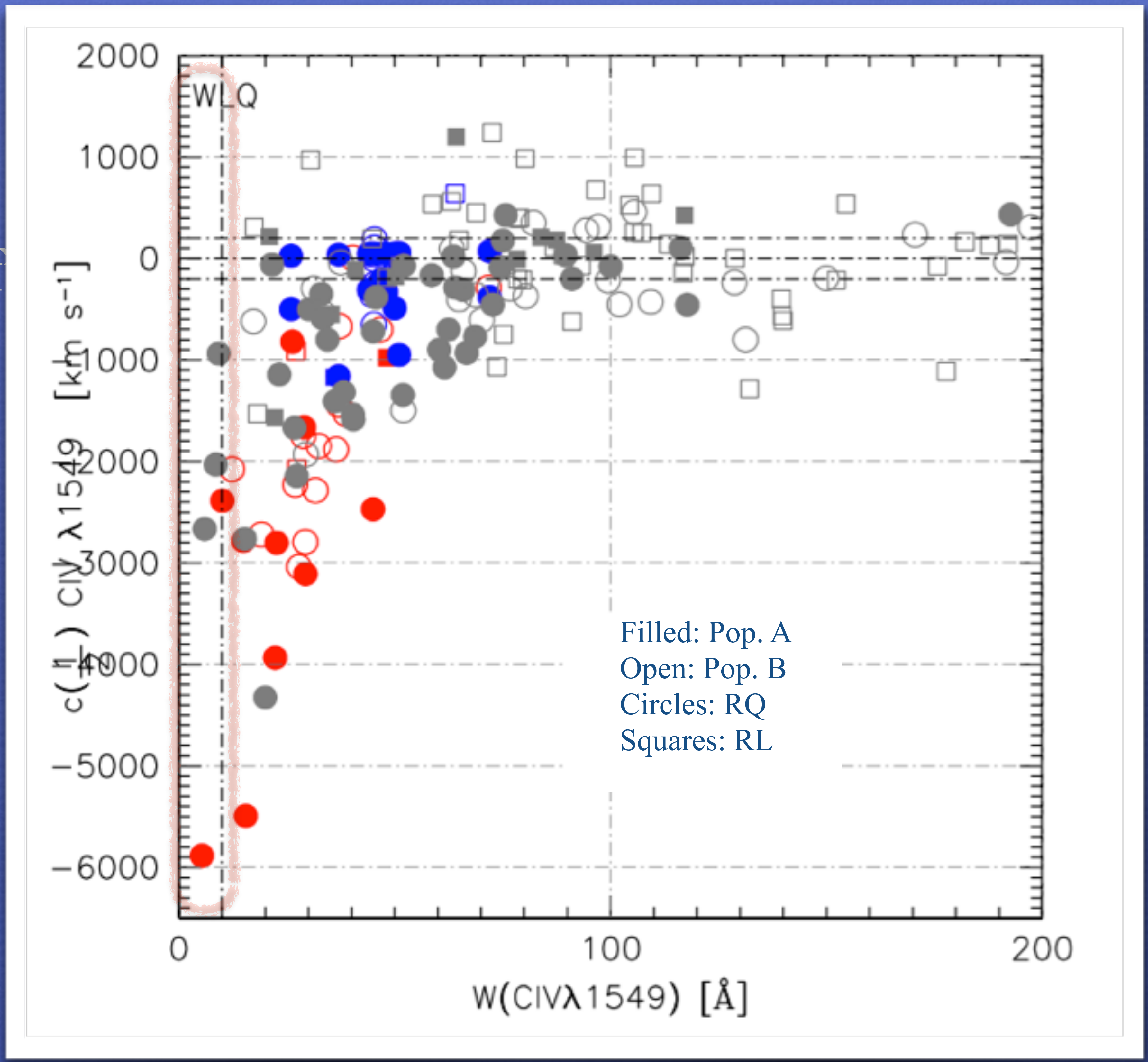

WLQs in the optical plane of 4D Eigenvector 1

Most —all of the ones at high-*z* — are extreme Pop. A sources with $R_{FeII} > 1$, with CIV showing extreme outflow velocities

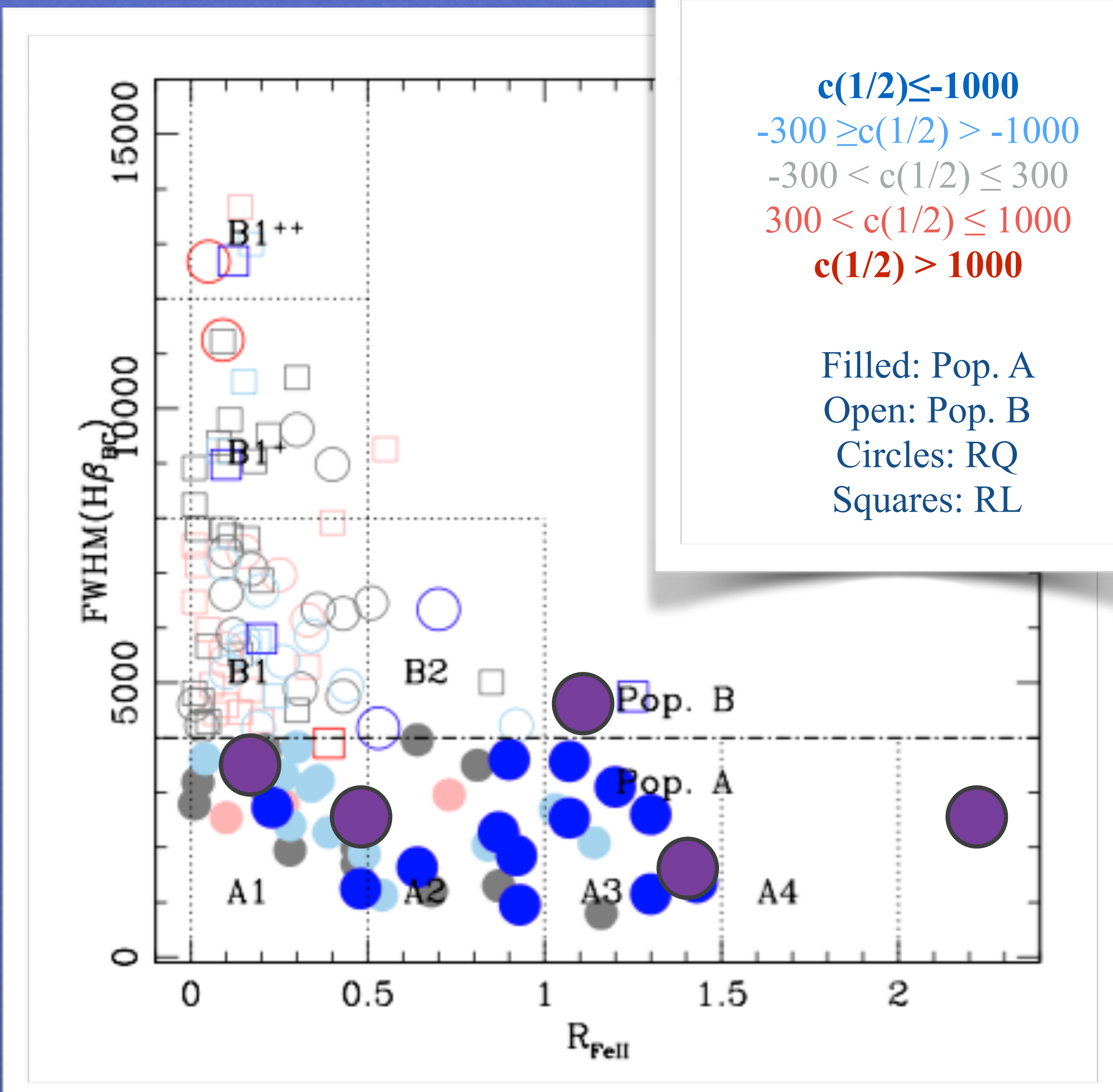

c(1/2)≤-1000
-300 ≥c(1/2) > -1000
-300 < c(1/2) ≤ 300
300 < c(1/2) ≤ 1000
c(1/2) > 1000

Filled: Pop. A
Open: Pop. B
Circles: RQ
Squares: RL

Table 4
Line Luminosities and Blueshifts

Name	log L[Hα] (erg s^{-1})	log L[Hβ] (erg s^{-1})	log L[Mg II] (erg s^{-1})	log L[C IV] (erg s^{-1})	Δv[Mg II] (km s^{-1})	Δv[C IV] (km s^{-1})
J0836	$44.29^{+0.21}_{-0.06}$	$43.71^{+1.09}_{-0.19}$	$43.56^{+0.09}_{-0.06}$	43.54 ± 0.07	197 ± 216	2266 ± 191
J0945	44.64 ± 0.05	44.02 ± 0.08	44.29 ± 0.02	43.75 ± 0.12	1281 ± 183	5485 ± 380
J1321	$43.89^{+0.03}_{-0.04}$	$43.32^{+0.39}_{-0.09}$	$43.48^{+0.11}_{-0.02}$	$43.95^{+0.26}_{-0.06}$	202 ± 188	396 ± 189
J1411	$44.03^{+0.03}_{-0.06}$	43.52 ± 0.20	43.34 ± 0.06	$43.60^{+0.16}_{-0.06}$	−136 ± 181	3142^{+370}_{-208}
J1417	$44.15^{+0.05}_{-0.03}$	43.45 ± 0.11	43.88 ± 0.02	$43.55^{+2.38}_{-0.23}$	624 ± 180	5321^{+4179}_{-652}
J1447	$43.99^{+0.02}_{-0.03}$	$43.41^{+0.51}_{-0.07}$	$43.56^{+0.09}_{-0.02}$	$43.89^{+0.50}_{-0.15}$	1 ± 185	1319^{+750}_{-381}

Note. Δv[Mg II] and Δv[C IV] are line of sight blueshifts of the peaks of the Mg II and C IV profiles, respectively. Δv is based on the observed wavelength of each line center (expected to be at rest-frame 2800 Å for Mg II and 1549 Å for C IV) compared to the systemic redshifts in Table 1. Blueshifts are defined to be positive for approaching motions.

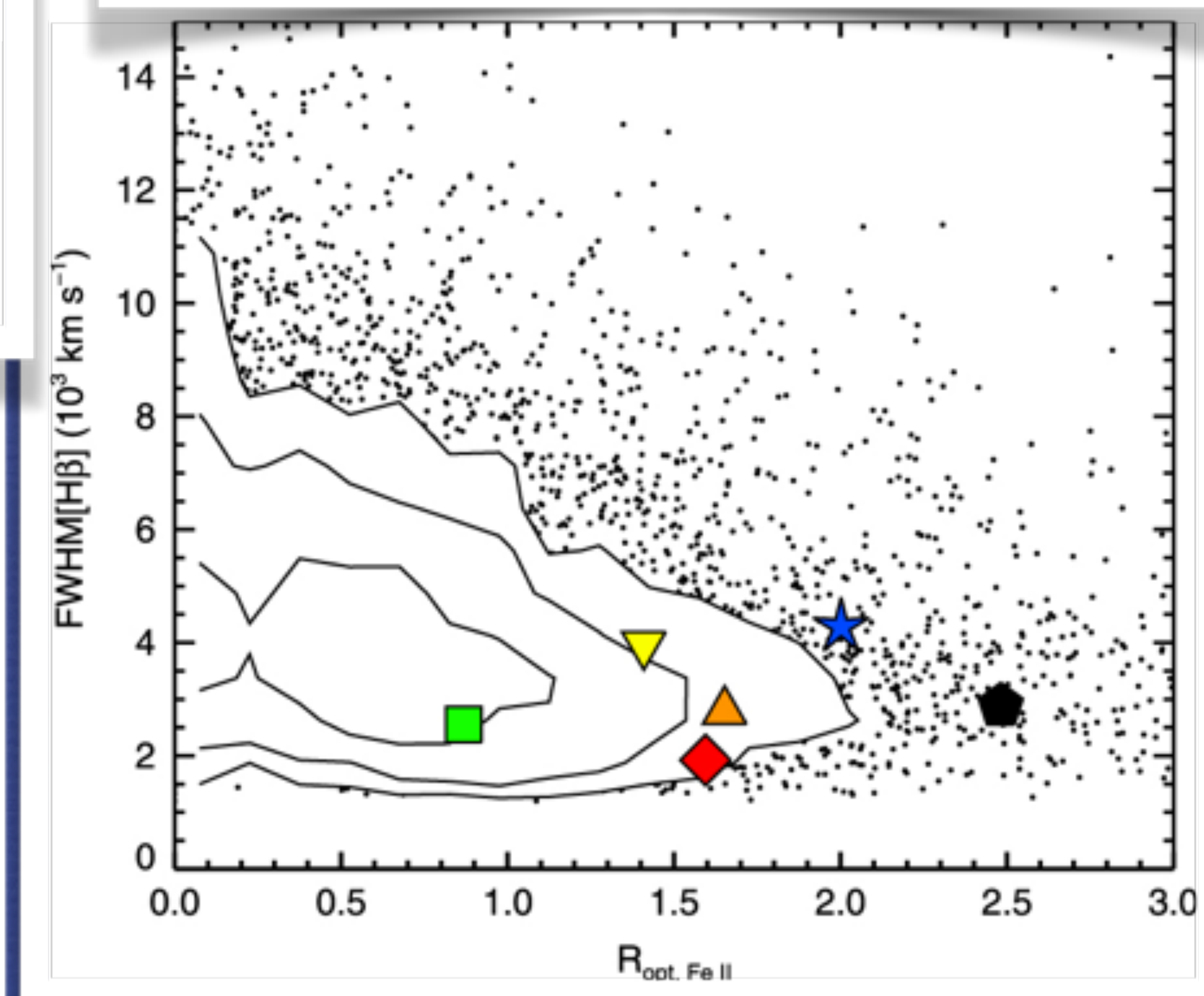

Plotkin et al. 2015

General conclusion

The MS in 4DE1 allows contextualization of spectral parameters related to the conditions of the LIL/HIL emitting gas. It is most likely a sequence of $L_{\rm Edd}$

The MS / 4DE1 is a helpful tool for contextualizingUV and optical data from large surveys. It yielded a straightforward interpretation of WLQs but its understanding is sketchy at best.

Limitations are presently associated with the estimate of a viewing angle for individual RQ sources, the photoionization modeling of FeII emission, the role of BH spin, and the interpretation of some features in the emission line profiles.

The goal is still to map the 4DE1 parameter space into a physical space involving M,